Analysis and engineering of feedstocks for industrial bioprocesses

By

Austin D. Comer

A dissertation submitted in partial fulfillment of

the requirements for the degree of

Doctor of Philosophy

(Chemical and Biological Engineering)

at the

UNIVERSITY OF WISCONSIN-MADISON

2018

Date of final oral examination: 8/1/2018

The dissertation is approved by the following members of the Final Oral Committee:

Brian F. Pfleger, Professor, Department of Chemical and Biological Engineering

Jennifer Reed, Associate Professor, Department of Chemical and Biological Engineering

Thatcher Root, Professor, Department of Chemical and Biological Engineering

John Yin, Professor, Department of Chemical and Biological Engineering

Katherine Mcmahon, Professor, Department of Civil and Environmental Engineering

Abstract

Biological production of fuels and chemicals has been a popular area of research for decades. The potential for producing valuable fuels and chemicals, typically supplied from petroleum sources, using renewable feedstocks is attractive both economically and environmentally. As our long-term survival on this planet is determined by our ability to manage our resources carefully, the use of biological production methods will become critical. In this body of work, we study the feedstocks used to power industrial bioprocesses. First, we show the economic impact of replacing glucose with methane, methanol, or acetate as a carbon source. Methane and acetate both have promise as replacements for glucose, but both may have technical hurdles to implementation. Under current market prices, methanol is not an economically viable replacement for glucose. Next, we study the potential of the marine cyanobacterium, *Synechococcus sp. strain* PCC 7002, to act as the primary glucose source for industrial bioprocesses. Cyanobacteria have higher biomass productivity than terrestrial plants, do not require arable land, and do not compete with food sources. We show the ability to improve the accumulation of glycogen, a glucose polymer, under diurnal growth conditions and improve understanding of how nitrogen starvation relates to glycogen production. We then approach replacing expensive fertilizers with municipal wastewater to reduce cyanobacterial growth costs. Wastewater contains compounds that are toxic to *S.* PCC 7002, which limits its use as a nutrient source. We show an approach to refactor wastewater media to sustain robust cyanobacterial growth. Finally, we constructed and tested an open raceway pond, which mimics industrial-scale facilities. The data from each Chapter was combined to produce a technoeconomic analysis that describes the cost of producing cyanobacterial biomass containing high glycogen content on an industrial scale. We show that the improvements in glycogen production, biomass production, and wastewater tolerance decrease the cost of growing cyanobacteria by 30%.

Acknowledgments

My ability to complete my PhD and survive graduate school is due in large-part due to the enormous amount of support I am lucky enough to have in my life. First and foremost, I would like to thank my wife, Taylor Garcia, for her continuous support. She, more than anyone else, has felt the effects of my research on our lives and has chosen to continue to show support, love, feedback, and perspective throughout my graduate career. Her support represents the single largest contribution to my success and happiness in graduate school and for that, I owe her a great debt of gratitude. I would also like to thank our fur-baby, Moonpie, for his unwitting and unrelenting support for the past three years. No one else literally jumps for joy every time I walk through the door. Beyond my immediate family, I have received continuous support and feedback about my research and career from the remainder of my family. My parents, David and Laura Comer, have been able and willing to provide advice and support throughout my life and education. My sister, Ashley Comer, has not only been a source of light-hearted positivity in my life, but she is able to provide positive support and feedback despite the physical distance between us. Further, Glenn and Glenna Garcia have been extremely supportive and helpful throughout this journey. Beyond that, my extended family has provided support from a distance throughout my career and life and I love them dearly for it.

Another critical component to my successful completion of this thesis is the extended group of friends and lab mates that have provided support, friendship, and unrestrained feedback as I have developed as a scientist. Among this group, my lab mates have been an inexhaustible resource. We have had a number of extremely knowledgeable post-doctoral researchers that have helped me in my research. Matthew Copeland helped me to get my feet on the ground and start doing research in the lab. Andrew Markley, Chris Jones, and Jeff Cameron helped me to learn everything I could need to know to work with cyanobacteria and were all willing to act as sounding boards for experimental planning. There were also a number of graduate students that directly helped me with planning experiments or fielding ideas including Nestor Hernandez, Travis Korosh, Ryan Clark, and Gina

Gordon. Throughout my time in the Pfleger lab, there have been many other lab members that have acted as friends and have provided feedback including Matthew Begemann, Daniel Mendez-Perez, Mark Politz, Jackie Rand, Chris Mehrer, Rung-Yi Lai, Michael Engstrom, Tayor Cook, Dylan Courtney, James Papadopolous, Jonathan Greenhalgh, Michael Jindra, and Franchesca Gambacorta. There are a number of people who have supported my research more directly, including Hugh Purdy, Matthew Long, Professor Reed, Professor Root, Jackie Cooper, Eric Codner, Steve Schumacher, Matthew Seib. I would also like to thank Kathie Heinzen, Michael Morris, and the many other staff members within the department who have put up with my numerous requests for assistance. I would also like to extend my thanks to the other friendships I have built within this department, including those with Sean Tacey, Ellen Murray, Daniel McClelland, Kevin Barnett, and many, many others. I am sure have missed naming many people in writing these acknowledgments that have had a great impact on my graduate career, but know that appreciate your support immensely.

I also want to take the time to thank my defense committee who have taken time out of their schedules to read this thesis and attend my defense. In particular, Professor Reed has provided me with both research resources as well as guidance in the work performed in Chapter 3. This was especially helpful in getting my graduate career started. In addition, Professor Root was invaluable in the construction and initial running of the open raceway pond system discussed in Chapter 6. Finally, Professor Brian Pfleger has been my advisor and general source of guidance throughout my graduate career. He has gone to great lengths and efforts to keep me on track and guide my research to become a consistent, valuable body of work. His contributions to my PhD have been critical for the production of this document and in securing my future career. For this, I owe him many thanks.

Table of Contents

Page

List of Figures

Chapter 1: Introduction and Thesis Overview

Introduction

Industrial bioprocesses are typically broken into two main components. The first component is the use of a microbe or other biological agent to convert a carbon substrate into a value-added fuel, chemical, or pharmaceutical. This is most commonly carried out using a heterotrophic organism grown on glucose as the primary carbon source. The second half of a typical industrial bioprocess is the purification of the final product. This requires separation from the cells that originally produced the product as well as unit operations designed to concentrate the product to a required concentration or purity. These downstream operations may also include further chemical alteration of the product.

When engineering an organism for an industrial bioprocess, a chemical engineer will consider how different factors affect the final economics of such a process. The final product titer that an organism can produce will drive downstream separation costs. The productivity of the organism will determine the capital expenses for growth and fermentation. Finally, the yield of product from the provided carbon source will affect the overall economics. Yield is most important when the product of interest is high volume and low cost, such as fuels or basic chemicals, but will still impact the overall economics of every industrial bioprocess. This thesis is focused on understanding how different feedstocks will impact overall economics of industrial bioprocesses and working to reduce those costs through engineering a cyanobacterium to produce high levels of glucose at a low cost.

Thesis Overview

Chapter 2 is a literature review of the bioeconomy and background on metabolic modeling, industrial growth of photosynthetic organisms, and glycogen production. Cyanobacteria have been used as a host for direct chemical production using sunlight and carbon dioxide as primary nutrient inputs. This process appears very attractive as a renewable chemical production platform or a

biomass production approach that does not require arable land for use. We consider how this can be incorporated into traditional industrial processes as well as other potential alternative feedstocks to sugar.

Chapter 3 outlines my work analyzing alternate carbon feedstocks for bioprocesses. Historically, glucose has been used as the carbon source for the majority of industrial bioprocesses. This is due to its low cost, abundance, and nearly universal biological preference. Recently, alternative carbon sources have gained popularity due to their abundance and low cost. Specifically, methane, methanol, and acetate. We analyze how these alternative carbon sources could be used by model organisms to produce a range products using flux balance analysis (FBA). Yields restricted by FBA are more informative than simple maximum theoretical yields calculated through chemical conversion. We show how the use of consistent yield ratios between carbon sources as well as general feedstock costs allow us to understand the economic impact on the production of products from different feedstocks.

Chapter 4 outlines metabolic engineering efforts aimed at maximizing the intracellular production of glycogen from cyanobacteria. Namely, efforts in rigorous analysis of existing strains in variable media conditions as well as genomic manipulations aimed at increasing glycogen accumulation. We are able to show that some genomic alterations allow for increases in glycogen, but many alterations fail to impact final titer or productivity. Further, we can better understand the economic potential of cyanobacteria to replace terrestrial sugar-producing plants.

Chapter 5 aims to achieve the robust growth of *S.* PCC 7002 on municipal wastewater. Cyanobacterial growth in wastewater presents a challenge due to a variety of stressors. There are both toxic compounds and a complex microbiome of other organisms that can impact the growth potential of *S.* PCC 7002 in municipal wastewater. We show that through mixing of different potential feed streams, we can match high biomass and glycogen titers found in Chapter 3 by wild-type *S.* PCC 7002 in both continuous and diurnal light conditions. We can also better understand the economic impact of diurnal growth on cyanobacterial glycogen production.

Chapter 6 describes the construction and testing of a set of open raceway ponds (ORPs) for the scale-up testing of different cyanobacterial strains and media conditions. ORPs mimic the most cost-effective way to grow cyanobacteria on a large scale. This pair of 50L open raceway ponds are able to show the growth potential of a cyanobacteria under industrially relevant geometries. This work paves the way for future research including testing outdoor cyanobacterial growth and chemical production in both lab media and wastewater.

Chapter 7 will summarize the total work of this thesis and discuss possible future directions to continue forward with this research. Following this discussion will be appendices covering my early, unpublished work in the Pfleger lab and my laying the ground work for a cyanobacterial tool development project.

Chapter 2: Literature Review

The bioeconomy

Biological production of fuels and chemicals has been a popular area of research for decades. The potential for producing valuable fuels and chemicals that are typically supplied from petroleum sources using renewable feedstocks is attractive both economically and environmentally. As our long-term survival on this planet is determined by our ability to manage our resources carefully, the use of biological production methods are likely to become critical.

The bioeconomy is built around the core conversion of renewable feedstocks to value-added chemicals. This is most commonly in the form of carbohydrate conversion to fuels, pharmaceuticals, or specialty chemicals.[78, 45] This process is most efficient when producing higher cost products with lower volumes. The first generation of biofuels and chemicals focused almost exclusively on ethanol production from corn or sugar cane, which contains very accessible carbohydrates. This is a well studied process and is performed industrially in yeast.[9, 49] This biofuel is used as a gasoline additive to assist in complete combustion. Unfortunately, ethanol is a poor biofuel for a number of reasons. Ethanol has a high vapor pressure, low energy density, and cannot be used directly in our current fuel system. Further, the use of corn as the primary feedstock competes with food production. These limitations have spurred movement to second and third generation biofuels and chemicals as overall better replacements for petroleum derived fuels.

Second generation biofuels and chemicals have garnered growing interest and research effort recently. Second generation biofuels and chemicals use non-food biomass as its primary input.[45] These processes use different lignocellulosic biomass substrates as the process feedstocks. This substrate can be difficult to break down into sugars due to the presence of lignin. They also typically produce toxic compounds in addition to sugars that reduce the range of organisms that can be grown in the resulting media. Similarly, third generation biofuels and chemicals use algal biomass as the main feedstock. Generally, algae has faster biomass productivities than terrestrial plants and

can be grown in wastewater.[82] This range of advantages make both second and third generation biofuels and chemicals very attractive assuming that technical hurdles to production and use can be overcome.

The final class of chemicals and biofuels production is not as clearly defined. This would be the production of products from non-standard feedstocks, such as natural gas. The main motivation for this class of production stems from very low natural gas prices and low cost natural gas and synthesis gas derived products, which includes methanol and acetate.[18, 17] The abundance of natural gas and the lack of economic applications in its use can be seen in images of the North America at night (Figure 1). These images show large clusters of flares at fracking sites near the Eagle Ford and Bakken shale formations. Methane is produced in abundance from these fields and the price of natural gas is so low that it is more economical to simply burn the methane rather than produce energy or chemicals.[71] Finding a scalable process that can use a distributed source of natural gas for production of value-added chemicals is attractive.

Methane and synthesis gas, a mixture of carbon monoxide and hydrogen, are common starting products for some conversion processes into more valuable products (Figure 2). In traditional gas-to-liquids (GTL), methane or other carbon sources can be converted to synthesis gas. Methane is converted to synthesis gas through a process called steam reformation. Coal or other solid carbon sources can be converted to synthesis gas though gasification.[84] Synthesis gas has a number of applications, but one common application is conversion to methanol for the production of other chemicals. This is completed through a catalytic methane to methanol conversion. Methanol has a large market, but it is often converted onto more valuable chemicals through additional chemical processes.[84] Alternatively, methanol can be converted to acetate through methanol carbonylation. This acetate production represents an additional low cost feedstock. The cost of the discussed substrates increase as more steps are required for chemical conversion. This results in higher feedstock costs. Theoretically, each feedstock is also more readily assimilated into central metabolism as it is further processed. This combination of effects means that it is difficult to assess

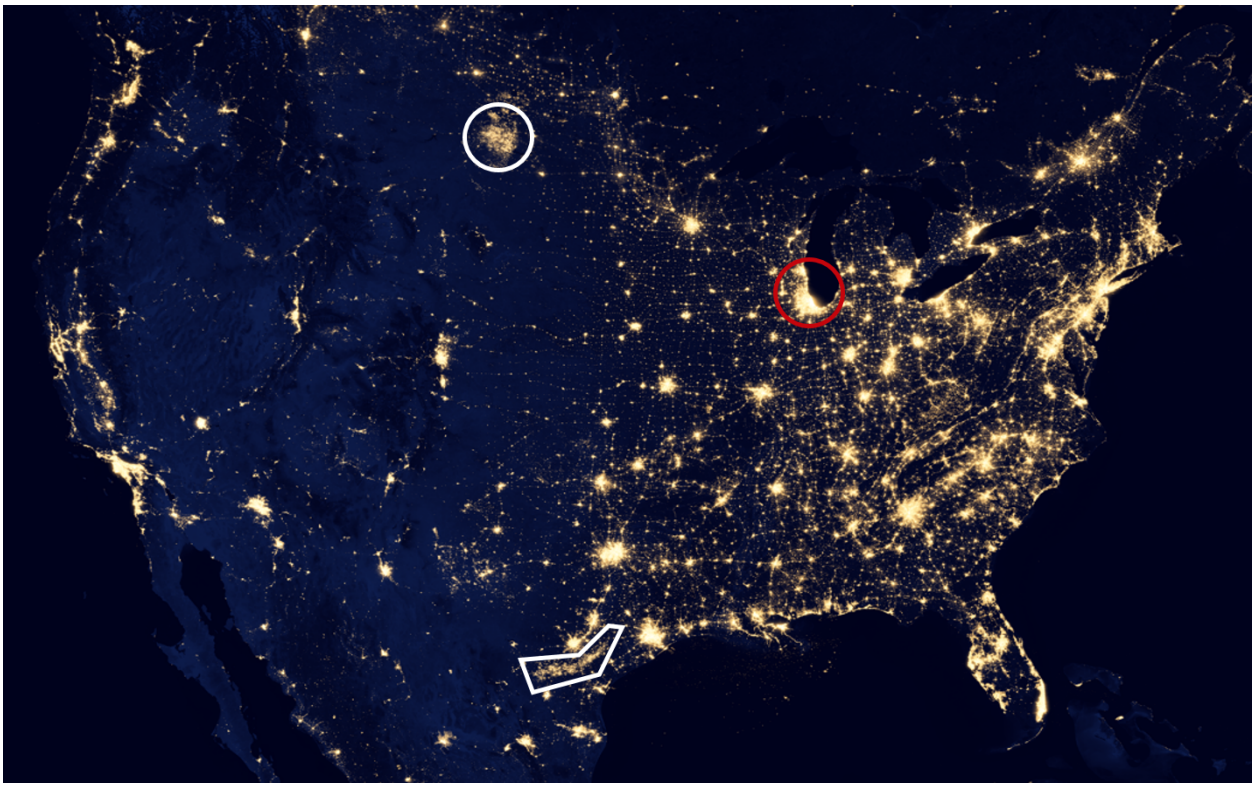

Figure 1: A picture of North America taken at night. The northern and southern circles represent the Bakken and Eagle Ford shale formations, respectively. The lights in these areas are from a large number of flares burning methane produced during the fracking process. The red circle highlights the Chicago metropolitan area as a comparison in size and brightness.

which feedstocks are valuable for use in industrial bioprocesses in comparison with the use of glucose, the current status quo.

Beyond this current set of chemical processes, there are a number of groups considering the biological conversion of methane, synthesis gas, methanol, and acetate to a large variety of value-added products. These direct conversions are difficult because they typically require the use of unusual organisms (except in the case of acetate) that are designed to consume these unique feedstocks. There are multiple companies working on these conversions industrially as well. Intrexon and Calysta are working on methane conversion using methanotrophs and LanzaTech is working on the conversion of synthesis gas to acetate.[65] Further, an integrated synthesis gas to acetate process with a downstream yeast process for conversion of acetate to biodiesel has been

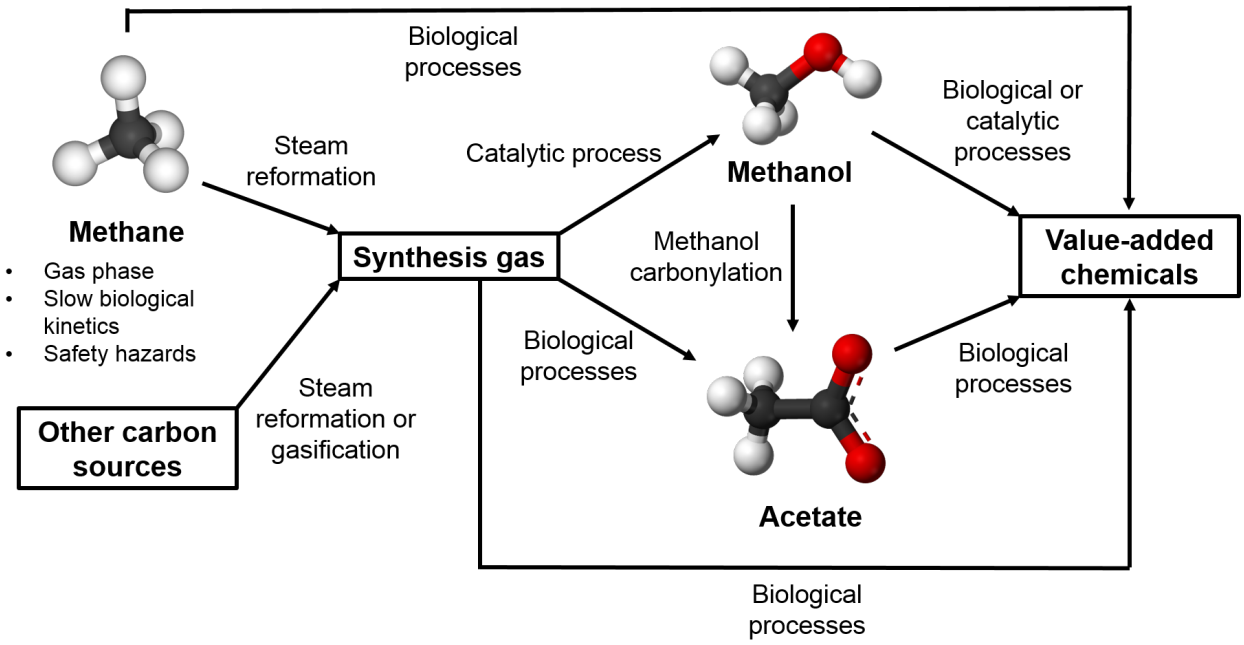

Figure 2: The production of basic chemicals from methane using traditional chemical methods as well as current and potential biological processes that could supplement or replace these conversions.

shown to work at lab scale.[33] Other groups have also considered using model organisms as the chemical production host and integrating the necessary assimilation pathways for their feedstock of interest. The weakness in this process is that these organisms are not optimized to handle these feedstocks and may require significant engineering efforts to successfully support both growth and chemical production on alternate carbon substrates. On the other hand, using a non-model organism for this conversion requires the development of an entire genomic toolbox in order to engineer the organism for chemical production. Further, these organisms have poorly studied metabolism that would make both computational and rational approaches to metabolic engineering difficult to implement.[53, 34]

These chemicals can be assimilated into biological systems for energy and carbon. These alternate substrates have some potential for chemical production based on their low price and the fact that they avoid the toxins present in lignocellulosic derived biomass, the food competition of corn-based biomass, and the unknown cost of algal biomass. Avoiding the core pitfalls of these

alternative technology still leaves a number of potential technical hurdles, including mass transfer and low energy density.

Beyond changing substrates, the range of target chemicals and fuels has expanded well beyond ethanol. In the last decade, research has shifted towards production of other short-chain alcohols, such as butanol and pentanol, which can act as drop-in replacements for fuels.[40, 39] Extensive work on production of medium chain alcohols, such as octanol and decanol, has also achieved increased yields and titers of these molecules.[51] These molecules are even better direct replacements for fuels. Further, work to improve the production of biodiesel has continued with efforts to increase the titer of fatty acids that can be converted to diesel. Unfortunately, none of these processes have been commercialized for biofuel production. In addition, a new focus on terpenes as potential replacements for jet fuel has also been explored.[64] This class of molecules can cover a wide range of physical properties, which allows for production of different classes of fuel. Beyond the production of fuel, there have been a number of successful biochemical commercialization projects that have produced polymer precursors, basic chemicals, and compounds for cosmetics. Some examples include 1,4-butanediol, 1,3-propanediol, Vitamin C, farnesane, and isoprene.[45] These chemicals have all been commercialized for full conversion of sugar substrates to chemical products through synthetic biology alone. Our lab has worked to increase the production of medium-chain fatty acids, which have a variety of valuable applications.[26, 86] There has also been a rapid expansion in the discovery and production of natural products. These include compounds such as medications and antibiotics[55] as well as plant bacterial resistance molecules[20]. There are many more examples available, especially when we consider mixed biological and chemical conversion (like the classic example of artemisinin).[38] This is not uncommon for a variety of chemicals and some pharmaceuticals.

Metabolic modeling

Flux balance analysis is a powerful tool to help us understand metabolism and probe production potential of an organism. FBA is a tool that looks at the steady state intracellular status of an organism based on a genome-scale metabolic model specific to that organism.[59] The model includes metabolic reactions, genes, and proteins, which allows for basic evaluation of the metabolic state of genetically modified strains. This approach requires the use of optimization software to analyze the genome-scale metabolic modeling in the context of some optimization parameter and set of constraints. These constraints are typically some form of media conditions and the most common optimization is the maximization of biomass production, to measure maximum growth rate.[59]

This approach can be taken further to investigate many components of the metabolic model. One engineering oriented example is flux couple a product of interest with growth. This growth coupling forces product synthesis in order to maximize growth. In another example, strains containing different knockouts can be more easily evaluated for changes in product production or growth. FBA has a number of additional uses, such as predicting maximum product production, evaluating novel pathways, or identifying missing reactions in a genome-scale metabolic network.[73] FBA has been further altered to include methods to look at non-steady state applications, the addition of signaling networks, and more.

Phototrophic organisms

Phototrophic organisms fall into two general classes: multicellular plants and macro algae and single-cell microalgae. Phototrophic organisms are named as such because they harness the energy of the sun to provide the majority of the intracellular energy required for growth through a process called photosynthesis. This energy collected by plants makes up the majority of our energy and food systems. Food chains begin consistently with an autotrophic organism, typically one that

requires light to survive. The process of photosynthesis is the basis for our food chain. Further, petrochemicals, our primary source of energy, are originally sources from carbon material, most of which was created from photosynthesis.[66]

Photosynthesis is broken into two general parts, light reactions and dark reactions (Figure 3). The light reactions are named due to their requirement for light. Light reactions use photons from the sun to create energy and reductive power which are collected into storage molecules, typically adenosine triphosphate(ATP) and nicotinamide-adenine dinucleotide phosphate (NADPH). These storage molecules are created by splitting water to create oxygen using the energy of a photon. This energy and reducing power can be used to reduce carbon dioxide through the dark reactions to create bioavailable carbon compounds, carbohydrates, which can act as the primary carbon source for biomass production. This is completed using the most abundant enzyme on earth, RuBisCo.[2] Photosynthesis reconnects with central metabolism within glycolysis through production of the compounds glyceraldehyde 3-phosphate (G3P) and 3-phosphoglycerate (3PG). This set of reactions is called the Calvin-Benson cycle and provides the majority of energy for both plants and single-cellular phototrophs. During the night, photosynthesis shuts down and energy is supplied from energy storage molecules built up during the light cycle. This rhythm is a diurnal cycle that is controlled by the exposure time and intensity to the sun.[46] Overcoming the lack of growth and chemical production during the dark cycle is a significant challenge in working with phototrophic organisms.[50]

Phototrophic organisms make very attractive engineering targets for a number of reasons. First and foremost, photosynthetic organisms are grown with inexpensive and often unused feedstocks. Light is easily accessible from sunlight and especially abundant in many areas. Carbon dioxide is both inexpensive and considered a waste product from most industrial processes, including many processes from power plants to cement production. If we can harness the photosynthetic ability of a phototroph to process a waste carbon source into a valuable fuel or chemical in an economical way, we create a strong carbon neutral process that would be very attractive for industrial use.[7]

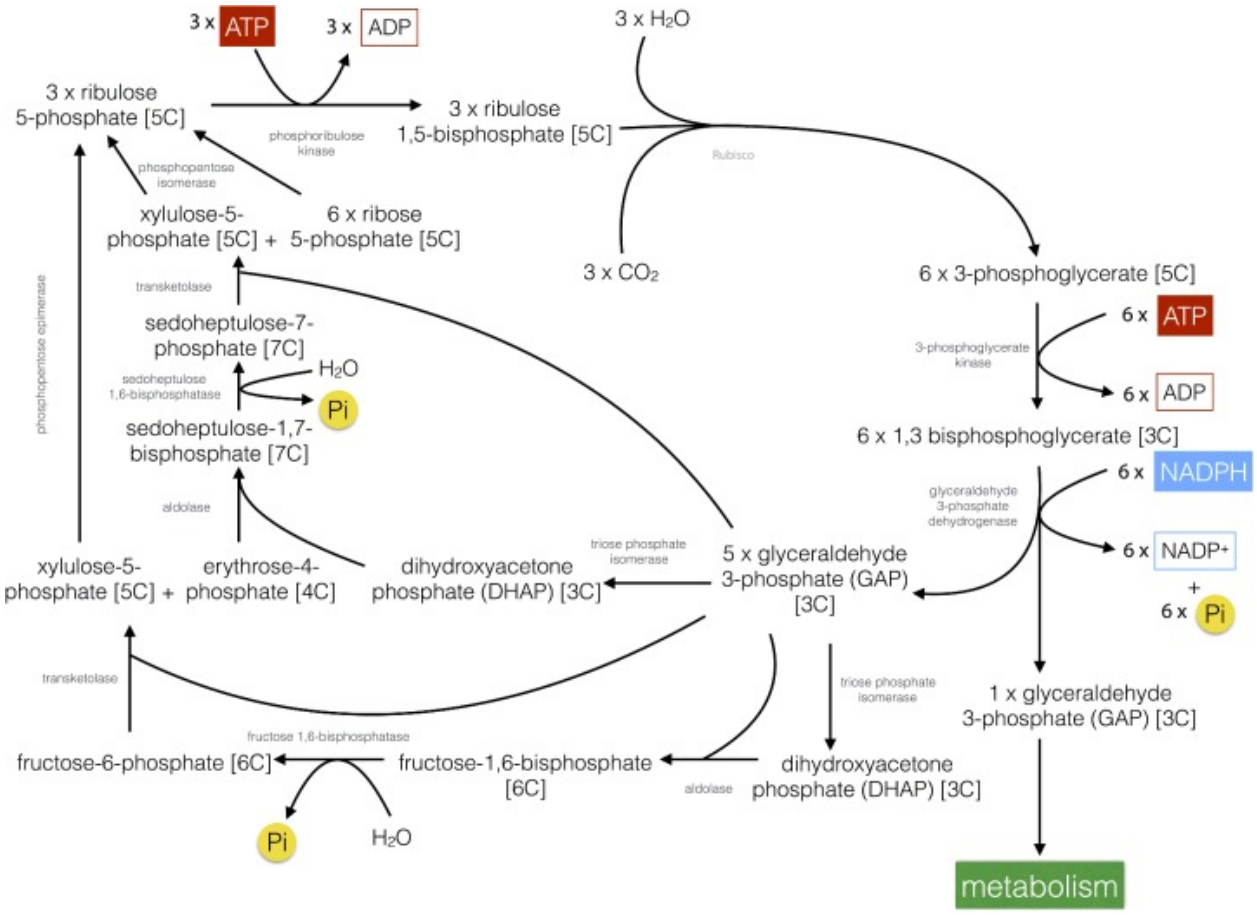

Figure 3: The Calvin-Benson cycle for the assimilation of carbon dioxide into central metabolism using Rubisco and energy from photosynthesis. Figure adapted from [66]

Cyanobacteria, also known as blue-green algae, are attractive hosts for chemical production because they have very fast growth rates compared to both terrestrial plants and many other algae. Cyanobacteria are photosynthetic prokaryotes that have relatively low nutrient requirements for growth. Beyond this, cyanobacteria can be grown using non-arable land and thus not compete with food or other agricultural land. This distinction could become critical as our population continues to grow and increases demand on our arable land to supply food.[41] Often, cyanobacteria growth is considered for areas that are particularly dry or otherwise difficult to grow crops in. As prokaryotes, creating genetic tools for the manipulation of cyanobacteria is much easier than plants or eukaryotic algae. This toolbox is also beginning to become well developed as many labs work across a variety

of different cyanobacterial strains.[68, 56] Cyanobacteria are also resistant to a wide range of toxins and stresses. This can be seen in the ability for many strains to grow in wastewater derived from a variety of sources. These sources can include municipal wastewater, industrial wastewater, and agricultural runoff.[5, 13] Some strains of cyanobacteria are more susceptible to these toxins than others and must be either engineered or the environment must be adjusted for growth under these conditions.

Cyanobacteria have already been successfully engineered to produce a range of chemicals directly from carbon dioxide and sunlight including short-chain alcohols, fatty acids, carbohydrates, and terpenes.[40, 39, 44, 22] Further, there are multiple strains of cyanobacteria that naturally accumulate high levels of glycogen or fatty acids as a form of energy storage. Glycogen can be hydrolyzed to glucose, but is more often considered a side product of central metabolism. There have been successful efforts to reduce glycogen production through engineering nitrogen regulation and the glycogen biosynthesis pathway.[27, 80, 1] On the other hand, fatty acids can be converted to biodiesel. This process is practiced in some areas at industrial scales, but the biodiesel is generally more expensive then petroleum-derived diesel.

For this work, we are considering the cyanobacteria *Synechococcus sp. strain* PCC 7002, shown in Figure 4, previously known as *Agmenellum quadruplicatum*. *S.* PCC 7002 is one of the fastest growing strains of cyanobacteria originally isolated by Van Baalen in coastal ocean.[79, 75] The natural environment for coastal cyanobacteria has highly variable salt content, but *S.* PCC 7002 has been shown to grow best in brackish water, a mixture of salt water and fresh water./citeAikawa2014 This range of salt tolerance is helpful in many applications, but does make growth in municipal wastewater more difficult for this organism. *S.* PCC 7002 is a naturally competent organism, meaning it will take up free DNA in solution. This quality makes transformation very easy and overcomes one basic hurdle to tool development in novel organisms.[74, 23]

Further, this cyanobacteria has had extensive tool development in promoter, induction, ribosome binding site, selection, counter-selection, genomic integration, and CRISPRi systems. Our lab has

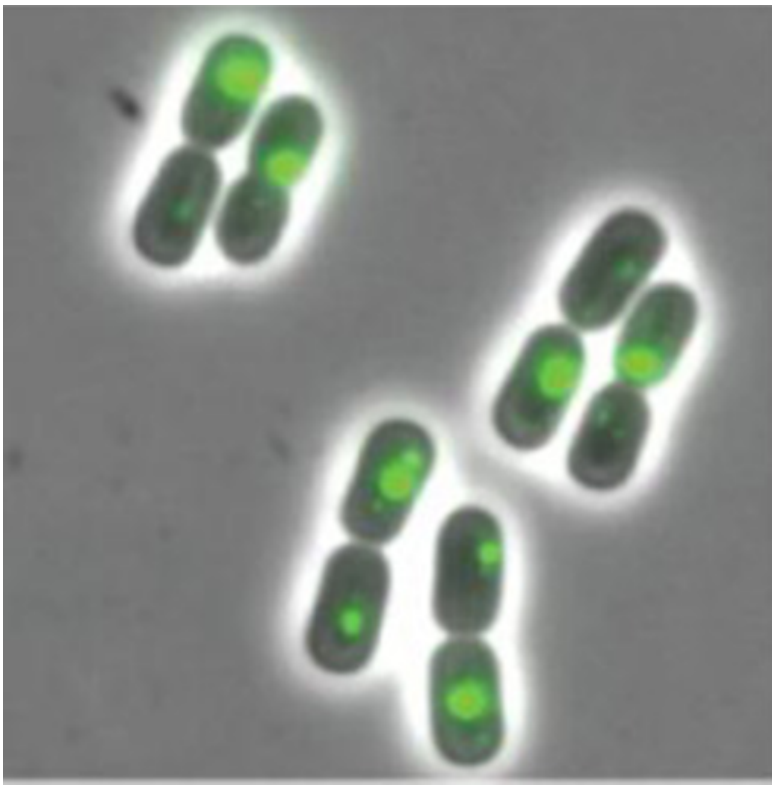

Figure 4: A microscope image of the cyanobacteria *Synechococcus sp. strain* PCC 7002 with a GFP tag on the carboxysome within the cell. Figure adapted from [14]

pioneered the first promoter system designed from a natural *S.* PCC 7002 strong promoter.[47] This promoter was trimmed down to a short sequence that removed expression variability with light. Alternate inducible versions of the promoter were made by adding a pair *lacO* sites around the core promoter. This study also validated the use of ribosome binding site calculators in *S.* PCC 7002.[47] Our lab was also the first to design an acrylic acid based counter-selection system for the production of scarless knockouts in *S.* PCC 7002.[6] Finally, we also developed a CRISPRi system for gene expression control and as a metabolic engineering tool.[24] These advancements have allowed for relatively high control over gene expression from the genome and has made genetic modification of *S.* PCC 7002 simple. In addition, the fast growth rate of this organism does make the time to introduce a genetic change or iterate through learning cycles lower. This set of qualities and developments has made *S.* PCC 7002 one of the model cyanobacteria that is closely studied for

chemical production.

Industrial cyanobacteria growth

There are two major hurdles to the use of cyanobacteria as an industrial production organism. The first is product selection and the second is overcoming industrial growth limitations. These factors are influenced further by the types of growth vessels that we can use for cyanobacterial growth. Cyanobacteria can be grown in open raceway ponds (ORP) or closed photobioreactors (PBR). Depending on the type of system available, our range of useful products that we can make and methods for overcoming cost limitations will vary.

Open raceway ponds are large, shallow ponds in the shape of a race track that use a paddle wheel to continuously mix the growth culture (Figure 5). These systems are typically open to air, but there are examples of covered systems that reduce water loss due to evaporative cooling. These systems are advantageous due to low capital costs and relatively low running costs. This disadvantage is the the amount of light delivered to each cell is very low. This will be limiting for both growth rate and final titers.[14] Further, open systems do not allow for the production of many volatile compounds and also leave the system open to contamination by bacteriophages or competing phototrophs. There have been a number of suggested improvements to the traditional ORP system to increase productivity and final biomass titer.[87, 11, 76]

On the other hand, a closed photobioreactor has a number of growth advantages over an open raceway pond (Figure 6).[15] The improved reactor geometry allows for much better light delivery per cell, which greatly improves growth rates and final biomass titers.[14] The closed system decreases the amount of water lost due to evaporation as well as decreases contamination likelihood and product loss. These improvements mean that PBR are far better systems for cyanobacterial growth and product production from the standpoint of growth alone. Unfortunately, photobioreactors are both very expensive to construct and very expensive to run. These costs typically make production of value-added products in a PBR more expensive than production in an open raceway

Figure 5: Figure of a large-scale open raceway pond for algal growth. Figure adapted from the MicroBio Engineering website @ https://microbioengineering.com/rw1000/

pond.[25] The exceptions to this would include the production of very high value products or the use of PBR systems that are so much more efficient for light distribution, that the extra capital costs are worthwhile.

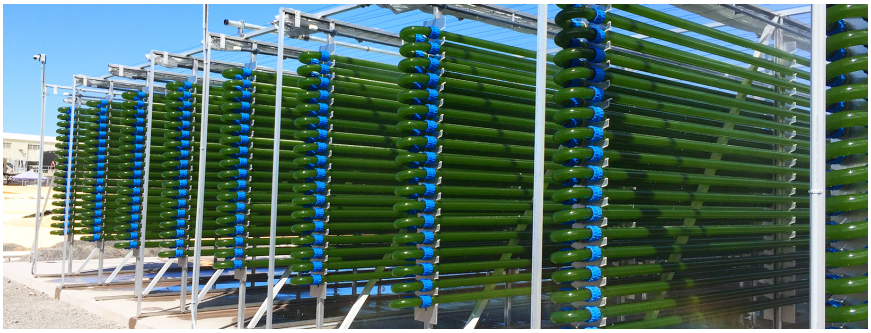

Figure 6: A large horizontal stacked tube photobioreactor system for high productivity growth of algae. reference Varicon Aqua @ http://www.variconaqua.com/

Given that any economically feasible cyanobacterial chemical production is more likely to occur

in an open raceway pond, this limits the range of products that can be made. Contamination prevents the production of compounds that can be easily assimilated by contaminating heterotrophs. The open system also prevents the production of any volatile compounds, which eliminates the ability to produce fuels or volatile chemicals. Further, the low final product tier means the water soluble extracellular products will be extremely expensive to separate without unique chemical properties that allow for easy separation. Finally, pharmaceuticals will be difficult to make because an open system could allow for contamination by cyanotoxin producing phototrophic competitors. This would mean very rigorous purification and testing would need to be done on the product . This limits our range of products greatly and biases intracellular products for ease of separation.

In order to drive down the cost of growing cyanobacteria, multiple approaches have been considered. Some groups have considered mixotrophic cyanobacterial growth.[43, 12] This involves using an alternate carbon source to improve growth rates or allow growth to continue during the dark cycle. Unfortunately, these approaches have focused primarily on carbon sources that can be consumed by the majority of heterotrophs, such as glucose, and would only act to invite contamination. Another popular option is the use of wastewater to replace liquid fertilizers required to grow cyanobacteria.[5, 91] This introduces other organisms into the system in exchange for a very low cost feedstock. This can also introduce toxins that cause growth and production issues for cyanobacteria. Further process improvements include unit operations for more efficient carbon dioxide delivery, better separations, less water and temperature loss by covering ponds, or more efficient culture mixing. Many of the alterations can decrease costs or increase growth rate as well as final product and biomass titers.

Glycogen production

Glycogen is a common energy storage molecule used in a number of organisms. Glycogen is a polymer of glucose molecules linked with alpha-1,4 bonds for linear chains and by alpha-1,6 bonds at branch points.[28] These molecules are built up starting from the products of photosynthesis, G3P

or 3PG. G3P or 3PG is built back up through gluconeogenesis to glucose-6-phosphate, isomerized to glucose-1-phosphate by phosphoglucomutase, and converted to ADP-glucose by *glgC*.[92] Finally, ADP-glucose is polymerized by *glgA* into glycogen. Glycogen branching is controlled by the branching and debranching enzymes *glgB* and *glgX*, respectively.[92, 77] These enzymes can adjust how compact the glycogen granules are based on the amount of branching, which can impact the volume efficiency of energy storage. In many cyanobacteria, glycogen is the main source of energy storage by which cells can regulate energy availability between periods of light and dark, as well as periods of high and low nutrients. In the wild, this energy storage is a survival adaptation.

In order to access the energy stored in the form of glycogen, cyanobacteria must take advantage of glycogen degradation pathways, shown in Figure 7. Glycogen can be degraded linearly by *glgP* and *agpA*. Once linear degradation to a branch point is complete, the last 4 glucose units must be cleaved by the debranching enzyme *glgX* and are degraded by a number of enzymes including *malQ*, which is responsible for breaking maltotetrose and maltotriose units into smaller components.[92] These pathways allow cellular access to energy and carbon through glycolysis and central metabolism from stored glycogen. The amount of glycogen released through each of these processes is determined by the amount of branching in the glycogen.

Historically, glycogen production has been probed at a few points within this pathway as well as through environmental changes. For *S.* PCC 7002, glycogen production is induced by different forms of nutrient starvation. Most commonly, nitrogen starvation will induce rapid buildup of intracellular glycogen.[1] The master nitrogen regulator controls this response and can be triggered by other forms of nutrient or light limitation. Historically, the *glgC* node has seen the most manipulation in *S.* PCC 7002. Groups have worked to knockout this node to reduce glycogen accumulation within the cell to increase the available energy for chemical production.[80] This manipulation has been shown to be successful in eliminating the majority of glycogen accumulation, although it has not increased chemical production. A similar analysis and result was achieved for a *glgA* strain.[85] Glycogen production has also been probed under different salt conditions. *S.* PCC 7002 was found in brackish

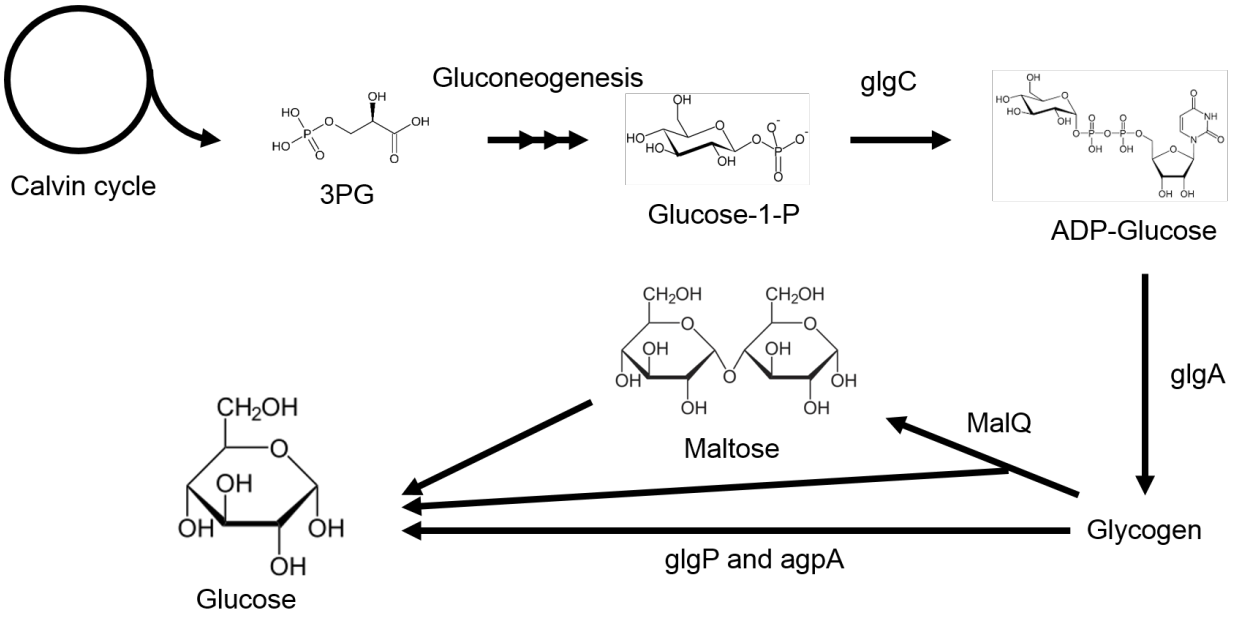

Figure 7: Glycogen is produced from the products of the Calvin-Benson cycle reforming glucose 1-phosphate though gluconeogenesis and phosphoglucomutase. This is converted to glycogen through *glgC* and *glgA*. Glycogen structure is altered by branching and debranching enzymes, *glgB* and *glgX*. Finally, glycogen can be degraded using linear depolymerases *glgP* and *agpA* as well as the branched chain pathway including *malQ*.

water and thus, unsurprisingly, grows and produces the most glycogen under these conditions.[1] Both fresh water and salt water growth of *S.* PCC 7002 reduces biomass production and glycogen content.

Summary

Overall, the bioeconomy is rapidly changing in both the range of feedstocks used for biological processes and the types of products being made. Feedstock cost is a powerful driver of overall costs in high volume markets and will affect product costs in all markets. Finding less expensive and more efficient feedstocks increase the viability of all industrial bioprocesses. Currently, alternate low cost molecules, such as methane, methanol, and acetate, are very attractive as replacements for sugar. However, it is difficult to analyze the cost effectiveness of the alternate substrates. Further, the

drive to second and third generation biofuels is pushed by a desire to find abundant and inexpensive sources of carbohydrates. Fortunately, cyanobacteria offer a number of advantages that make cyanobacterial carbohydrate production a promising path for low cost feedstocks. Cyanobacteria have higher biomass productivities than plants, do not require arable land, and do not compete for food resources. Cyanobacteria can also harness sunlight as their main energy source and the waste stream, carbon dioxide, as their primary carbon source. Currently, cyanobacterial biomass production does not appear to be economically viable. There needs to be further research on boosting productivity, titers, and carbon partitioning.

Chapter 3: Metabolic modeling and economic analysis of alternate feedstocks for industrial bioprocesses

Introduction

Abundant, low cost C1 compounds such as methane, methanol, and carbon monoxide have garnered attention as potentially inexpensive sources of carbon and energy in biocatalytic processes for producing commodity chemicals. [17, 29, 83][1] Over the last decade, natural gas supply has reached all-time highs with costs consistently lower than petroleum. Despite these economic advantages, large volumes of natural gas are flared at wellheads daily to reduce greenhouse gas emissions or directly leaked, both intentionally and unintentionally, to the environment during production.[31, 71] Nighttime satellite images of these areas show light intensities equivalent to major US cities and illustrate the enormous potential that is wasted. Alternative uses, such as pipelining to refineries, catalytic conversion to syngas or methanol, or combustion for electricity and heat have not been deployed due to costs, wide geographic distribution, and/or poor proximity to end-users. Given that feedstocks are the major operating cost of producing biomanufactured chemicals, the choice of carbon source can have a significant impact on profitability.[35] Given the potential process advantages, the economic potential of C1 feedstocks for biomanufacturing of commodity chemicals warrants evaluation.

Cost is not the only criteria when considering methane, as gas phase feedstocks suffer from a few bioprocess drawbacks. First, uptake of gas phase feedstocks can be mass-transfer limited and significantly slower than uptake of traditional aqueous feedstocks, such as sugars and organic acids, depending on bioreactor conditions.[17] Second, methane utilization by methylotrophs requires an electron acceptor – most frequently oxygen – which raises safety concerns over potentially

[1] This work was completed with guidance from Dr. Matthew Long and Professor Jennifer Reed and was published in part or whole.[16] Specifically, Dr. Matthew Long assisted in FBA formulation and in the interpretation of results and Professor Reed assisted in manuscript edits and contributed computational resources.

explosive mixtures of feedstock gases.[83] Third, the conversion of methane to methanol, catalyzed by methane monooxgynease, is a slow step that limits overall productivity. For these reasons, we were curious if alternative derivatives of C1 compounds, methanol and acetate, would have economic advantages over glucose. Methanol, produced by steam reformation to syngas and catalytic conversion to methanol, is the first intermediate in methane assimilation. Acetate can be produced from natural gas by combining catalytic water-gas shift with anaerobic fermentation of the resulting syngas by acetogens. These so-called biological gas-to-liquid (Bio-GTL) processes have been recently demonstrated for producing lipids and biodiesel.[32] This low-cost process makes acetate an interesting potential feedstock to replace glucose in biocatalytic processes. Feeding aqueous methanol or acetate would circumvent many of the technical hurdles in a bioreactor while potentially leveraging the low-cost and abundant supply of C1 feedstocks.

The last factor in selecting a feedstock is the relative amount needed to generate a given amount of product. Sugars are the dominant feedstock for bioconversions because metabolism efficiently extracts energy and electrons for use in synthesizing chemical products. Assimilation of C1 compounds is not as energy efficient given higher energy and reducing power costs. There are several pathways for assimilating methane and methanol; each differs in energetic yield, connections to central metabolism, and kinetics. Methane and methanol assimilation both occur through the assimilation of formaldehyde. The first step in methane catabolism is oxidation to methanol by a methane monooxygenase (Hwang et al., 2014).[34] Methanol is further oxidized to formaldehyde by an alcohol oxidase or methanol dehydrogenase.[53, 83] Formaldehyde is then assimilated through one of three pathways: the ribulose monophosphate (RuMP) pathway, the dihydroxyacetone (DHA) pathway, or the serine pathway (Figure 8).[88] The DHA — found only in fungi — and RuMP — common in gamma-proteobacteria and only found in bacteria and archea — pathways both use a five carbon sugar as a substrate to assimilate formaldehyde and produce a six carbon sugar.[34, 53, 83, 88] Every three turnovers of these cycles produces a single dihydroxyacetone phosphate. In contrast, the serine pathway — common in alpha-proteobacteria — assimilates formaldehyde

through reaction with glycine to create serine.[34, 88] Every two turnovers of this cycle assimilates two formaldehydes and one carbon dioxide to produce a 2-phosphoglycerate (the base cycle can be augmented with other reactions to produce acetyl-CoA and TCA cycle intermediates with additional cycles and assimilation of CO_2. To obtain energy, formaldehyde is oxidized to carbon dioxide to generate reducing equivalents that can be converted to ATP via the electron transport chain and ATP synthase.[88] Overall, the RuMP pathway is considered the most efficient pathway in terms of energetic yield and is the preferred C1 assimilation pathway in studies of C1 catabolism as a feedstock.[53] Beyond the formaldehyde assimilating pathways, there is a small class of C1 catabolizing, non-photosynthetic bacteria that use the Calvin-Benson-Bassham (CBB) cycle to assimilate carbon dioxide by oxidation of C1 carbon sources to produce the energy needed to run the CBB.[34] This does not appear to be an efficient pathway and is not biologically common, so we did not include it in our analysis. In addition, Bogorad, I. W. et al. created a synthetic methanol condensation cycle (MCC) for the efficient assimilation of methanol by using a combination of the RuMP cycle and synthetic non-oxidative glycolysis in E. coli.[8] We tested this pathway for improved yield as part of a set of analysis looking at the impact of including carbon efficient assimilation pathways and show little difference on predicted product yields in E. coli.

Acetate is typically assimilated into central metabolism as acetyl-CoA. Acetate is a common by-product during rapid growth in bacteria and re-assimilates during stationary phase at the cost of one ATP. For this reason, most organisms, including those studied here, have pathways for assimilating acetate. In *E. coli*, and many other microorganisms, acetate assimilation proceeds through acetyl-phosphate (catalyzed by ackA/pta). In other organisms, such as the cyanobacterium *Synechococcus sp. strain* PCC 7002 studied here, acetate assimilation proceeds through a transient acyl-AMP intermediate as part of an acyl-CoA ligase mechanism.[6] Other pathways for acetate assimilation involve CoA transfer from other metabolites (e.g. propionyl-CoA, succinyl-CoA).

To assess the tradeoffs between feedstock cost and product yield, we have performed an economic analysis using maximum theoretical yields calculated by flux balance analysis of genome-

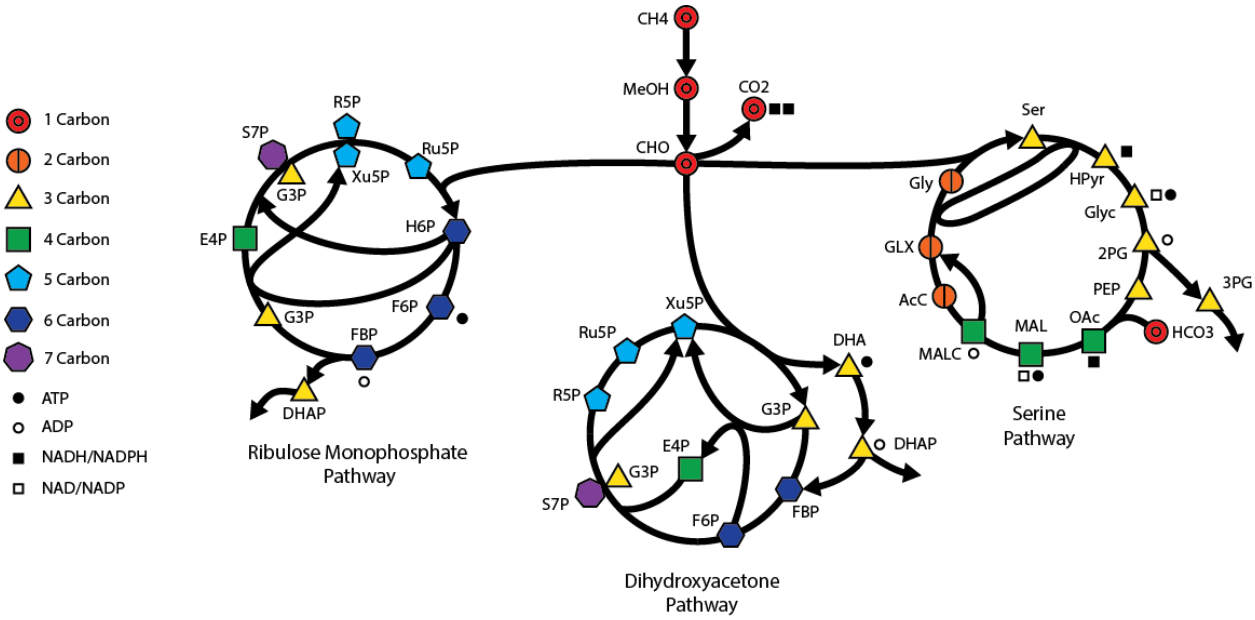

Figure 8: A visual representation of the three formaldehyde assimilation pathways analyzed in this work.

scale metabolic models. We performed the analysis on models of three organisms, the bacterium *Escherichia coli*, the yeast *Saccharomyces cerevisiae*, and the cyanobacterium *Synechococcus sp. strain* PCC 7002, augmented with all three common methane assimilation pathways (serine, RUMP, DHA). For each model, we calculated the theoretical yield for every metabolite in each model from each feedstock – glucose, methane, methanol, and acetate as well as xylose and glycerol for E. coli only. We use the calculated theoretical yields and current feedstock prices to create surfaces of feedstock costs. Our analysis shows that despite the lower stoichiometric yield from methane, methane feedstock costs are consistently lower than glucose when used as carbon and energy sources to make products. Conversely, methanol is equal to or costlier than glucose. Acetate is much more difficult to give an accurate estimate of comparable feedstock cost with glucose given current technological change and price variation. Our analysis suggests that methane is the most promising C1 feedstock, assuming it is possible to overcome any technical hurdles associated with its use as a feedstock.

Metabolic modeling for estimating yield ratios

Established genome-scale metabolic models of *E. coli* (iJO1366) (Orth et al., 2011), *S. cerevisiae* (iMM904) (Mo et al., 2009), and *Synechococcus sp. strain* PCC 7002 (iSYP708) (Vu et al., 2013) were used to calculate theoretical yields.[60, 52, 81] Each model was augmented with reactions necessary for C1 metabolism, including methane/methanol exchange, methane/methanol transport, methane/methanol oxidation, the RuMP pathway, the DHA pathway, the serine pathway, and formaldehyde oxidation to carbon dioxide. Acetate assimilation pathways were already present in each model. For *S.* PCC 7002, which lacks a glyoxylate shunt, acetate is assimilated as acetyl-CoA that is respired through an alternate TCA cycle present in cyanobacteria. The resulting reducing equivalents are used to create ATP through the electron transport chain and to fix CO_2 via the Calvin cycle to fix. A complete table of the modeled media and uptake constraints are in Supplementary Tables 1-3. All reactions that were added to the base models are listed in Supplementary Table 4-6. Reactions for heterologous pathways or carbon efficient pathways were not included in the augmented model during yield ratio calculations. These were only included individually for additional analyses. Please note genome scale metabolic models are only capable of simulating the biological features that are encoded within the model. Our chosen *S. cerevisiae* and *S.* PCC 7002 models are less developed than the widely accepted *E. coli* model and therefore may not capture all biological features.

Flux balance analysis (FBA) was used to calculate the maximum theoretical yield of specific metabolites under carbon-limited conditions for each augmented model.[59, 62] The yields were calculated for every metabolite within a model. The formulation is shown below where I is the set of all metabolites and J is the set of all reactions. I^{target} is the target metabolite for the current iteration. $S_{(i,j)}$ is the stoichiometric matrix, υ_j is the flux vector, and p_i is a metabolite accumulation rate vector. p_i is constrained to zero for all metabolites besides the metabolite whose yield is being maximized (I^{target}). Biomass generation was either unconstrained or forced to be greater than or equal to 10% of the maximum biomass exchange flux for each substrate. Calculations were

performed for the carbon sources: methane, methanol, glucose, acetate, glycerol (*E. coli* only), and xylose (*E. coli* only).

$$\max_{\upsilon,p} \sum_{i \in I^{target}} p_i \tag{1}$$

$$\sum_{j \in J} S_{i,j} \cdot \upsilon_j = p_i \quad \forall \quad i \in I \tag{2}$$

$$p_i = 0 \quad \forall \quad i \notin I^{target} \tag{3}$$

$$\alpha_j \leq \upsilon_j \leq \beta_j \quad \forall \quad j \in J \tag{4}$$

All models were solved with the assumption that cells could uptake unlimited amounts of O_2 (aerobic conditions) and other inorganic nutrients (metals, phosphate, ammonium, protons, etc.) required for growth and/or to balance metabolism. Carbon uptake was restricted to a maximum of 10 mmol/gDW/hr of each substrate. The *E. coli* model included a term for maintenance energy, which was set to 3.15 mmol/gDW/hr as determined by Orth et al.[60] In the yeast model, we added all augmented reactions to the cytoplasm compartment. The cyanobacterial model (iSYP708) contains a light uptake constraint of zero forcing cells to uptake a single carbon/energy source. These simulations were performed to evaluate the impact of different carbon sources on improving chemical production through a diurnal light/dark cycle.[50]

In order to assess the relative value of feedstocks for producing chemicals, we performed flux balance analysis of three genome-scale metabolic models augmented with reactions required for assimilating C1 substrates. We compared the maximum theoretical yield of each metabolite from alternative carbon sources – methane, methanol, and acetate – to the corresponding yield on glucose (Figure 9a-c). In each case, there was a strong correlation with a high R^2 value for a linear regression through the origin. In subsequent analyses, we used the slope of the regression to represent the ratio of theoretical yield of chemicals from each feedstock and organism. Among the feedstocks, glucose

gave the highest theoretical yield followed by acetate, methanol, and methane, consistent with the number of carbons in each feedstock. Interestingly, methane, which is more reduced than methanol, has lower yields. This can be explained by the high cost of activating the C-H bond in methane, which requires a reducing equivalent. This investment is not recovered in the net exothermic reaction of methane conversion to methanol. When normalized by carbon number in the feedstock (Figure 9d) the curves collapse and show interesting differences in slope depending on the organism. For *E. coli*, these curves collapse with $YR_{methanol} > YR_{methane} \approx YR_{glucose} > YR_{acetate}$. For *S. cerevisiae*, these curves collapse with $YR_{methanol} \approx YR_{glucose} > YR_{acetate} \approx YR_{methane}$. For *S.* PCC 7002, these curves collapse with $YR_{methanol} \approx YR_{methane} > YR_{acetate} > YR_{glucose}$. Figure 12 summarizes the ratios of theoretical yield.

Both methanol and glycerol had higher carbon yields than glucose for *E. coli* while only methanol had a higher carbon yield for *S. cerevisiae* (Figure 9d and Figure 12). For *S.* PCC 7002: methane, methanol, and acetate all had higher carbon yields than glucose, which suggests *S.* PCC 7002 may not utilize glucose as efficiently. The maximum P/O ratios for each metabolic model was calculated (Figure 75). The *E. coli* model had a higher P/O value (1.375) than the *S. cerevisiae* model (1.125), which could explain why maximum yields for some compounds were higher in *E. coli* than *S. cerevisiae*. *S.* PCC 7002 had the highest P/O ratio at 2.5; however, this is based on genome annotations and should be confirmed experimentally.

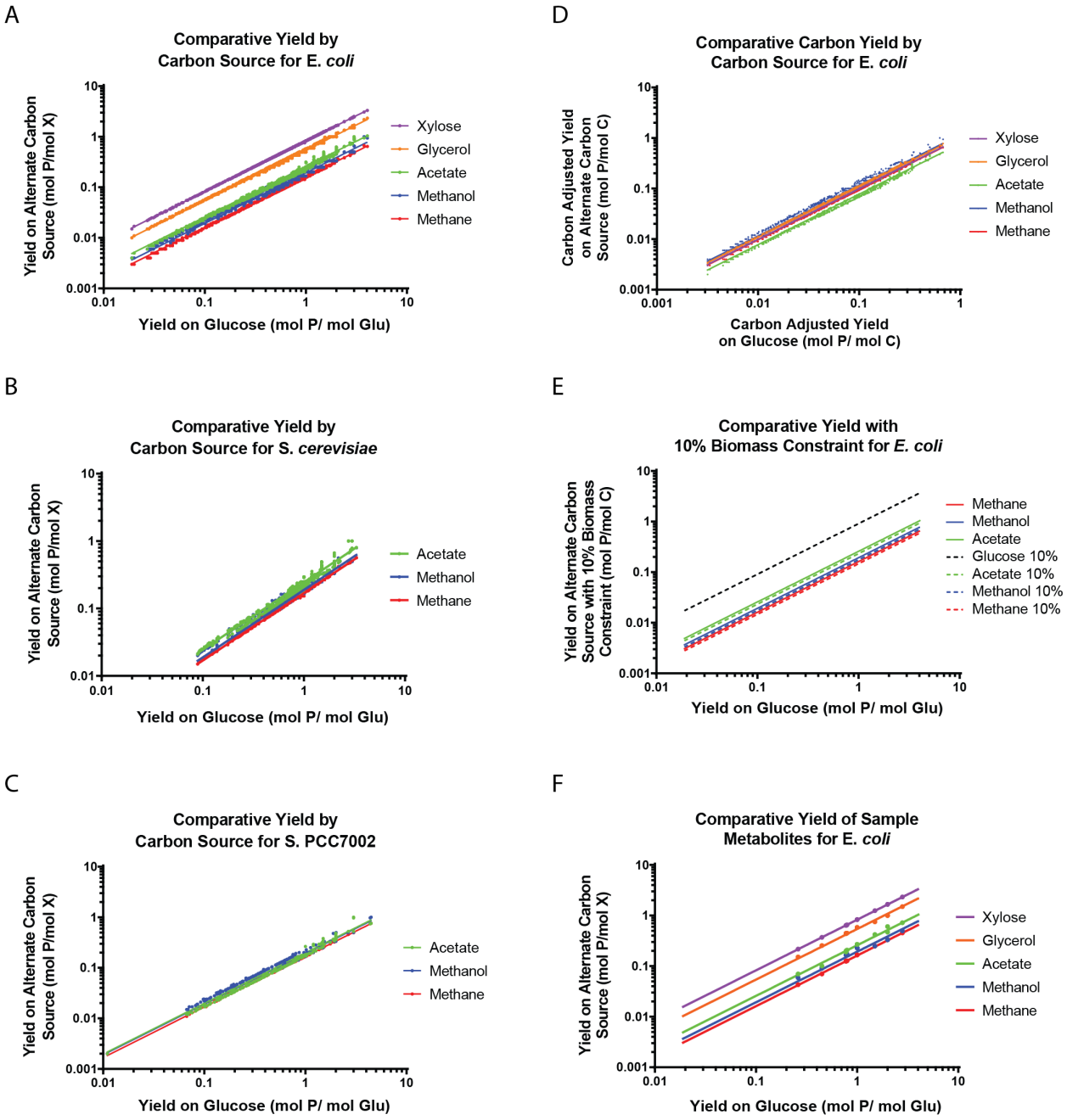

Figure 9: Summary of the yield ratio data calculated using flux balance analysis. Panel A shows the yield of each metabolite in the *E. coli* genome-scale metabolic model on glucose and on the alternate substrates methane, methanol, acetate, glycerol, and xylose as well as the linear regression that define the yield ratio for each alternate carbon source. Panel B shows the yield of each metabolite in the *S. cerevisiae* genome-scale metabolic model on glucose and on the alternate substrates methane, methanol, and acetate as well as the linear regression that define the yield ratio for each alternate carbon source. Panel B shows the yield of each metabolite in the *S.* PCC 7002 genome-scale metabolic model on glucose and on the alternate substrates methane, methanol, and acetate as well as the linear regression that define the yield ratio for each alternate carbon source. Panel D uses the same data from panel A, but compares the yields on a per carbon basis. This collapses the different yield ratios onto a much tighter set of lines. Panel E shows the yield ratio lines from Panel A as well as the lines from a set of FBA simulations requiring 10% of maximum biomass production. This shows that our results are not an artifact of having no biomass requirement given the small change. Panel F shows the yield ratio lines from Panel A with a selected subset of metabolites

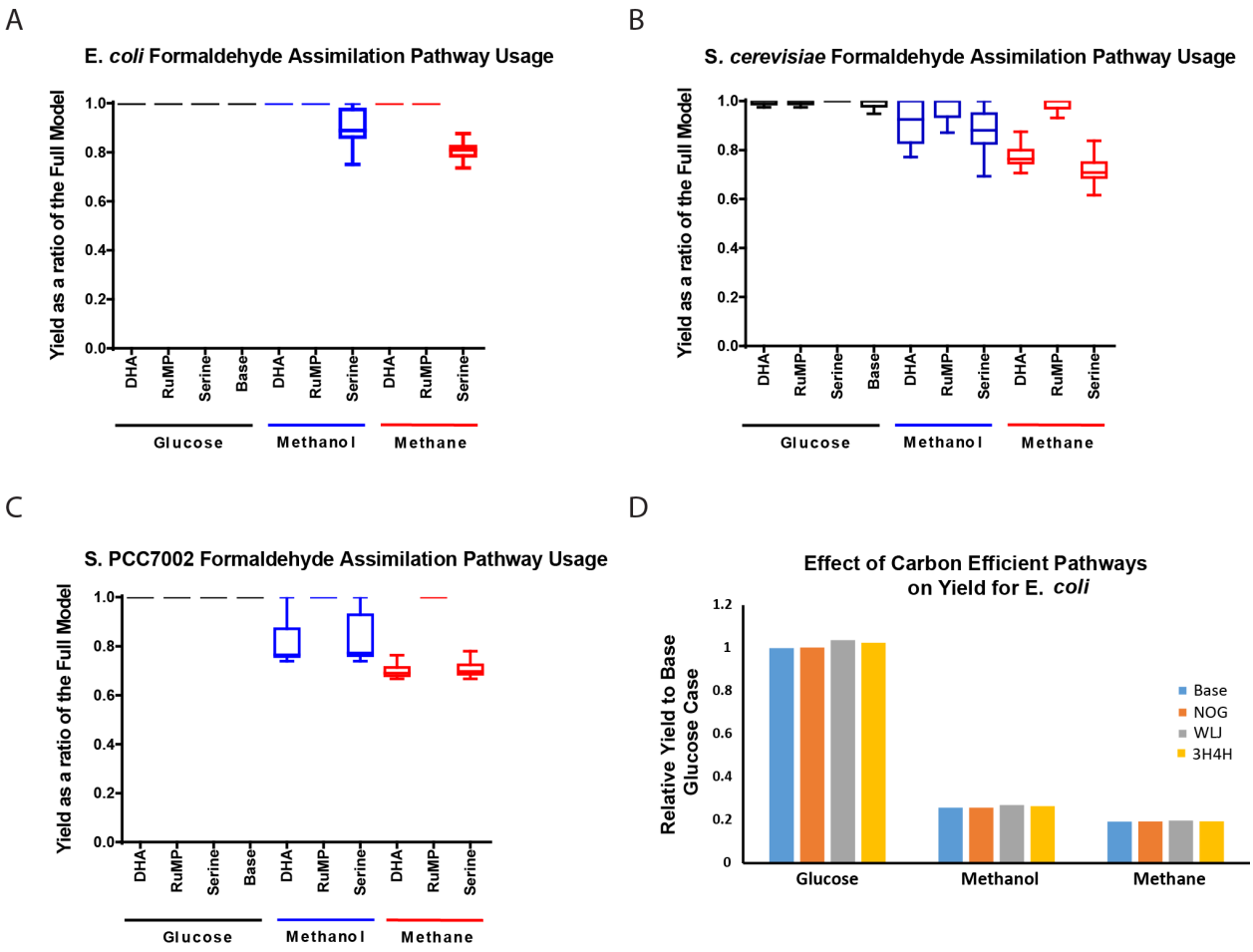

Figure 10: Panels A, B, and C show changes in the distribution of product yields when using single formaldehyde assimilation pathways instead of all three simultaneously under different media conditions for *E. coli*, *S. cerevisiae*, and *S.* PCC 7002, respectively. Panel D shows how the addition of carbon efficient pathways has little effect on product yields.

Economic analysis using yield ratios

To evaluate each feedstock, we calculated the relative feedstock costs for producing one mole of each metabolite in the metabolic models. Dividing the molar price of each feedstock by the theoretical yield of that feedstock yields the individual feedstock cost. Here, we used the equation below to calculate an average relative feedstock cost (RC) between glucose and an alternate carbon source. YR represents ratio of theoretical yields (molar yield on the alternative carbon source divided by molar yield on glucose), P_a is the molar price of the alternate carbon source, and P_g is the molar price of glucose. YR is estimated by a linear regression through the origin between the molar yields of each metabolite when produced using glucose and the alternative carbon source. The sensitivity of the relative feedstock cost was calculated by varying feedstock prices and creating a surface for visualization.

$$RC = \frac{P_a}{P_g} * \frac{1}{YR} \tag{5}$$

Molar yields indicate that glucose is the preferred feedstock for biological chemical production, but on a per carbon basis, other feedstocks are more efficient. To evaluate the relative costs of different feedstocks, we created relative cost surfaces using estimated ranges of feedstock prices and the ratios of theoretical yield calculated from FBA. We used bulk purchase pricing and stock market values (specifically, natural gas and sugar prices) over a 5-year period to determine each carbon source's range of bulk purchase prices. We estimate that sugar prices are currently between \$0.10 and \$0.30/lb (\$0.0264/mol to \$0.0792/mol), methanol prices are between \$1.00-1.60/gal (\$0.01068/mol to \$0.01709/mol), and methane prices are between \$2.75-\$4.50/MMBTU (\$0.0022/mol to \$0.0036/mol). It was more difficult to determine an estimate for acetate prices. Acetate comes in multiple forms and could be made commercially via a Bio-GTL process, which has not been economically analyzed in the public literature. Using bulk pricing for both sodium acetate and acetic acid, we calculated the highest price that we used (approximately \$0.50/kg, or

$0.03/mol). Acetate production from syngas in Bio-GTL processes could have very high yield and therefore be less expensive.[32] Therefore, we used a high molar conversion of syngas to acetate with a low cost of syngas to represent the lower bound on price ($0.05/kg, or $0.003/mol). This range is a best estimate and more information could adjust this range further.

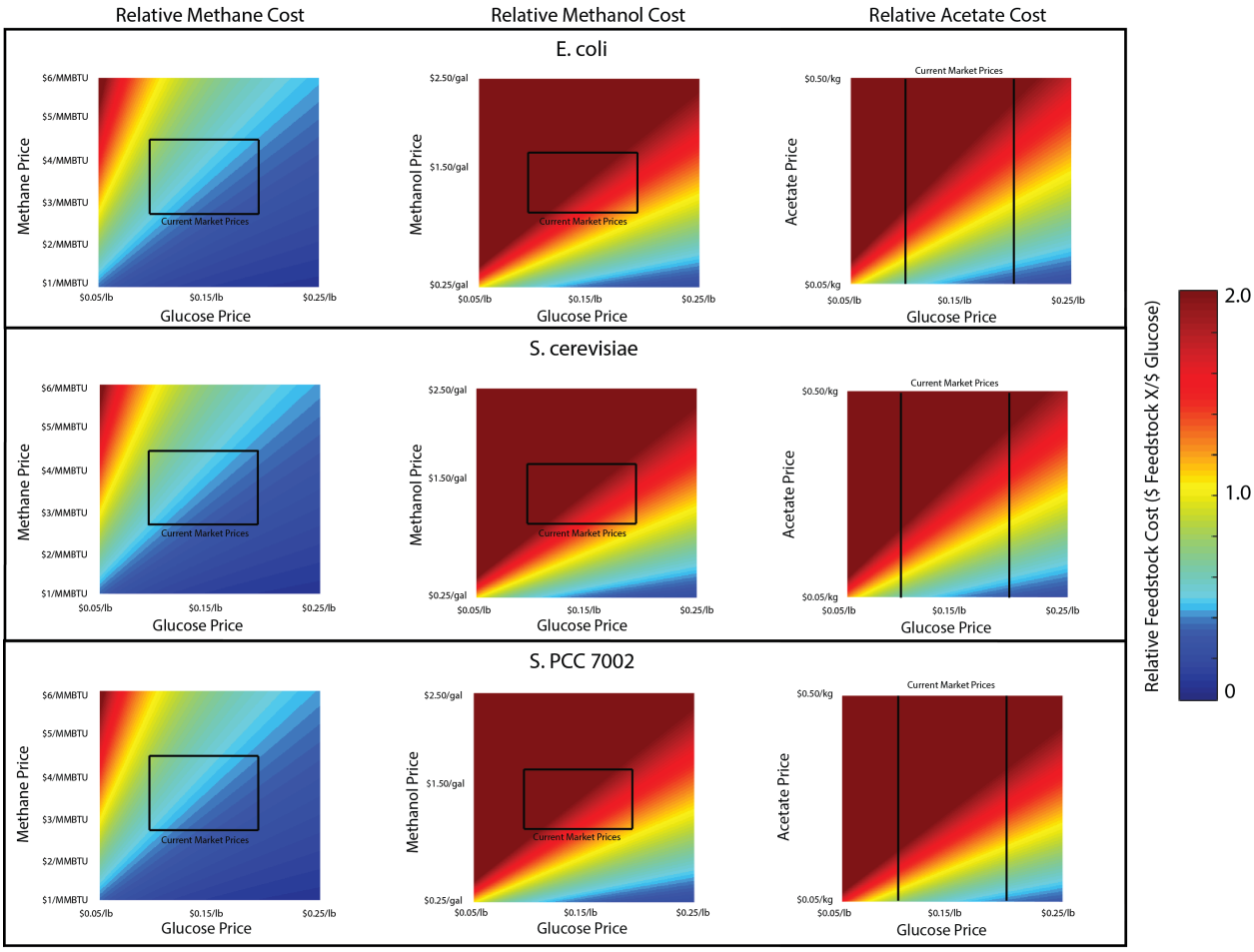

Figure 11: This figure shows the relative cost of switching from glucose to an alternate feedstock across a number of scenarios. Cool colors represent lower cost for switching and warm colors represent higher cost from switching. The top row describes the results in *E. coli*, the second row describes the results in *S. cerevisiae*, and the third row describes the results in *S.* PCC 7002. The left column is the cost for switching to methane, the center column is the cost for switching to methanol, and the last column is the cost for switching to acetate. The black boxes represent the current range of market prices for each feedstock. The horizontal axis of each graph represents increasing glucose price and the vertical axis represents increasing alternate carbon source price.

Relative cost surfaces were constructed by plotting the relative feedstock cost of metabolites in

an organism's genome-scale model (Figure 11). The sliding color scheme represents the regions where the alternative carbon source is more expensive than glucose (red) for producing the average chemical, less expensive than glucose (blue), or equivalent (yellow). The surfaces showed little variation between three organisms studied, with glucose having a slightly bigger economic advantage in yeast. The surfaces show that methane is the only feedstock that is consistently less expensive than glucose at current feedstock prices. Conversely, methanol is more expensive than glucose as a feedstock over the range of current prices. The large uncertainty in acetate prices prevents a general statement, but low acetate prices have the potential to be a less expensive feedstock than glucose, albeit still more expensive than methane.

Conclusions

Our analysis, based on feedstock price and theoretical conversion yields, suggests that methane is the most attractive feedstock for microbial cell factories. This assumes that technical barriers to using methane can be overcome. For instance, biological assimilation kinetics of methane tend to be relatively slow and are a rate-limiting step in methane conversion to value-added chemicals. The main cause of the slow kinetics is the long turnover time of the methane monooxygenase active site.[34] The reactivation of the active site is a slow process that results in an overall low methane assimilation rate. With protein engineering, it could be possible to overcome this barrier. There are also difficulties in scaling-up microbial production using a methane feedstock. Methane assimilation pathways require both methane and oxygen supply for effective function. This combination of gases can be explosive, which introduces a safety concern when using industrial-size reactors. Another difficulty is the slow mass transfer of methane into aqueous solutions (Conrado and Gonzalez, 2014). If these barriers are overcome, methane has the potential to be a more profitable feedstock than glucose.

A caveat to this analysis is that it only considers feedstock costs and does not consider differences in other costs associated with these feedstocks, such as operating costs, capital costs, conversion inefficiencies (i.e. operating at a fraction of theoretical yield), separations, wastes, etc. A true measure of profitability will require a more detailed technoeconomic analysis of any potential process. For instance, if a technological advance in methane-to-methanol catalytic conversion occurs, the price of methanol could drop considerably and make methanol more competitive with glucose. Methanol provides other technical advantages over methane such as faster mass transfer, faster uptake rate, simplified gassing, and reduced safety concerns that our feedstock analysis does not consider. However, considering current prices, it is clear that methane is the preferred feedstock.

If we are unable to engineer microbes for efficient methane assimilation for chemical production (i.e. achieve yields approaching theoretical limits), the more attractive strategy would be to convert methane to acetate (via syngas) instead of converting methane to methanol. The price of acetate is

a large uncertainty in our analysis, but new BIO-GTL technologies that leverage less-expensive, nitrogen-containing syngas could make the lower end of our estimate range a reality. Assuming a low-cost bio-GTL process works at industrial scale, then acetate would compete with glucose as a feedstock.

Our analysis shows a consistent trend when comparing theoretical yields on different feedstocks, suggesting that a general relationship is derivable. This trend is interesting because it suggests that product yield varies with carbon source identity independent of the specific product (i.e. products have similar relative yields on different carbon sources). We postulate that this linear relationship is obtained because of the structure of metabolism in which catabolic and anabolic pathways are linked by common central metabolites. In other words, all of the substrates we simulated connect to central metabolism through the catabolic pathways described in the introduction, in the process generating NAD(P)H and ATP to varying extents depending on the substrate. Conversely, all products (except those metabolites found in the catabolic pathways) are produced from the same anabolic pathways independent of carbon source. Therefore the difference in a product's yield on different carbon sources can be traced to the difference in NAD(P)H/ATP produced via the catabolic pathways used to convert carbon sources into precursors for that product.

Thermodynamics could provide a possible explanation for the linear relationship between product yields on different feedstocks. A thermodynamic estimate of the maximum theoretical product yield from a specific substrate can be calculated using the carbon number and degree of reduction of both the substrate and product.[21] This is calculated using the equation below, where f_{max} is the number of moles of product that can be made from 1 mole of substrate, w and j are the number of carbon atoms in the substrate and product and γ_s and γ_p are the degree of reduction of substrate and product, respectively.[21]

$$f_{max} = \frac{w\gamma_s}{j\gamma_p} \tag{6}$$

For a given product, j and γ_p will remain constant when comparing different substrates, while w and γ_s will be unique to the substrate used. This allows for a comparison between maximum theoretical yields of different substrates on a thermodynamic basis. The numerator of the above equation is 8 for methane, 6 for methanol, 8 for acetate, and 24 for glucose. This implies yields from glucose will be 3 times higher than from methane or acetate and 4 times higher than yields from methanol. When normalized for carbon content, methane generates a theoretical yield twice that of glucose. In our analysis, when yields were normalized to the carbon number in the feedstock, the largest difference between feedstocks was significantly less than 2 (Figure 9). Therefore, the degree of reduction is not completely responsible for remaining difference in yields on various feedstocks. One reason for the discrepancy is the requirement of additional electrons and energy in the specific biological pathways (e.g. MMO) used to conduct the transformations. For this reason, analysis using genome-scale metabolic models is an improvement over analysis using just stoichiometry.

	Substrate	Ratio of Theoretical Yield	R_0^2
E. coli Yield Ratio	Methane	0.162 ± 0.0002	0.9989
	Methanol	0.193 ± 0.0009	0.9811
	Acetate	0.258 ± 0.0009	0.9881
	Glycerol	0.542 ± 0.0011	0.9962
	Xylose	0.827 ± 0.0002	0.9999
E. coli Carbon Adjusted Yield Ratios	Methane	0.970 ± 0.0010	0.9989
	Methanol	1.157 ± 0.0051	0.9811
	Acetate	0.775 ± 0.0027	0.9881
	Glycerol	1.083 ± 0.0022	0.9962
	Xylose	0.992 ± 0.0002	0.9999
E. coli 10% Biomass Constraint Yield Ratios	Methane	0.147 ± 0.0002	0.9979
	Methanol	0.176 ± 0.0008	0.9818
	Acetate	0.233 ± 0.0008	0.9873
	Glucose	0.913 ± 0.0005	0.9997
S. cerevisiae Yield Ratios	Methane	0.169 ± 0.0002	0.9992
	Methanol	0.188 ± 0.0009	0.9835
	Acetate	0.244 ± 0.0017	0.9691
S. cerevisiae Carbon Adjusted Yield Ratios	Methane	1.015 ± 0.0011	0.9992
	Methanol	1.130 ± 0.0056	0.9835
	Acetate	0.732 ± 0.0050	0.9691
S. PCC7002 Yield Ratios	Methane	0.168 ± 0.0001	0.9999
	Methanol	0.191 ± 0.0015	0.9804
	Acetate	0.198 ± 0.0023	0.9554
S. PCC7002 Carbon Adjusted Yield Ratios	Methane	1.010 ± 0.0006	0.9999
	Methanol	1.146 ± 0.0088	0.9804
	Acetate	0.593 ± 0.0069	0.9554

Figure 12: A table describing the calculated linear regressions through the origin for each yield ratio.

	E. coli					
	Glucose	Xylose	Glycerol	Acetate	Methanol	Methane
Glycine	2.804	2.326	1.5	0.72	0.5	0.456
Leucine	0.778	0.639	0.439	0.202	0.167	0.126
Lysine	0.776	0.638	0.448	0.191	0.167	0.125
Serine	2	1.667	1	0.472	0.333	0.333
Tryptophan	0.449	0.371	0.255	0.101	0.091	0.07
Pyruvate	2	1.667	1	0.607	0.333	0.333
Succinate	1.5	1.25	0.75	0.423	0.25	0.25
Hexadecanoate	0.261	0.217	0.152	0.07	0.059	0.043
Butanol*	1	0.833	0.583	0.271	0.229	0.167
3-methylbutanol*	0.796	0.654	0.449	0.208	0.174	0.127
Isobutanol*	1	0.833	0.583	0.269	0.229	0.167

Figure 13: Quantitative maximum theoretical yields for a selected set of metabolites in *E. coli*.

	S. cerevisiae			
	Glucose	Acetate	Methanol	Methane
Glycine	3	0.784	0.5	0.5
Leucine	0.753	0.175	0.163	0.132
Lysine	0.708	0.179	0.165	0.127
Serine	2	0.43	0.333	0.333
Tryptophan	0.426	0.087	0.091	0.073
Pyruvate	2	0.5	0.333	0.333
Succinate	1.5	0.386	0.25	0.25
Hexadecanoate	0.212	0.055	0.052	0.037
Butanol*	1	0.264	0.237	0.167
3-methylbutanol*	0.776	0.178	0.163	0.132
Isobutanol*	1	0.224	0.214	0.167

Figure 14: Quantitative maximum theoretical yields for a selected set of metabolites in *S. cerevisiae*.

	S. PCC7002			
	Glucose	Acetate	Methanol	Methane
Glycine	0.79	0.134	0.176	0.134
Leucine	0.508	0.086	0.114	0.086
Lysine	0.099	0.019	0.024	0.017
Serine	0.752	0.128	0.168	0.128
Tryptophan	0.26	0.044	0.058	0.044
Pyruvate	2	0.405	0.333	0.333
Succinate	1.474	0.32	0.25	0.25
Hexadecanoate	N/A	N/A	N/A	N/A
Butanol*	1	0.286	0.243	0.167
3-methylbutanol*	0.8	0.158	0.184	0.133
Isobutanol*	1	0.182	0.238	0.167

Figure 15: Quantitative maximum theoretical yields for a selected set of metabolites in *S.* PCC 7002.

Chapter 4: Metabolic engineering of cyanobacteria for glycogen production

Introduction

Third generation biofuels use algal biomass as a feedstock for the production of biofuels.[2] This can be further generalized as the use of algal biomass for the production of any value-added chemicals. This work focuses on improving the production of easily extracted sugars using the cyanobacteria *Synechococcus sp. strain* PCC 7002. The cyanobacterial biomass could then be hydrolyzed using the same methods applied to corn to produce readily bio-available sugars in high abundance.[69] Cyanobacteria are attractive for sugar production because they have much higher biomass productivities than terrestrial plants, no arable land requirements, and the ability to use wastewater for growth.[82] When compared to production of second generation biofuels, algal biomass may have fewer toxic components to inhibit downstream heterotrophic growth. These advantages drive down the cost of cyanobacterial sugar production and open the door to algal biomass feedstocks for industrial bioprocesses.

The primary strategy we will focus on is the production of intracellular glycogen. This is naturally accumulated as energy storage in many cyanobacteria under a variety of nutrient limited conditions as well as energy storage to survive during the dark cycle.[92] This accumulation is triggered by nitrogen depletion and can give very high intracellular glycogen content in wild-type *S.* PCC 7002 under continuous light conditions.[1] Under diurnal conditions, glycogen is produced during the light cycle and consumed for energy during the dark cycle (Figure 16).

The production of glycogen occurs only under light exposure. The Calvin cycle and light reactions are used to capture carbon and produce energy.[66] The carbon enters central metabolism

[2]The work presented in the chapter includes contributions from Dylan Courtney, Dr. Andrew Markley, and Dr. Travis Korosh. Dr. Korosh created the *glgC* knockout strain and Dr. Markley created the *glgC* overexpression strain. The CPF1/Cas12 genomic editing toolbox developed by Dylan Courtney was used to make some of the knockout strains. Dr. Markley designed the original glycogen screen and assisted in initial testing of thew glycogen screen.

in lower glycolysis as 3-phosphoglycerate of glyceraldehyde 3-phosphate and works upwards through gluconeogenesis. Glucose-1-phosphate is converted into ADP-glucose by *glgC* and ADP-glucose is polymerized to glycogen by *glgA*. The structure of glycogen can be further altered by branching and debranching enzymes, *glgB* and *glgX*.[92]

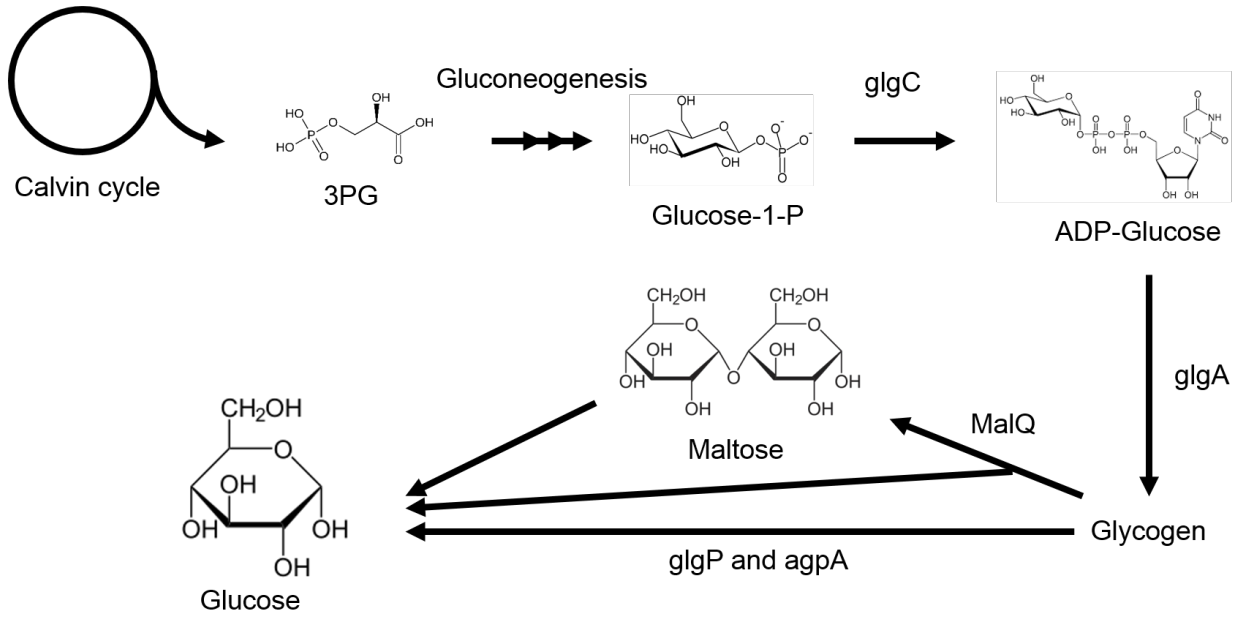

Figure 16: Glycogen is produced from the products of the Calvin-Benson cycle reforming glucose 1-phsohpate though gluconeogenesis and phosphoglucomutase. This is converted to glycogen through *glgC* and *glgA*. Glycogen structure is altered by branching and decranching enzymes, *glgB* and *glgX*. Finally, glycogen can be degraded using linear depolymerases *glgP* and *agpA* as well as the branched chain pathway including *malQ*.

Glycogen catabolism is conducted by the removal of single glucose-1-phosphate monomers by *glgP* and *agpA*, linear glycogen phosphorylases, or the removal of maltotetrose units at branch points by *glgX*, which are further broken down to glucose-1-phosphate monomers. These monomers can be processed for energy through glycolysis and central metabolism during the dark cycle or under other low-energy conditions. Traditionally, a cycle of glycogen production and degradation occurs under natural diurnal light cycles.[92]

First, I will discuss the validation and rigorous testing of previous engineering efforts on *glgC*. Second, I will discuss multiple genetic manipulations performed to attempt and increase glycogen

fraction in growing cells without compromising total biomass titer. I will then discuss a glycogen screen meant to identify mutants with high glycogen content. Finally, I will discuss the efforts in hydrolyzing, analyzing, and growing heterotrophic organisms on cyanobacterial biomass.

Methods

Biomass titer measurements

Biomass titers were estimated in one of two ways. First, we use optical density measurements with light at a wavelength of 730nm. This required sample dilution to within the linear range of the spectrophotometer used. Optical density (OD) measurements will detect both cell biomass and other components that absorb light. This becomes relevant when producing glycogen because OD730 measurements will detect glycogen as well as total cell biomass. Second, Biomass titers were also directly measured through dry cell weight measurements. A pre-weighed conical tube is filled with a recorded volume of cell culture. The conical tube is centrifuged at 5000xg for 20 minutes. The supernatant is vacuum aspirated and the pellet is resuspended in 1 volume of water. Next, the suspension is centrifuged at 5,000xg for 20 minutes and the supernatant is vacuum aspirated. The samples are then flash frozen in liquid nitrogen or frozen overnight in a -80C freezer. Once frozen, the samples are lyopholized and final weights are measured.

Glycogen content and glycogen titer measurements

Glycogen content is measured by extracting glycogen as glucose from lyopholized biomass samples through hydrolysis. A direct biomass titer is calculated using the dry cell weight method described above. Next, 5-20mg of dessicated biomass is added to a 5mL glass reactor. To this, 1mL of 4% sulfuric acid is added. The reactor is sealed with a cap containing a second septa to prevent vapor loss during hydrolysis. The reactors are placed in a silicon oil bath at 121°C for 1 hour and then cooled in an ice water bath for 20 minutes. Samples are transferred into 1.7mL microfuge

tubes, centrifuged for 10 minutes at 20,000xg, filtered through a 0.22um filter, and stored at -20C until analysis. This is based on the biomass hydrolysis process used by NREL.[69]

Glucose concentration of the hydrolyzed sample is measured using HPLC. A 5mM sulfuric acid mobile phase is used with a Rezek ROA-Organic Acid column. Samples are measured for 25 minutes using a refractive index detector detector and compared to a prepared standard curve.

Cyanobacterial culturing

Cyanobacterial cultures were grown in 60mL of Media A in a 250mL baffled flask unless otherwise specified. Typically, cultures were grown under continuous light provided by LED strips in a shaking incubator. The incubator is heated to 27°C unless otherwise specified and has a constant carbon dioxide concentration of 1%. Each time a biomass titer is measured through direct sampling, the cultures are first weighed and water is added to adjust for volume loss due to evaporation. In the case where cultures are grown diurnally, the cultures are grown at 27°C in the shaking incubator with a diurnal cycle programmed into an 8-cycle controller. The controller is programmed by setting the length of time and light intensity for each of the 8 segments of the controller scheme. Light is measured as a percentage of maximum intensity.

Genetic modification of cyanobacteria

Genetic alterations were made using the natural homologous recombination ability and competency of *S.* PCC 7002.[74] Integrations were completed using *E. coli* shuttle vectors with 500bp homology regions to the target integration site. Transformation was performed by adding 1.5ug of plasmid DNA to 1mL of culture grown to OD730 = 0.9-1.0. The cells are exposed to light for 4-24 hours and then 150uL are plated onto media A plates with 1.5% agar. Colonies appear within 4 days. We use the CPF1/Cas12 system for targeted *glgP* and *agpA* knockouts and 2-step selection and counter-selection for all other knockouts. CPF1/Cas12 was delivered by conjugation on an RS1010 plasmid into *S.* PCC 7002.

Bacterial growth curves

E. coli growth in lab media and on hydrolysate is measured using a Tecan M1000 plates reader. A 96-well plate has 150uL of fresh media with culture added to an optical density of 0.05. Plates are incubated in a 37°C shaking incubator with a gas transfer film covering the wells. Samples are taken at 30 or 60 minute intervals to measure optical density.

Flocculation and sedimentation measurements

Flocculation is induced by the addition of calcium hydroxide to reach a target pH. Samples are mixed by inversion for 10 seconds in a 15mL conical tube and placed on a rack with height measurements. Samples are allowed to sediment for 20-90 minutes with time lapse video taking pictures every 30 seconds. Sample height is recorded at each picture and used to calculate a floc size using Stokes law on the fastest velocity recorded.

Overexpression of *glgC* for glycogen accumulation

Our first approach looked to ”push” glycogen biosynthesis through overexpression of the glycogen biosynthesis pathway to improve glycogen accumulation. We hypothesized that the production of ADP-glucose was rate limiting and tested this by overexpressing *glgC*, the gene responsible for glucose 1-phosphate conversion to ADP-glucose. Overexpression of *glgC* is predicted to increased synthesis of ADP-glucose. This faster synthesis rate would allow for increased glycogen accumulation under continuous light conditions, where glycogen degradation does not readily occur. We overexpressed *glgC* by adding a second copy to the genome in the *glpK* locus under the strong IPTG-inducible promoter, cLac143. Cultures were grown with continuous induction of the *glgC* overexpression cassette with 0.1mM IPTG. The Δ*glgC* strain was made using the acrylic acid selection/counter-selection system and confirmed using colony PCR.[6]

glgC overexpression and Δ*glgC* strains under continuous light yield time-dependent results

(Figure 17). We can see that presence of the *glgC* overexpression cassette or knockout introduces a growth defect. The overexpression cassette introduces a mild growth defect whether or not IPTG is present, while the knockout arrests growth after 2 days. During early growth, the *glgC* overexpression strain shows approximately double the glycogen content when compared to either wild-type or the uninduced *glgC* overexpression strain. However, this effect fades over time until, after 4 days, the *glgC* overexpression strain is indistinguishable from the wild-type. The Δ*glgC* strain produces little to no glycogen.

The growth defect decreases the glycogen production potential of the *glgC* overexpression strain. On the other hand, the increased glycogen content early in the experiment implies that *glgC* overexpression could be overcoming a metabolic bottleneck. The disappearance of the increased glycogen content over time is likely caused by the nitrogen starvation effect within the cell inducing high expression of all genes in the glycogen synthesis pathway to a higher degree than the designed *glgC* overexpression cassette. This could also imply that *glgC* is predicted to produce better results. Finally, the lack of glycogen production in the Δ*glgC* strain aligns with expectations and previous results.[80] The small signal present at late time points represents a small amount of glucose present in glycolysis, likely representing the flux to glycogen that is plugged by the *glgC* knockout. Overall, the overexpression of *glgC* alone is not enough to improve glycogen content or titers above wild-type production levels.

To probe the effect of light conditions on titer and productivity as well as effectiveness of genetic manipulations, we probed the same set of strains under diurnal light conditions. We predict glycogen content and biomass productivity to drop when we use diurnal cycling conditions for growth. This is caused by decreased overall light delivery for energy production and carbon uptake. With decreased average volumetric light delivery, the cyanobacteria will grow at a slower rate and be less likely to partition carbon. Further, maximum biomass titers are predicted to decrease. This leaves more nitrogen leftover in the media and decreases the nitrogen starvation phenotype that gives higher glycogen content. We also expect to see the glycogen content vary across night and day

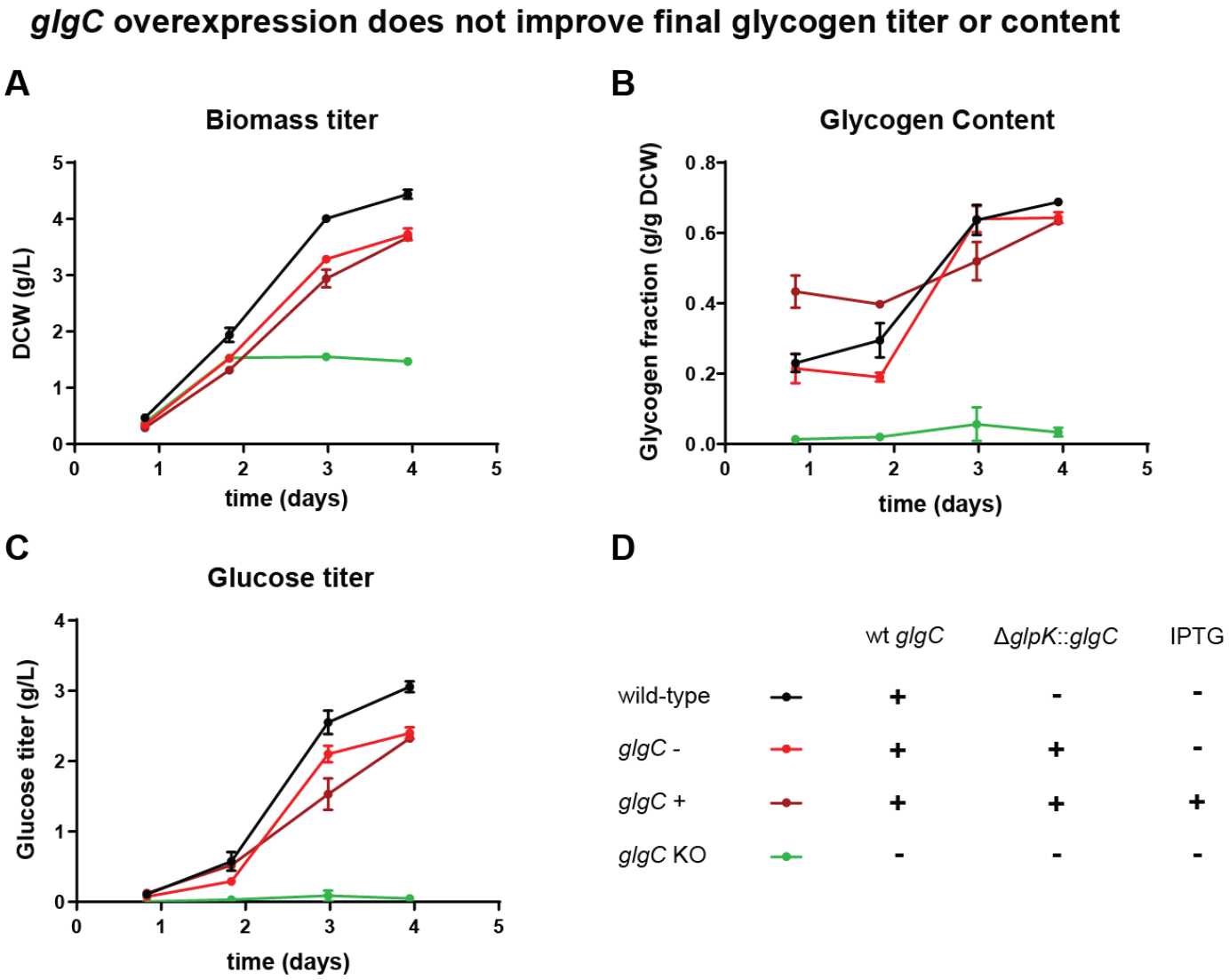

Figure 17: Biomass and glycogen production by *S.* PCC 7002 strains under continuous light conditions in media A. This experiment investigates the value of overexpressing *glgC* in the glycogen biosynthesis pathway. Panel A shows the biomass production measured directly as dry cell weight (DCW). Panel B shows fractional glycogen content measured through biomass hydrolysis. Panel C shows glycogen titer measured as glucose. Panel D describes the genotypes of the strains measured in Panels A-C.

cycles. This is caused by the production and consumption cycles of glycogen that occur to regulate cell growth across light/dark cycles.[63] These cycles should reduce glycogen accumulation and more accurately represent the industrial production potential of the strain. Figure 18 shows the light conditions we used in our diurnal cycle, a 10 hour dark cycle with a 14 hour variable light

cycle that more closely represents outdoor light delivery than simplistic on/off systems.

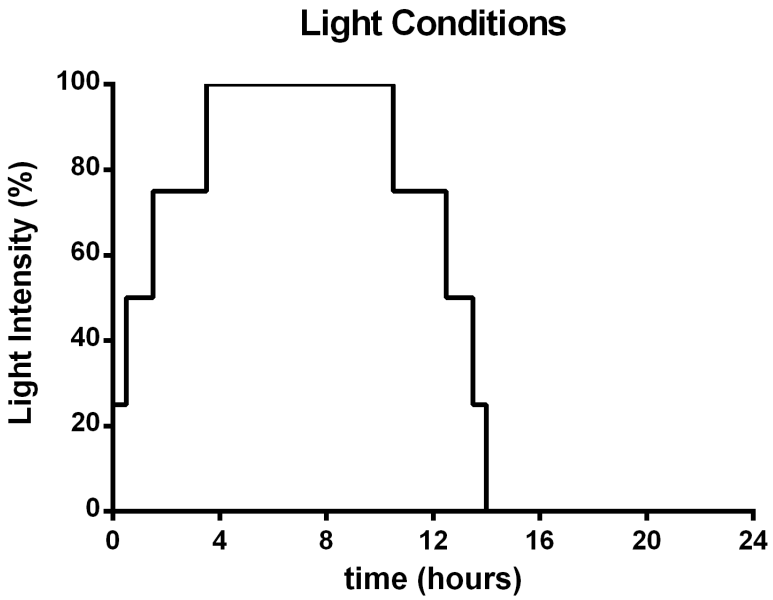

Figure 18: The diurnal light conditions used in all diurnal experiments discussed in this thesis. We programmed an 8-phase controller for light output as a fraction of maximum light output on a 24-hour cycle.

The effect of diurnal growth can be seen in the ”saw-tooth” pattern in panel A of Figure 19. During early growth, the *glgC* overexpression strain had approximately double the glycogen content of both wild-type and the uninduced *glgC* overexpression strain. The difference in glycogen content decreases over time until the strains are not substantially different. The Δ*glgC* strain produces little to no glycogen over the growth period and appears to have arrested growth.

We found the time-dependent increase in glycogen content in the *glgC* overexpression strain was maintained under diurnal conditions compared to continuous light conditions. The arrested growth in the Δ*glgC* strain occurs when the cultures have run out of nitrogen and would normally switch to glycogen production, which increases the optical density. The inability of the Δ*glgC* strain to produce glycogen means that these cultures instead stop increasing in optical density once nitrogen is depleted. Overall, the *glgC* overexpression validation experiments imply that genetic manipulations can influence glycogen content under industrial conditions, although those changes

have yet to shown any late growth impact. This experiment also confirms that glycogen content is lower under diurnal cycling and represents an additional production hurdle to the industrial relevance of cyanobacteria.

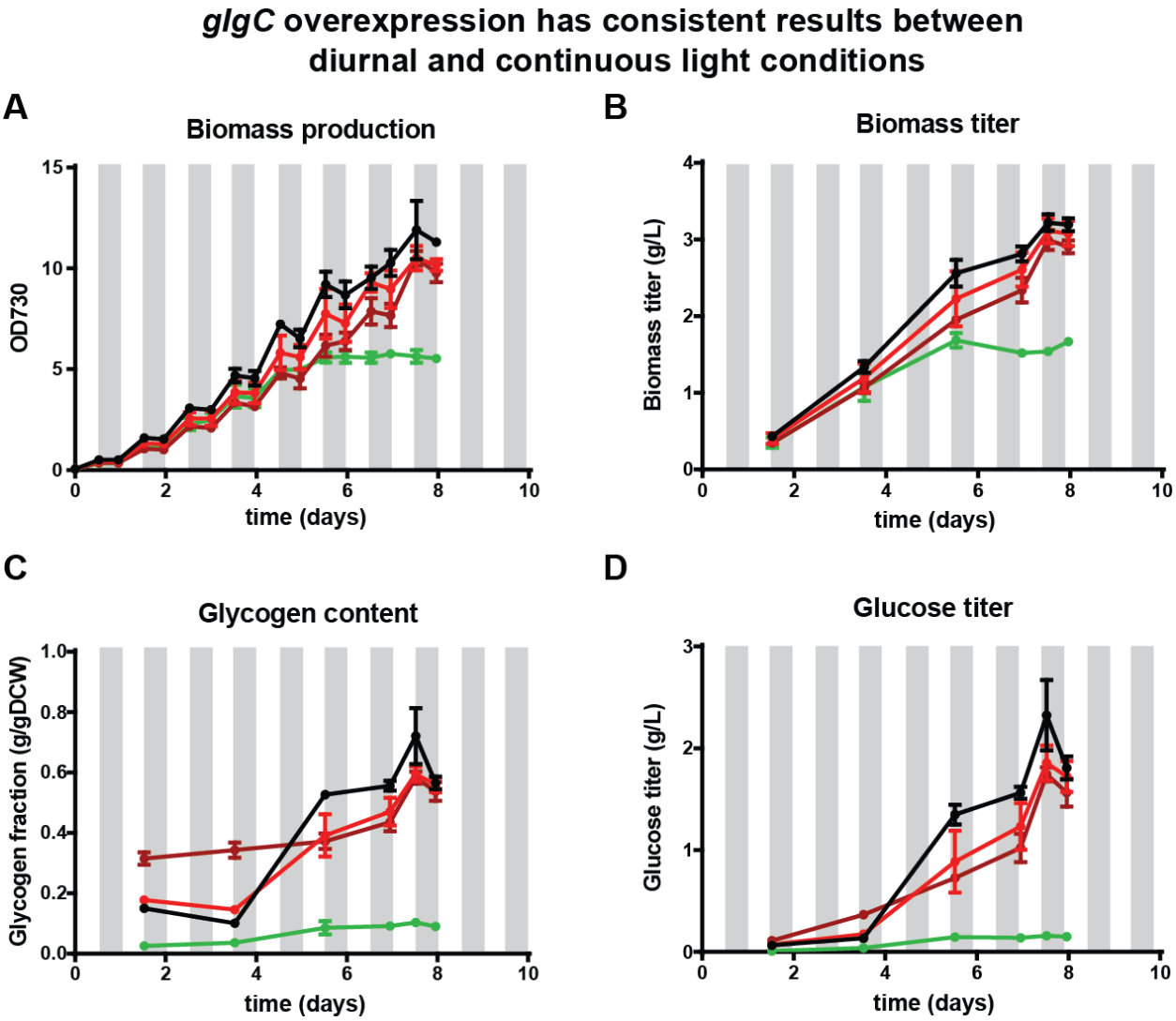

Figure 19: Biomass and glycogen production by *S.* PCC 7002 strains under diurnal light conditions in media A. This experiment investigates the value of overexpressing *glgC* in the glycogen biosynthesis pathway under the more restrictive diurnal light conditions. Panel A shows the biomass production as optical density measured at 730nm. Panel B shows the biomass production measured directly as dry cell weight (DCW). Panel C shows fractional glycogen content measured through biomass hydrolysis. Panel D shows glycogen titer measured as glucose.

Improving glycogen accumulation through deleting glycogen degradation

We then investigated methods to reduce glycogen degradation to increase intracellular accumulation. This approach can harness the power of nitrogen starvation to induce glycogen biosynthesis while increasing accumulation by removing the degradation pathways. We considered three gene knockouts at two key nodes in glycogen metabolism: *malQ*, *glgP*, and *agpA*. *malQ* is responsible for the breakdown of short poly-maltose chains (maltotetrose and maltotriose) down to single maltose units. On the other hand, *glgP* and its isozyme, *agpA*, are responsible for removing terminal glucoses from linear glycogen strands. We created knockouts at these key nodes and measured the resulting changes in glycogen content and titer under different light conditions.

We hypothesize that Δ*malQ* will help increase glycogen accumulation by blocking consumption of glycogen for cellular energy. *malQ* is an intermediate step in the breakdown of branched glycogen chains from 4 glucose units or less in length. These linear branches cannot be broken down further by other depolymerases and are removed as maltotetrose or maltotriose and then broken into glucose monomers. Further, by testing under nitrogen replete conditions, we probe whether glycogen polymerization and depolymerization is a metabolic technique to control energy production using futile cycles. We created the Δ*malQ* strain using a selection/counter-selection approach to create a clean knockout of *malQ* without disrupting the downstream operon.[6] This required removing the majority of the *malQ* gene and leaving a small protein to allow readthrough into the remainder of the operon. This requirement also shows the value of having the genetic tools to create clean genomic knockouts.

The Δ*malQ* strain shows a consistent growth defect compared to wild-type as shown by the decreased biomass titer (Figure 20). Both strains under nitrogen deplete conditions have higher glycogen content than under nitrogen replete conditions. Under nitrogen replete conditions, the Δ*malQ*strain has higher glycogen content than wild-type. Finally, glycogen titer is lower for the Δ*malQ* strain under nitrogen deplete conditions and equal for nitrogen replete conditions.

We considered the Δ*malQ* strain under both nitrogen deplete and nitrogen replete conditions.

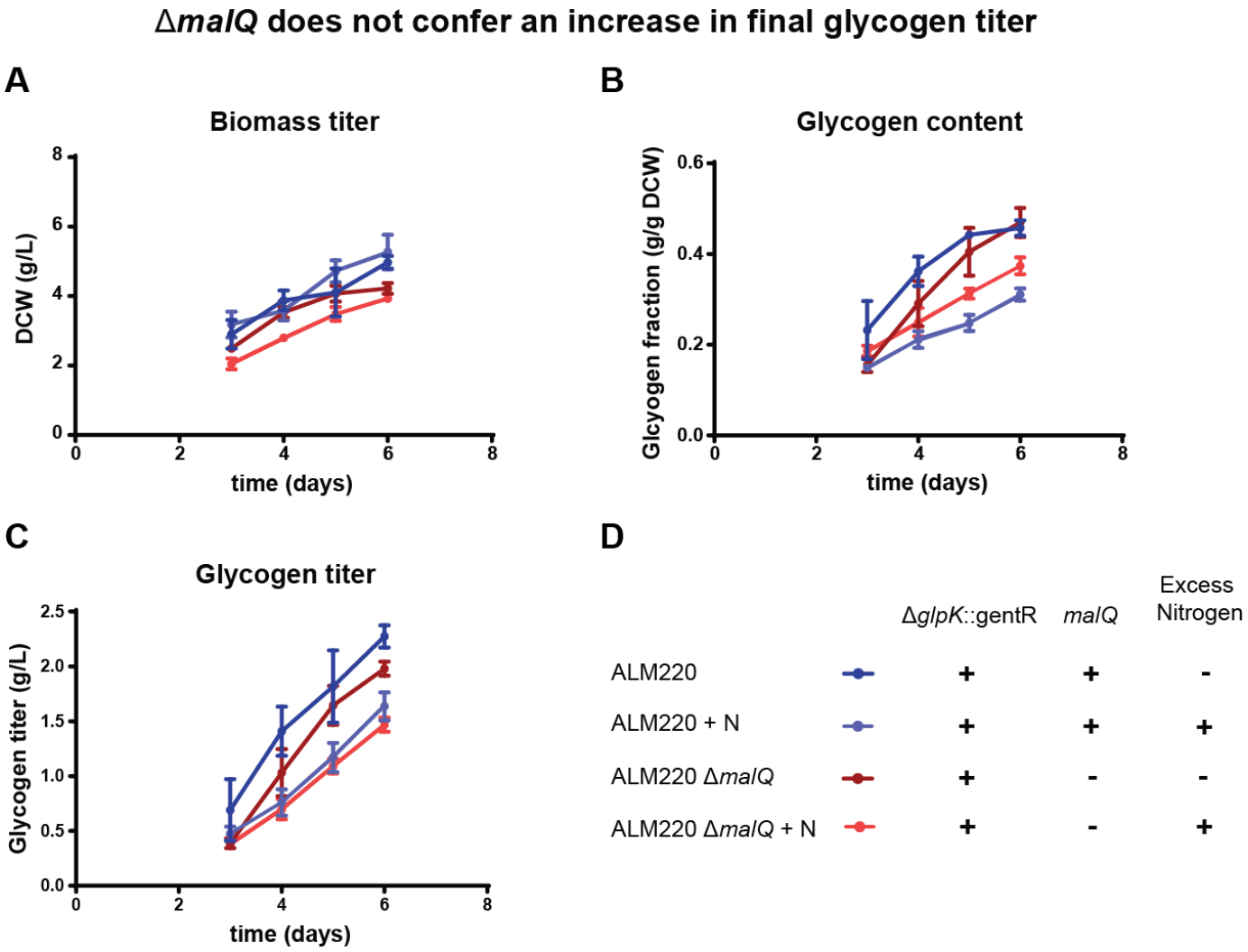

Figure 20: Biomass and glycogen production by *S.* PCC 7002 strains under continuous light conditions in media A. This experiment investigates the value of knocking out *malQ* in the glycogen catabolism pathway under both nitrogen deplete and replete conditions. Panel A shows the biomass production measured directly as dry cell weight (DCW). Panel B shows fractional glycogen content measured through biomass hydrolysis. Panel C shows glycogen titer measured as glucose. Panel D describes the genotypes and media conditions of the strains measured in Panels A-C.

Unfortunately, the Δ*malQ* is shown to have little-to-no effect on glycogen accumulation under the nitrogen starvation condition. We hypothesize that this is due to low pathway flux for glycogen depolymerization along this route. There does appear to be a substantial increase in glycogen content under nitrogen replete conditions compared to wild-type, but this increase in glycogen content is accompanied by a growth defect that results in lower glycogen titers. Unfortunately,

nitrogen replete conditions are unlikely to be industrially relevant for glycogen production. Overall, Δ*malQ* is either detrimental or non-impactful to glycogen accumulation.

We also considered the combined effect of a *malQ* knockout with the overexpression of *glgC*. Δ*malQ* might help to enhance the early effect of *glgC* overexpression by avoiding glycogen degradation. These genetic modifications were combined by knocking out the *malQ* gene in conjuction with the replacement of *glpK* by either an antibiotic marker or the *glgC* overexpression cassette.

The results in Figure 21 show that only the Δ*malQ* strain without *glgC* overexpression is the only strain with a growth defect. Amongst all 4 strains, there is little variation in glyocgen content and only the Δ*malQ* strain shows a decrease in glycogen titer.

The combination of these two genetic alterations appears to recover the growth defect seen in the *malQ* knockout strain alone. The total glycogen titer in the combined *malQ* knockout and *glgC* overexpression strain returns to matching the glycogen titer of wild-type cultures. This combined effect implies that combining *glgC* overexpression with genetic alterations that reduce glycogen breakdown may improve glycogen accumulation. Unfortunately, the combined *malQ* knockout and *glgC* overexpression strain does not provide a glycogen accumulation benefit over wild-type.

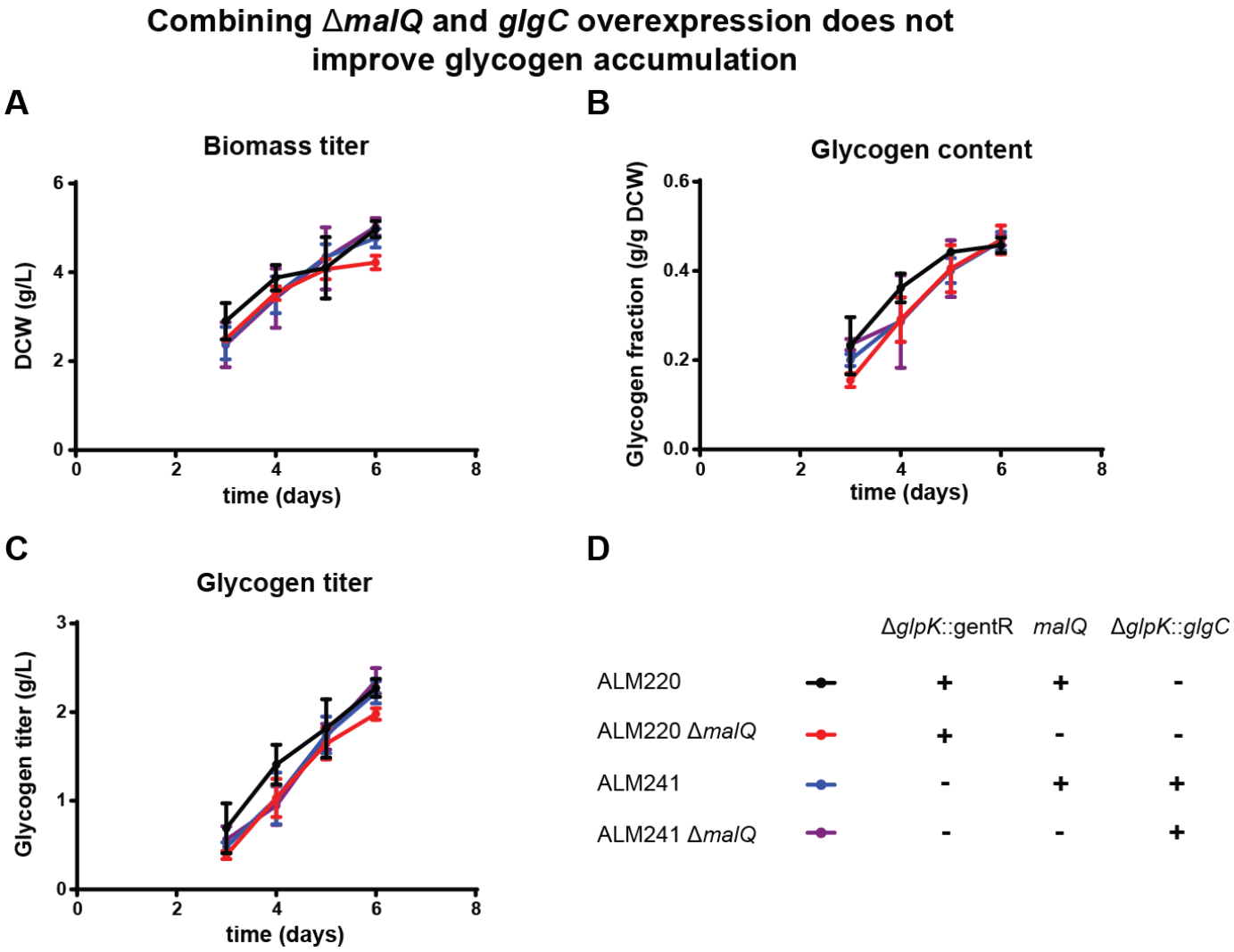

Figure 21: Biomass and glycogen production by *S.* PCC 7002 strains under continuous light conditions in media A. This experiment investigates the value of overexpressing *glgC* in the glycogen biosynthesis pathway in the context of knocking out *malQ* in the glycogen catabolism ptahway. Panel A shows the biomass production measured directly as dry cell weight (DCW). Panel B shows fractional glycogen content measured through biomass hydrolysis. Panel C shows glycogen titer measured as glucose. Panel D describes the genotypes of the strains measured in Panels A-C.

We hypothesize that the linear depolymerases have a greater effect on glycogen breakdown than *malQ* in *S.* PCC 7002. We probed the effect of knocking out the linear glycogen phosphorylase *glgP* and its isozyme, *agpA*. These phosphorylases remove terminal glucose monomers from linear chains of glycogen longer than 4 units.[92] Removing these phosphorylases should lead to enhanced accumulation of glycogen by reducing the breakdown of glycogen during growth. We expect this effect, like that of *malQ*, to be enhanced under diurnal conditions.

Under continuous light conditions, the single glycogen phosphorylase knockouts decrease the total biomass titer, and the double knockout has similar biomass titer to wild-type (Figure 22). The different strains show no variation in glycogen content. The glycogen titer of the single knockout mutants are lower than either wild-type or the double knockout, but this decrease is caused by the decrease in biomass production.

These results are not surprising given that cells grown under continuous light and low nitrogen conditions should only need to make glycogen, not break it down for consumption. This does make it less likely that glycogen biosynthesis and degradation pathways are used to manage excess energy in the cell during growth. Additionally, the accumulation of glycogen is dependent primarily on glycogen production from the light reactions. This will not vary greatly between these strains because the glycogen production pathway has not been altered. Overall, knocking out the glycogen phosphorylases *glgP* and *agpA* does not have a substantial effect on glycogen accumulation under continuous light conditions.

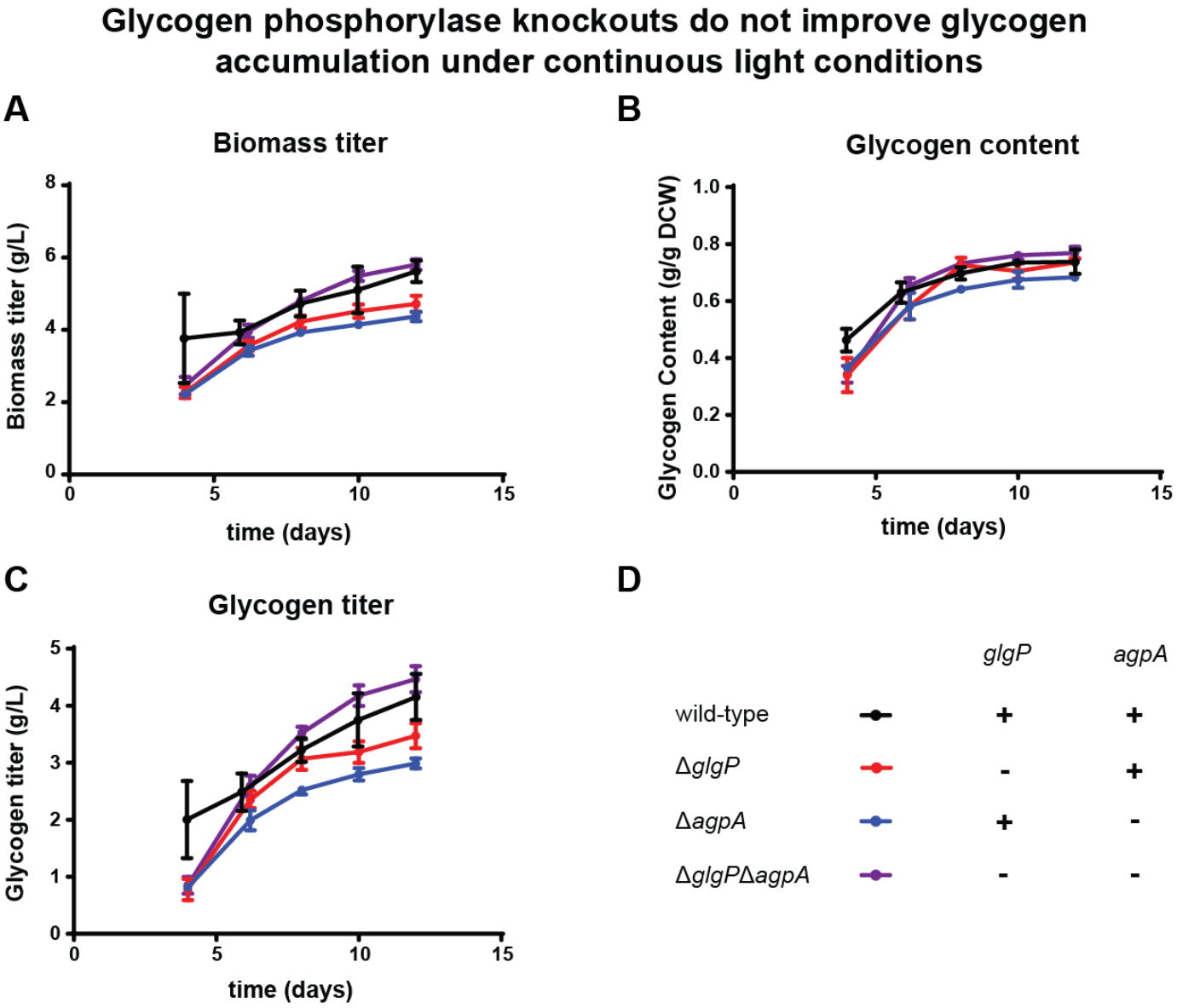

Figure 22: Biomass and glycogen production by *S.* PCC 7002 strains under continuous light conditions in media A. This experiment investigates the value of knocking out linear glycogen phosphorylases in the glycogen catabolism pathway. Panel A shows the biomass production measured directly as dry cell weight (DCW). Panel B shows fractional glycogen content measured through biomass hydrolysis. Panel C shows glycogen titer measured as glucose. Panel D describes the genotypes of the strains measured in Panels A-C.

We hypothesize that the inability to break down glycogen during the night cycle should increase overall glycogen accumulation compared to wild-type. It is possible that inhibiting the use of glycogen as an energy source during the night will induce a growth defect because the cells rely on the energy from glycogen to survive without light. This may be mitigated through use of alternate storage molecules besides glycogen, of which *S.* PCC 7002 has multiple.[90] These alternate storage molecules comprise much smaller energy or nitrogen reserves.

Under diurnal conditions, both the Δ*glgP*and the double knockout strains have higher biomass production than wild-type. All three knockout strains show a marginal glycogen content improvement over wild-type, which results in a 20% increase in glycogen titer for both the Δ*glgP* and the Δ*glgP*Δ*agpA* strains.

Knocking out glycogen depolymerases under diurnal light conditions has a stronger effect than in continuous light conditions (Figure 23). Both the Δ*glgP* and double knockout strains appear to increase glycogen accumulation compared to diurnally grown wild-type cells. Further, this increase can recover a majority of the glycogen titer lost when growing in diurnal conditions compared to continuous light conditions. This makes sense given that glycogen accumulation under diurnal conditions is dependent on both glycogen production and consumption because cells must consume glycogen for energy during the dark cycle. When the linear glycogen phosphorylases are knocked out, the cells cannot degrade glycogen for consumption and thus can accumulate higher net levels of glycogen. Further, the branched glycogen breakdown pathway is unlikely to be accessible because it requires that branch points only have a few monomers polymerized. The lack of linear depolymerases effectively eliminates cellular access to glycogen. The Δ*glgP* strain improves the industrial potential of cyanobacteria as a glucose source by improving glycogen titers under diurnal conditions by 20%. The Δ*agpA* strain shows no impact on glycogen accumulation either alone or simultaneously with Δ*glgP*. This implies that *agpA* either does not have glycogen phosphorylase activity, or works much less effectively than *glgP*.

It is also interesting to now that the increase in biomass titer is made up of additional glycogen

production (panels E and F of Figure 23). The titer of productive biomass is the same as cultures grown in continuous light. This implies that glycogen production occurs under nitrogen limitation until the glycogen and productive biomass absorb all of the light entering the culture. This association implies that careful control over the nitrogen content of a culture would give additional control over the final glycogen content within the culture. Both the productivity and total biomass titer are affected by total light delivery and the glycogen productivity will be affected by the total productive biomass produced from the nitrogen supplied to the culture. It is possible that a maximum cellular fraction of glycogen is reached or that there is signaling control to stop glycogen accumulation after a certain point.

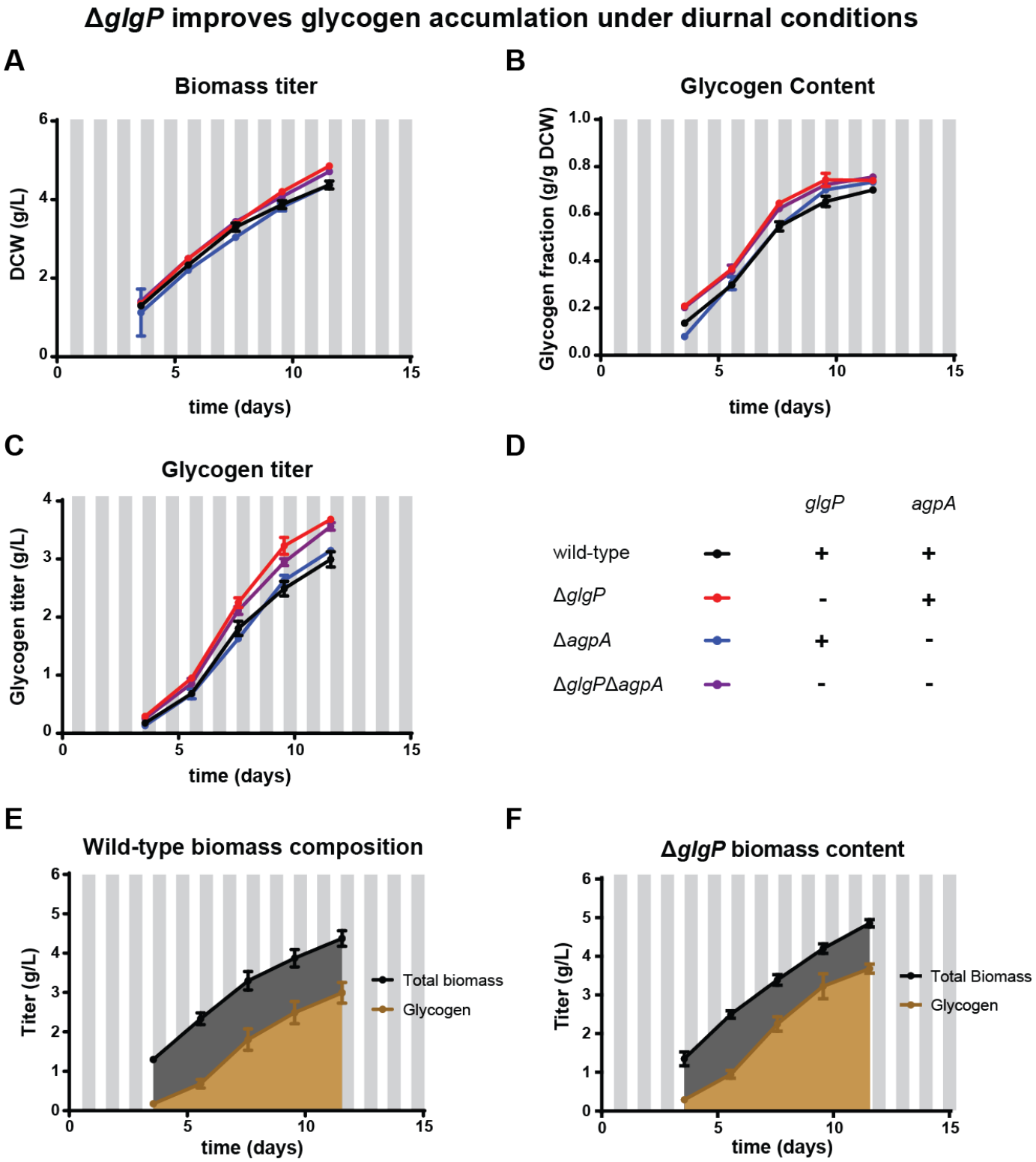

Figure 23: Biomass and glycogen production by *S.* PCC 7002 strains under diurnal light conditions in media A. This experiment investigates the value of knocking out linear glycogen phosphorylases in the glycogen catabolism pathway under more restrictive diurnal conditions. Panel A shows the biomass production measured directly as dry cell weight (DCW). Panel B shows fractional glycogen content measured through biomass hydrolysis. Panel C shows glycogen titer measured as glucose. Panel D describes the genotypes of the strains measured in Panels A-C. Panels E and F show the total biomass titer and total glycogen fraction of the wild-type and Δ*glgP* strains. These panels help emphasize the production differences between these strains.

We hypothesized that nitrogen starvation to different degrees could be used to push *S.* PCC 7002 to produce very high glycogen content. We made a set of modified media A conditions that deviate in the total amount of nitrate in the media. We tested over a range from one quarter of the nitrate in media A to four times the nitrate in media A. This range should cover different nitrogen starvation states and determine how initial nitrate concentration impacts productive biomass titer and glycogen content. Hypothetically, it is industrially relevant to nitrogen starve a culture to induce rapid glycogen production at a lower biomass titer. This could create a higher average productivity compared to growth in media A or nitrogen replete conditions because the growth phase would primarily encompass the exponential growth phase with simultaneous glycogen accumulation.

As seen in Figure 24, the growth of each culture is dependent on nitrogen dose. The cultures with higher nitrogen concentration grow the fastest and reach the highest titers. On the other hand, the low nitrogen conditions reach high glycogen content very early in growth and maintain it throughout the experiment. Glycogen content tends to decrease with increasing nitrogen dose. Overall, glycogen titer increases with nitrogen dose until the 2x condition, afterwards glycogen titer decreases again. In addition, productive biomass increases with nitrogen dose and is constant once a maximum is reached. This relationship can be used to decide on nutrient dosage required for a given volumetric light intensity or biomass titer.

This experiment shows that strong nitrogen starvation can be used as an additional tool for control of glycogen accumulation. By our first measurement of biomass titer and glycogen content, the cultures with the two lowest nitrogen levels have reached stationary phase. These cultures have reached over 70% glycogen content and could be immediately harvested. This is a faster time than the typical 12 days for media A. The optical densities imply that these cultures reached a high-glycogen, nitrogen-limited stationary phase in two or three days of growth (for 0.25x and 0.5x, respectively). Further, we find that maximum productive biomass titer is directly related to the amount of nitrate supplied. The remainder of biomass is made up of glycogen content. This experiment also shows that cyanobacteria appear to have a maximum fraction of total biomass that can

exist as glycogen (around 75%). This could be regulated by multiple mechanisms including direct glycogen synthesis pathway control as well as degradation of light harvesting components. The destruction of photosynthetic pathways would reduce pressure for the cell to find a sink for excess energy. It may be possible to push glycogen content beyond this point by disrupting cyanobacterial signaling pathways. Finally, this analysis gives us information to use in a technoeconomic analysis to determine if strong nitrogen starvation would decrease production costs by maintaining high productivity. This would result in lower culture titers and faster open raceway pond turnover. An example of these comparative processes in continuous light is shown (with estimated data) in Figure 25. In this example, the data is estimated from previous experimental data and results in approximately a 50% increase in productivity on a glycogen basis (approximately 6g collected in a 1L reactor versus 4g). We will evaluate this alternate production method as part of a technoeconomic analysis in Chapter 6. If the flocculation technique is independent of biomass titer, or does not suffer in effectiveness, this could increase daily productivities at the expense of water use. Overall, this experiment shows that we can fine tune the nitrogen dose in media to control growth rate, maximum biomass titer, and glycogen content under constant light delivery. We were also able to show that it is unlikely we can push cyanobacteria above the 75-80% glycogen content point without genetic alterations.

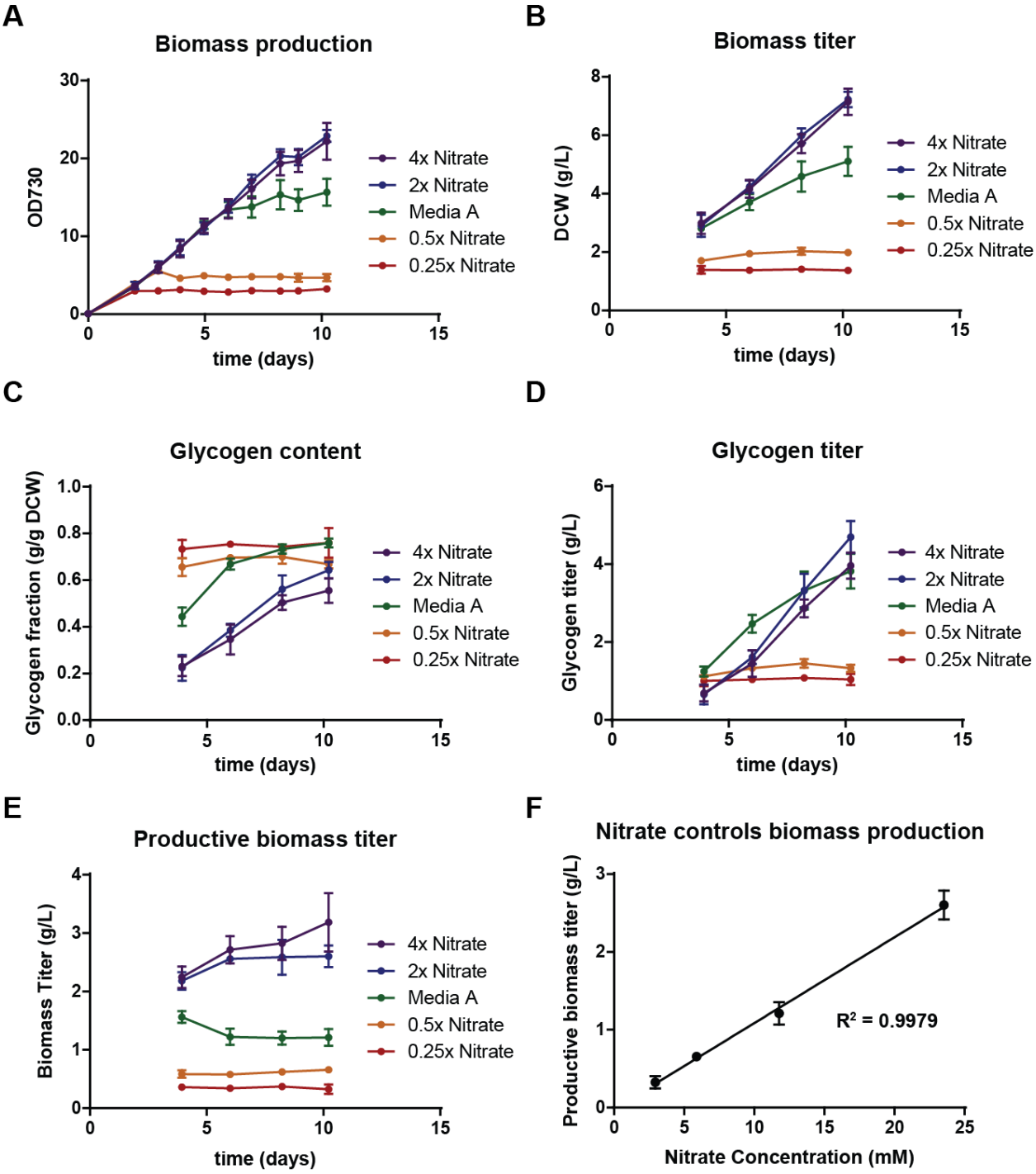

Figure 24: Biomass and glycogen production by *S.* PCC 7002 strains under continuous light conditions in a variety of nitrogen limited media A conditions. Conditions vary from 25% of the nitrogen in media A to 400% of the nitrogen in media A. Panel A shows biomass production as optical density at 730nm. Panel B shows the biomass production measured directly as dry cell weight (DCW). Panel C shows fractional glycogen content measured through biomass hydrolysis. Panel D shows glycogen titer measured as glucose. Panel E shows the fraction of total biomass that is not made up of glycogen. Panel F shows a relationship between nitrate dose and productive biomass production (for 0.25x, 0.5x, 1x, and 2x nitrate doses only).

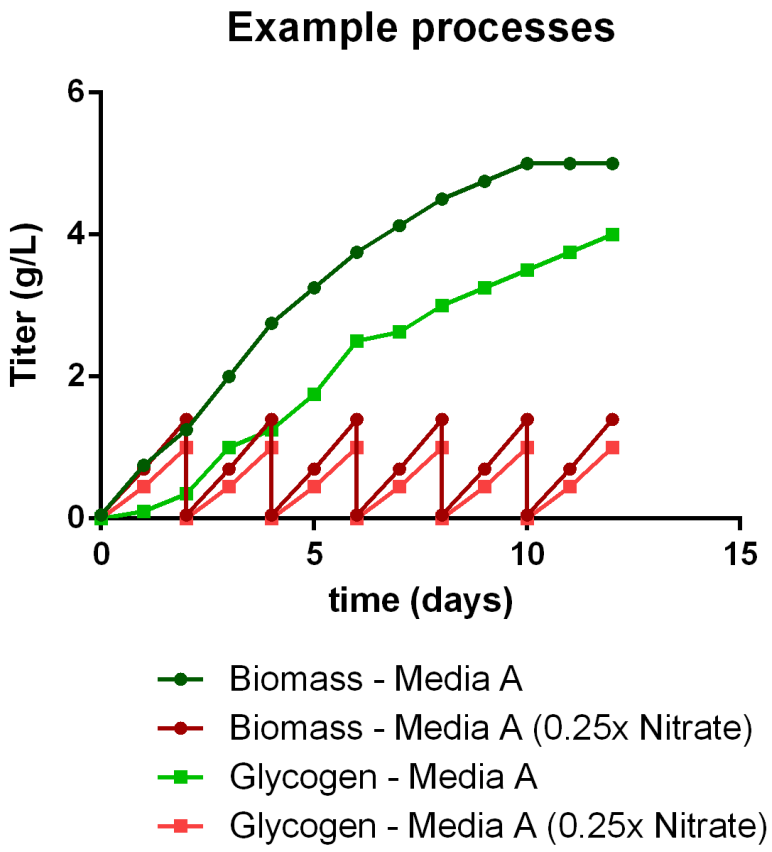

Figure 25: A theoretical growth curve for a highly nitrogen starved production process in comparison to media A growth conditions in continuous light. Cells can be harvested many times over after reaching maximum titer in low nitrogen conditions before a media A culture could be harvested.

Analysis of a growth-associated glycogen screen

A previous post-doctoral researcher named Andrew Markley proposed a screen for high glycogen accumulating cells by taking advantage of the natural role of glycogen within the cell. Being able to connect glycogen content to a growth-associated screen is a very powerful approach to screen many mutants. The screen is explained in Figure 26, first cyanobacteria is grown in a liquid culture, then applied to a series of agar plates which are placed in the dark. A plate is removed every two days and placed in the light to allow cells that survive the period of time in the dark to grow. The longer a plate is left in the dark, the fewer cells expected to survive. The cells that do survive, we expect to have increased glycogen content in comparison to the cells that die.

We decided to test the validity of this screen in a variety of ways. Andrew Markley first tested the screen on a designed library of overexpressed genes intended to increase glycogen content. Specifically, he attempted to create a library of *glgA*, *glgC*, and phosphoglucomutase overexpression cassettes with a library of ribosome binding sites to alter each gene's expression within the operon. He was able to isolate a single mutant that may have had increased glycogen content in comparison to wild-type *S.* PCC 7002. We decided to validate this mutant, ALM339, under more rigorous conditions. Although there appeared to be a modest improvement in glycogen accumulation, the library mutant was somewhat inconsistent (data shown in Figure 74 in the appendix).

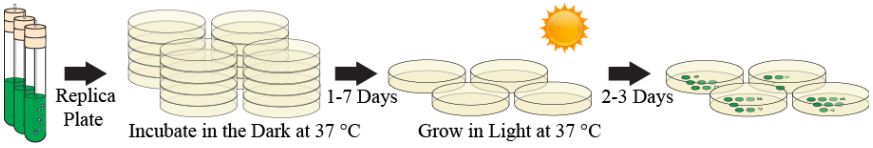

Figure 26: A visual explanation of the glycogen growth-associated screen. Cells are grown in liquid culture, plated on media A plates and placed in the dark, removed from the dark and grown in the light periodically, and then analyzed for growth.

To test the screening capability of the glycogen screen, we created an ribosome binding site (RBS) library to overexpress *glgC*. Our approach hedges our previous knowledge of the glycogen accumulation benefit of overexpressing *glgC* early in the growth cycle. This library should show

enrichment for high expressing *glgC* integrands that use an RBS with high predicted expression (see Figure 27). The selection for higher glycogen content should work for the *glgC* strain within a 2 day growth period with IPTG induction. The higher the accumulated glycogen content, the longer we predict a colony will survive on an agar plate in the dark. By comparing gross colony formation on plates from different lengths of time in the dark, we can determine whether the library has cells with higher glycogen content present. Further, these strains can be isolated, sequenced, and tested for a direct measure of glycogen content. This data will help validate the value of the glycogen screen. We decided to test this library against wild-type *S.* PCC 7002 and the *glgC* overexpression strain to determine whether enrichment of highly expressed RBSs occurred.

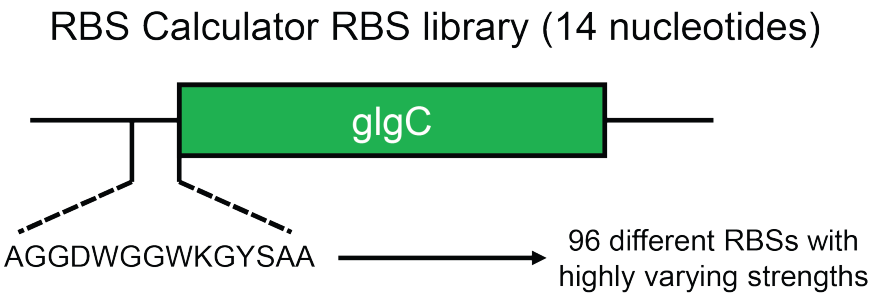

Figure 27: The small library of ribosome binding sites designed using a single degenerate oligo sequence allows for variation in the expression of *glgC*. Overexpression of *glgC* at low optical densities shows increased accumulation of glycogen. We aim to use this library to detect the ability of the screen to differentiate between mutants with higher and lower *glgC* overexpression.

We grew wild-type *S.* PCC 7002, an induced *glgC* overexpression strain, and the induced RBS library for two days in nitrogen limited media. We then applied 1mL of OD730 normalized culture onto a media A plate and spread the culture evenly until evaporated. The plates were placed in the dark at 37°C for 4 days, with one set of plates removed each day and placed in light to allow for cyanobacterial growth. The resulting plates are shown in Figure 28, where the wild-type and *glgC* overexpression strains survive for only 2 days and the RBS library still has colonies after 4 days in the dark. To determine if high expressing RBS variants from the library enriched in the surviving population, we sequenced a set of 10 colonies. This analysis found that the library was a random distribution of expression levels from the RBS library. This implies that the screen may not have

targeted colonies with higher glycogen content or that the screen has poor resolution, both of which reduce the value of this screen in practical applications.

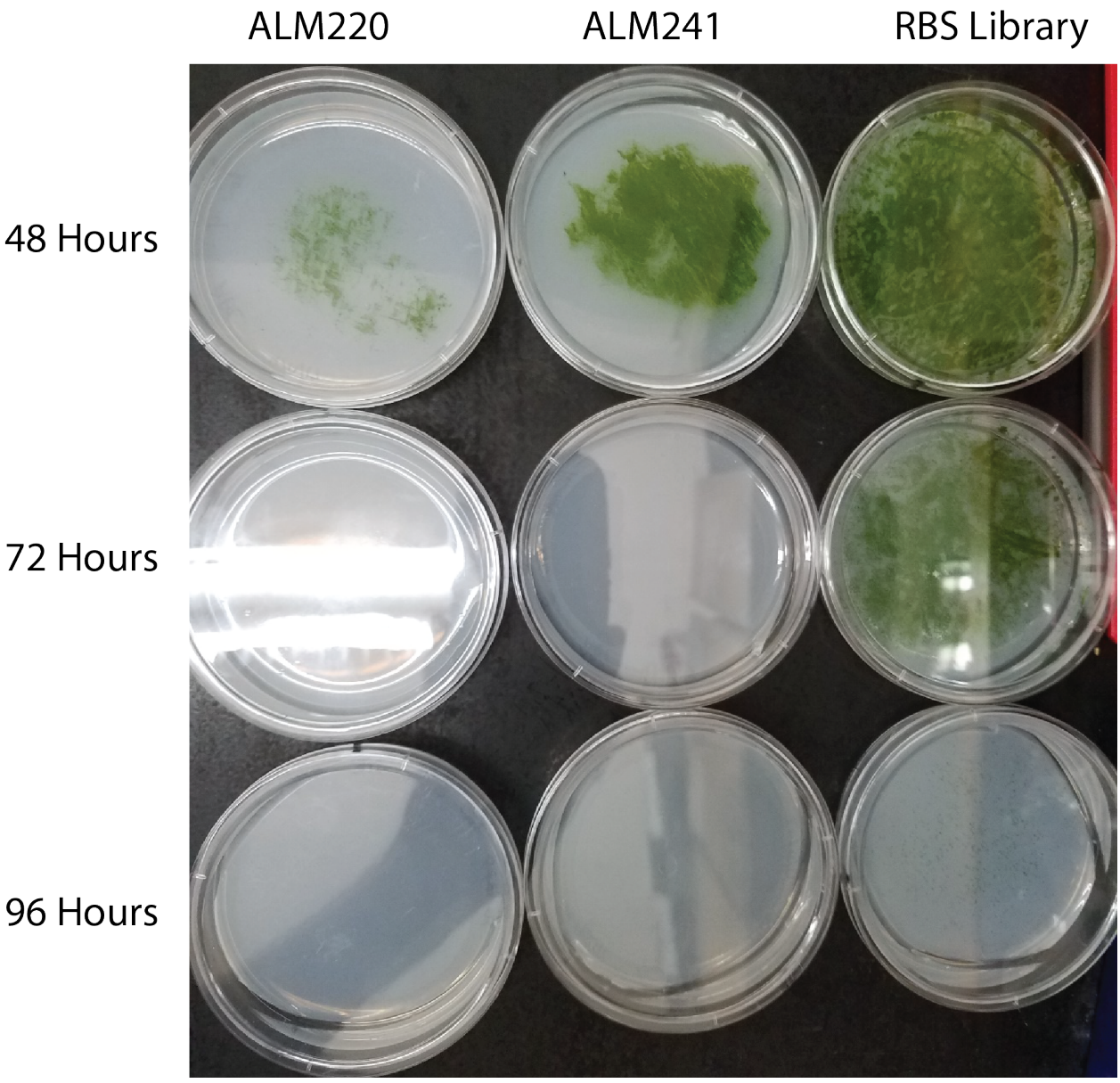

Figure 28: The comparison of Media A plates spread with different cultures of *S.* PCC 7002 that had been grown for 48 hours. The time each row of plates was left in the dark is denoted to the left. The longer a given strain was left in the dark, the fewer colonies are found on the plate. ALM220 is a gentamycin barcode strain and acts as a wild-type control, ALM241 is an induced *glgC* overexpression strain, and the RBS library is a mixed culture of all RBS combinations in the library.

To determine the glycogen content produced by each sequenced colony, we decided to test each in liquid culture. This should give more definitive results than searching for RBS enrichment and allows for a direct comparison of predicted *glgC* overexpression to glycogen content. These samples were grown for two days and then collected for biomass and glycogen measurements to determine the fraction of total biomass that is made up by glycogen. These results were then compared to the sequenced RBSs for each culture.

We first compared measured glycogen accumulation levels with RBS strength and found poor correlation (Figure 29). Further, a Spearman rank correlation between predicted RBS strengths and measured glycogen accumulation resulted in poor correlation to predicted RBS strength and no mutants accumulated more glycogen than the control (Figure 30). This led us to believe this screen may select for more than simply glycogen content or that glycogen content does not vary greatly with *glgC* RBS changes, which led us to an experiment aimed at probing the screen's effectiveness rigorously using previously studied phenotypes.

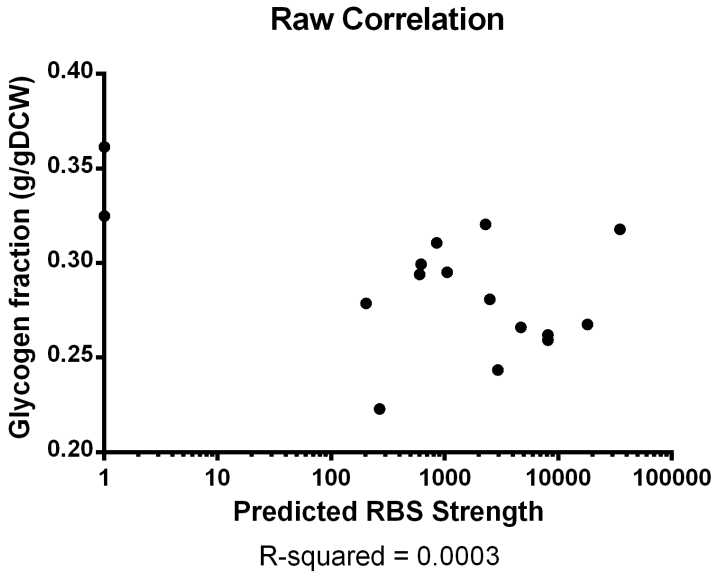

Figure 29: Comparison of the strength of the RBS on the *glgC* overexpression cassette against the measured glycogen content of each culture. Each culture was grown for 48 hours before the glycogen content was measured.

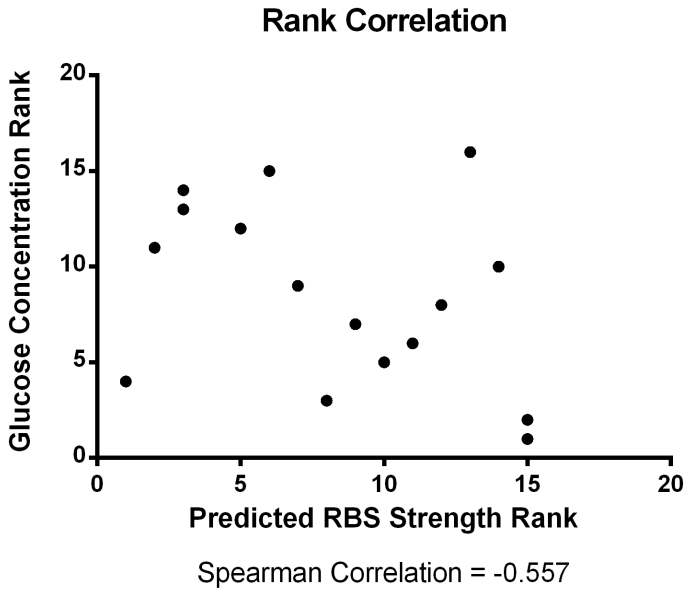

Figure 30: Comparison of the rank of the strength of the RBS on the GlgC overexpression cassette against the rank of the measured glycogen content of each culture. Each culture was grown for 48 hours before the glycogen content was measured. The ranks represent highest glycogen content and predicted RBS strength at 1 and the lowest glycogen content and predicted RBS strength (i.e. wild-type or inactive mutant) 16. Ties were given equal ranking.

In order to test the glycogen screen more rigorously, we decided to take advantage of the *glgC* overexpression strain with well-defined behavior as well as the nitrogen starvation effect to show the ability of the glycogen screen to detect cells with higher glycogen content. We compared wild-type cells grown in media A at three different time points: 2, 6, and 12 days. These three time points should have different levels of glycogen accumulation as seen in previous experiments. We compared these controls to a nitrogen replete condition grown for 12 days, induced and uninduced *glgC* overexpression strain grown for 2 days, as well as a Δ*glgC* strain grown for 2 days. We measured glycogen content, biomass titer, and survival through the glycogen screen across 12 days. This rigorous set of data is a more direct comparison because glycogen content of the cultures used in the screen were directly measured, as opposed to a post-factum analysis of surviving colonies.

Figure 31 shows the results of this analysis. Panel A indicates that glycogen accumulation occurs as predicted by previous work. The nitrogen replete wild-type culture has lower glycogen

content then the nitrogen deplete condition. By 6 days of growth, the wild-type strain in nitrogen deplete conditions has a high glycogen content, but a lower biomass titer. Finally, the two day growth results are nearly identical to the *glgC* study discussed previously. Unfortunately, the survival measurements from the screen do not align well with the glycogen content for the long growth times. Until day 6, the nitrogen replete culture grown for 12 days has higher survival than the nitrogen deplete condition. Further, the 6-day culture in nitrogen deplete conditions has the longest survival despite having almost identical glycogen content to the 12 day nitrogen deplete condition. On the other hand, the survival of the cultures grown for 2 days perfectly tracks with our expectations. The wild-type and uninduced *glgC* strain survive for the same amount of time and at the same dilutions. The induced *glgC* strain survives longer and at higher dilutions. The Δ*glgC* strain has the lowest survival.

We can show the screen correctly identifies cells with high glycogen content when grown for a short period of time. Unfortunately, these cells have lower glycogen content than cells grown in nitrogen deplete conditions for 12 days, but are able to survive longer during the screen. One explanation is that *S.* PCC 7002 has group protection properties, where cells show higher survivability when close to other cells. Further, cells grown in nitrogen deplete conditions for long periods of time seem to have a lower cell count and less productive biomass per OD730. This could also account for lower survivability during the glycogen screen. In addition, this experiment does not show the ability of this screen to identify small changes in glycogen.

Overall, we conclude that this screen seems effective with cultures at similar OD730 measurements during early stages of growth. When glycogen becomes a very significant portion of the cell biomass, the screen seems more confounded by cellular fitness and productive biomass, which reduces its effectiveness in the most important cases. It might be possible to improve the accuracy of the screen by normalizing to productive biomass titer. This can be estimated using the nitrogen starvation experiment. However, the requirement for a long growth step to probe for late-stage glycogen accumulating mutants will bias the culture towards fast-growing mutants.

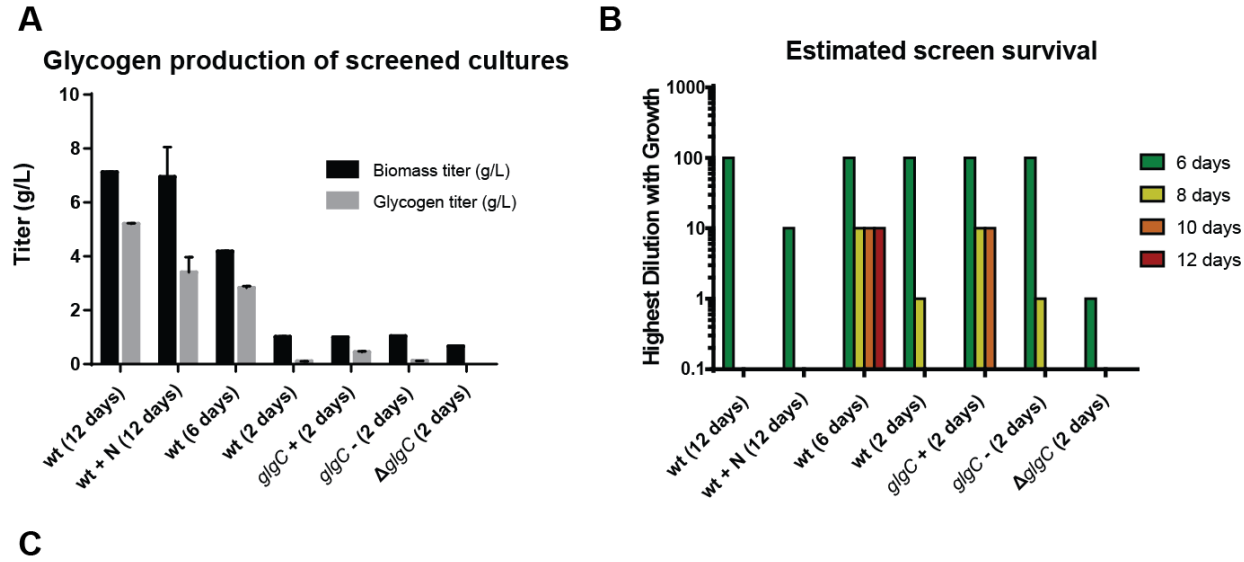

Figure 31: Panel A describes the biomass and glycogen production of different strains of *S.* PCC 7002 with different genotype and media conditions that were screened with the glycogen screen. Panel B describes the highest order of magnitude of dilution on which colonies grew. This estimate is required because cyanobacterial colonies grow better when adjacent to other cyanobacterial colonies. Panel C shows the physical spot plates upon which the glycogen screen was run. The left-most plate was in the dark for 2 days and each plate afterwards was in the dark for 2 additional plates. After time in the dark, each plate was exposed to the light for 3 days.

Downstream processing and use of cyanobacterial biomass

To round out this work, we have considered hydrolysis of, flocculation of, and heterotrophic growth on cyanobacterial biomass. In considering process parameters that would be relevant for cyanobacterial biomass hydrolysis, we studied a variety of conditions in which cyanobacterial biomass would hydrolyze to glucose and other basic cellular components. Further, we consider how different conditions could allow for effective sedimentation of cyanobacteria hedging base flocculation techniques. In Chapter 6, we consider how alternative methods could further improve flocculation as an extension on this work. Last, we discuss the growth of *Escherichia coli* on cyanobacterial hydrolysate in comparison to control media from equivalent lab materials.

Traditionally, biomass hydrolysis has been completed through application of high temperature in acidic conditions.[69] The temperature and time applied to a sample determine the extent of biomass breakdown. We use this process to analyze production of glycogen in biomass samples as well as hydrolyze samples in order to grow heterotrophic organisms. We wanted to determine if we could use less acid and longer times or even base-catalyzed hydrolysis as options for reducing costs in an industrial bioprocess. Theoretically, cyanobacterial biomass can be a drop-in replacement for corn in glucose fed biological processes.[5] We were able to show that with a decrease in acid concentration or time, there is less biomass hydrolysis (Figure 32). Additionally, the hydrolysis of biomass using base-catalyzed hydrolysis requires much higher base concentrations or higher hydrolysis time. Last, the cyanobacterial biomass we tested has a buffering effect, which requires higher concentrations of acid to hydrolyze higher biomass concentrations.

In order to study cell collection efficiency of our organism, we applied the technique of base flocculation to cyanobacteria using a pH shift with calcium hydroxide in Figure 33.[72] This was achieved through the addition of base to the cyanobacterial culture to achieve high pH levels. Once the pH is increased enough, flocculation and sedimentation occurs. The theory behind this process has been debated, but recent studies have shown using base for flocculation can be a cost efficient approach to biomass concentration.[72] Using base flocculation will increase material costs because

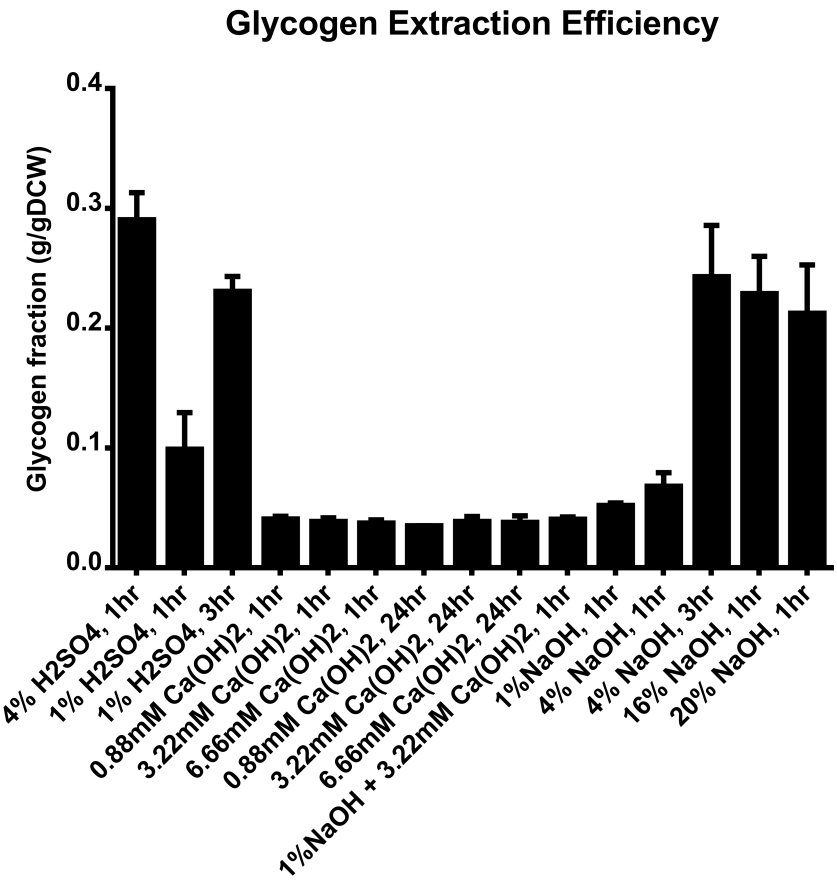

Figure 32: Glycogen extraction efficiency of different conditions under 121C using base or acid catalyzed hydrolysis of biomass.

performing acid hydrolysis will require additional acid to neutralize the calcium hydroxide.

Figure 34 shows quantitative measurement of the sedimentation rate of flocculated cells using base flocculation. These measurements are taken using time-lapse video over the experimental time frame. This analysis can be used to calculate floc size and drive a process model for flocculation and sedimentation costs. This figure shows a range of cultures at different pHs. Flocculation rate varies by pH and seems to have two critical levels: one at which flocculation begins to occur and another at which the speed of flocculation increases. The first critical level occurs somewhere in the pH range of 10.8-10.9, and flocculation appears to increase drastically in rate between pH 11.4 and 11.8, the second critical point. The ability to flocculate cyanobacteria quickly and at low cost

should make production of intracellular products in cyanoabcteria more viable.

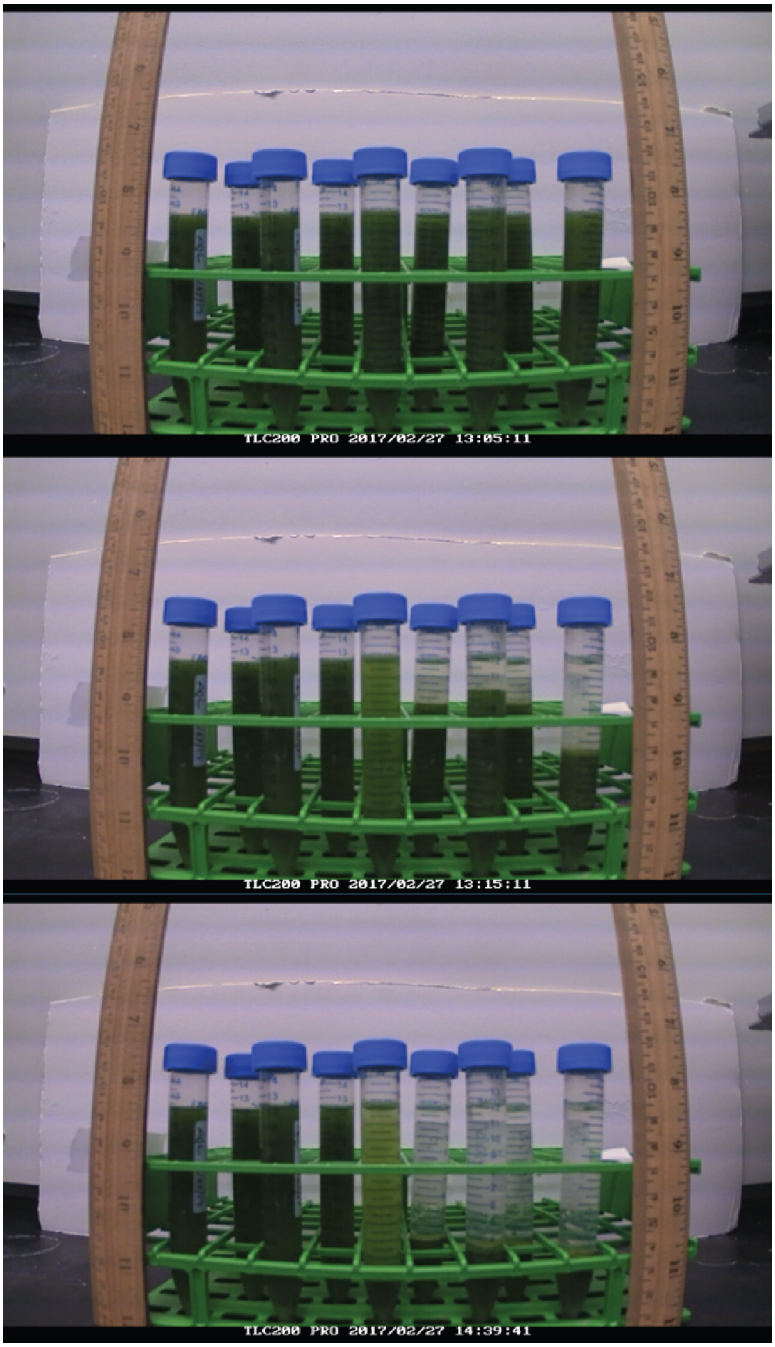

Figure 33: Snapshots from a time lapse video of flocculated cells that are undergoing sedimentation. The samples are increasing in pH from left to right.

Sedimentation is dependent on the size of the flocs that form from induced flocculation. We

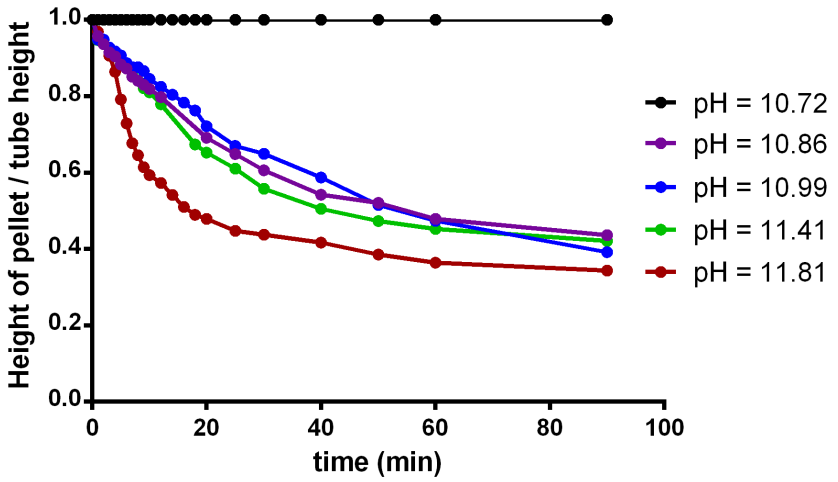

Figure 34: Quantification of time lapse video comparing sedimentation of *S.* PCC 7002 under different pH conditions. Height relative to the maximum height of the culture is tracked over the range of the time lapse video.

hypothesize that lower biomass titers would form smaller flocs and sediment slower. We tested this by diluting a single culture to a variety of optical densities and testing floculation rate in each culture at the same pH. Each culture was diluted, brought to pH 11.8, mixed vigorously for 10 seconds, and allowed to sediment.

The flocculation of cyanobacteria at low pH appears to be consistent despite variations in biomass titer of the culture (Figure 35). This is supported by consistent sedimentation rate across cultures sedimented from different biomass titers (Figure 36). The rapid flocculation of sample 2 is due to the higher pH. Among sample with consistent pH, the flocculation is very consistent despite an order of magnitude difference in biomass titer. This range of biomass titers covers the range of titers expected in an industrial setting given the available light delivery in an open raceway pond. This experiment disproves our hypothesis and implies that low titer cultures can still flocculate efficiently, which bodes well for industrial cyanoabcterial growth in an ORP.

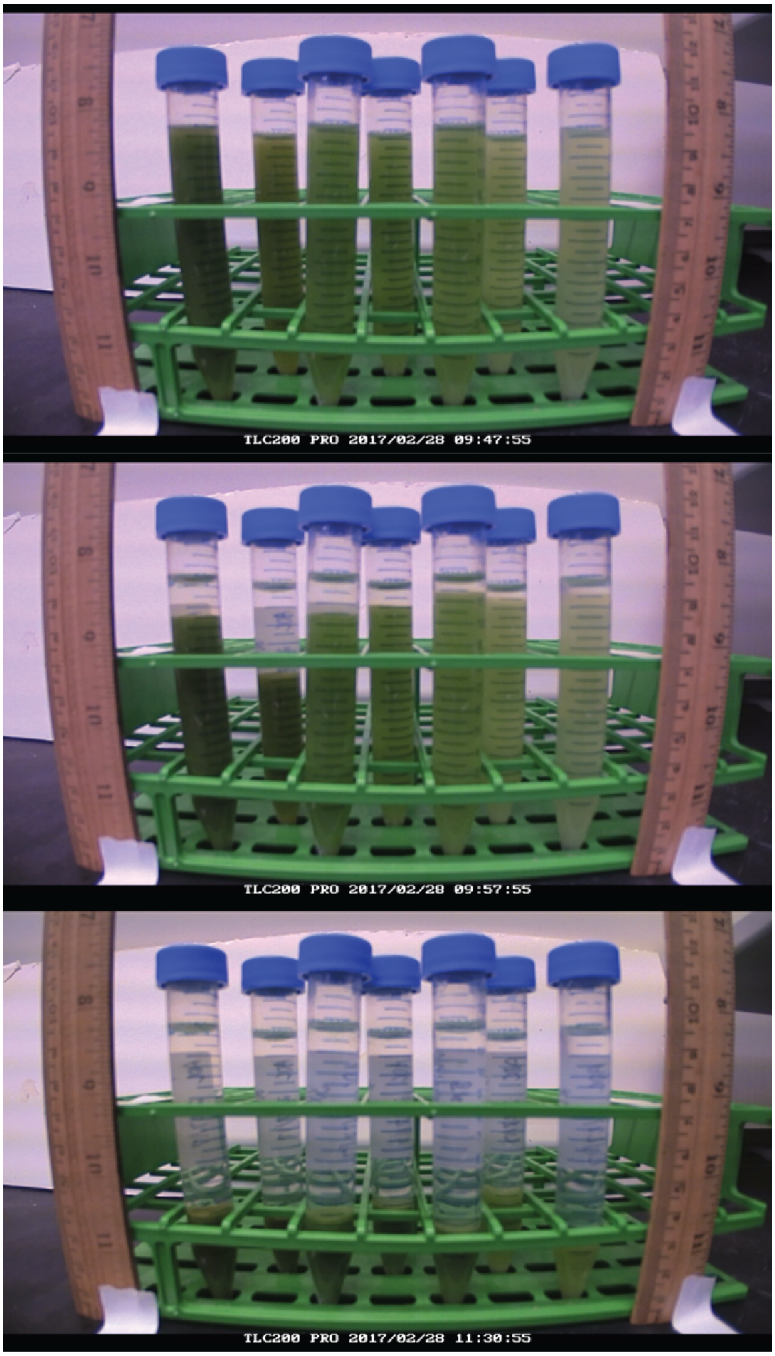

Figure 35: Snapshots from a time lapse video of flocculating cells. The sample decrease in biomass content from left to right.

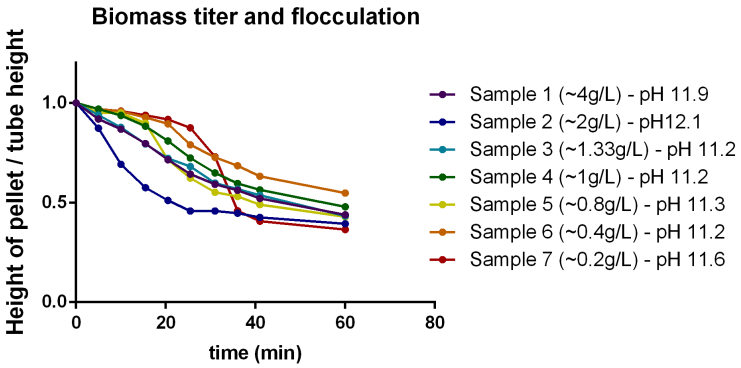

Figure 36: Quantification of time lapse video comparing sedimentation of *S.* PCC 7002 under different biomass titers with similar pH conditions. Height relative to the maximum height of the culture is tracked over the range of the time lapse video.

Cultures grown in municipal wastewater are exposed to different stresses and are likely to flocculate in a different manner. Further, other bacteria in the wastewater microbiome may influence sedimentation rates and alter the economic impact of wastewater media (Figure 37). The data in Figure 38 shows quantitative measurements of sedimentation rates of base flocculated cells. The cells grown in wastewater media show a drastic increase in sedimentation rate when exposed to similar concentrations of calcium hydroxide. This increased flocculation is likely due to other microbes in the culture. Further, cells in toxic wastewater media may be stressed and more likely to form flocs in response to a pH change.

Unfortunately, this flocculation method lacks synergy with the remainder of the process we are considering. Acid hydrolysis would require adding enough acid to first neutralize the calcium hydroxide added for flocculation and then acidify the solution for acid hydrolysis. This would both increase costs and increase the amount of salt in the final hydrolysate. While this will increase material costs, it may be less expensive or toxic to downstream processes compared to other flocculation methods. Flocculation shows even more promise if other methodologies can be used to induce a similar effect, especially given the faster rates of flocculation seen from wastewater grown cultures. One such technique would be the use of surface displayed proteins that can form covalent bonds with one another.[89, 67]

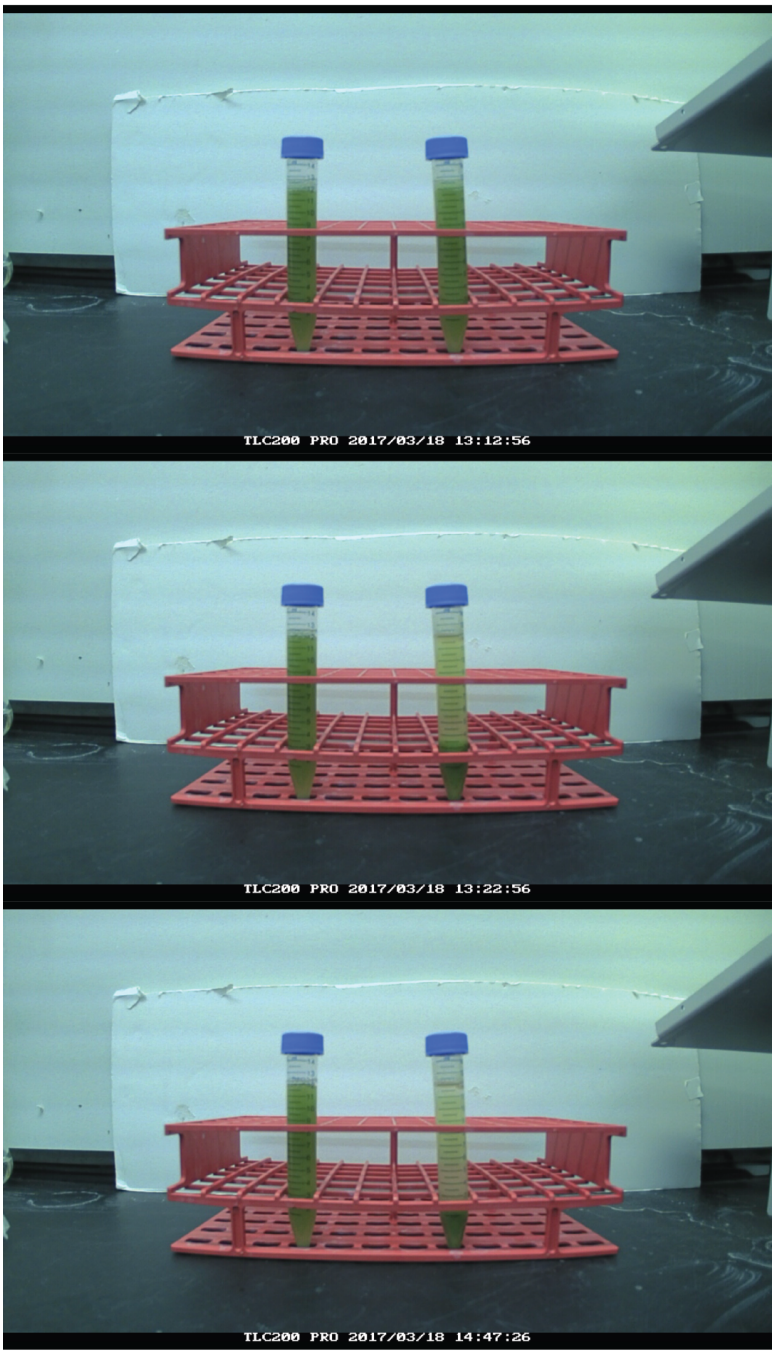

Figure 37: Snapshots from a time lapse video of flocculating cells. The left sample has no base added and the right sample has base added; both are in GBF media.

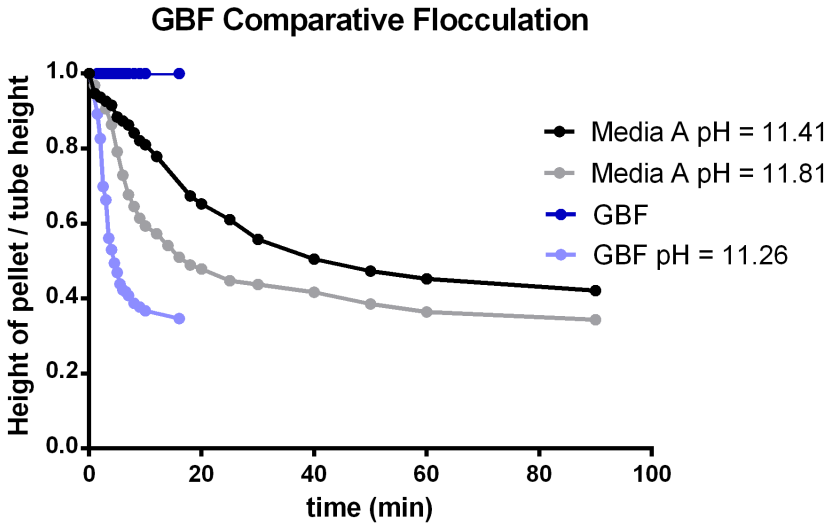

Figure 38: Quantification of time lapse video comparing sedimentation of *S.* PCC 7002 under GBF or media A growth condition after addition of base. Height relative to the maximum height of the culture is tracked over the range of the time lapse video.

Finally, we have done preliminary growth tests to show that *E. coli* can grow on cyanobacteria hydrolysate (Figure 39). We decided to compare the growth of this model organism on hydrolysate to growth on standard lab media. These are not directly comparable because the nutrient content of the lab media tends to be much higher than the total nutrient content of the hydrolysate. Further, *E. coli* is generally more sensitive to toxins than other model organisms such as *Saccharomyces cerevisiae*. We found that *E. coli* grew better than lab minimal media, but worse than on LB media. The minimal media was supplemented with glucose at the same concentration as the hydrolysate as the sole carbon source. The higher final biomass titer on the hydrolysate could represent the presence of alternate carbon sources that are unavailable in the minimal media. It could also mean the the hydrolysate is not limited in some substrate that is limiting in the M9 media.

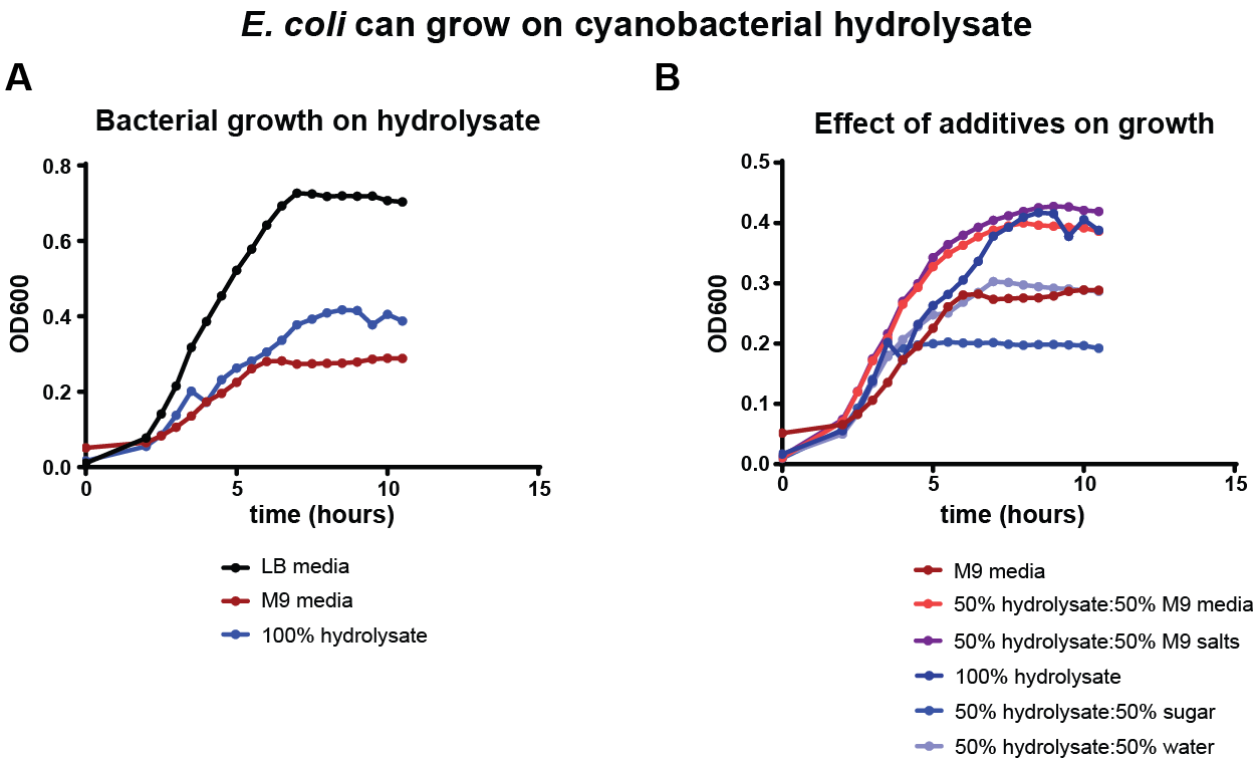

Figure 39: Panels A and B show growth of *E. coli* on different lab medias, cyanobacterial hydrolysate, and supplemented cyanobacterial hydrolysate. These were grown in 96 well plates and measured on a Tecan M1000 plate reader.

We also considered different minimal media additives that could be used to improve growth on

the hydrolysate. We first considered simply diluting the hydrolysate in water or in a sugar solution that matches the concentration of glucose measured in the hydrolysate. Interestingly, dilution in water showed better growth than dilution in sugar, while both grew to lower final biomass titers than pure hydrolysate. Next, we considered dilution in M9 media with matching glucose content to the hydrolysate as well as diluting with core M9 salts. The supplementation of M9 media improved growth rate, but not final biomass titer. A similar effect was seen when just adding M9 salts without glucose. This implies that the hydrolysate may need minor refactoring to allow for optimized growth by *E. coli*, but that the hydrolysate appears to have all the required nutrients for cellular growth.

Chapter 5: Improving cyanobacterial growth on municipal wastewater media

Introduction

The growth of photosynthetic organisms using municipal wastewater as a feedstock is not a novel concept, but historically many strains have needed engineering or environmental changes to support growth on different toxic feedstocks[61].[3] Multiple studies have also considered the cost savings of using wastewater instead of fertilizer in these processes.[5, 91] We have considered the use of *Synechococcus sp. strain* PCC 7002 for the partial detoxicification and elimination of excess nutrients in nutrient-rich streams within a municipal wastewater treatment plant. We target the gravity belt filtrate (GBF) as a source of nitrogen and phosphorus for an algal growth operation (Figure 40). This stream is part of the dewatering process downstream of the series of digestors found within the wastewater treatment plant. This waste stream is typically a high cost stream to remove excess nutrients from with many wastewater treatment plants opting for construction of struvite reactors to remove phosphate and recycle the excess nitrogen.[42] This presents an opportunity for value from both new and existing wastewater treatment plants of which even small algal growth operations could take advantage.

One of the biggest hurdles to the use of biological processes for nutrient removal from wastewater is that the ratio of nitrogen and phosphorus in the waste stream must be carefully balanced to match the uptake ability of the organism used. Without this match, there will be excess nitrogen or phosphorus in the spent growth medium that would need to be processed further. In our case, the GBF stream has excess phosphate that we will be unable to remove using *S.* PCC 7002.

[3] This work was performed with the help of Dr. Travis Korosh, who provided the ground basis of knowledge through both previous work and direct training. Specifically, Travis identified some mechanisms of GBF toxicity, taught me the techniques for GBF analysis, and gave feedback on experimental design. Jackie Cooper provided assistance in obtaining ICP-AES measurements and protocols for the nitrate/nitrite HPLC method. Matt Seib assisted with collection of wastewater samples.

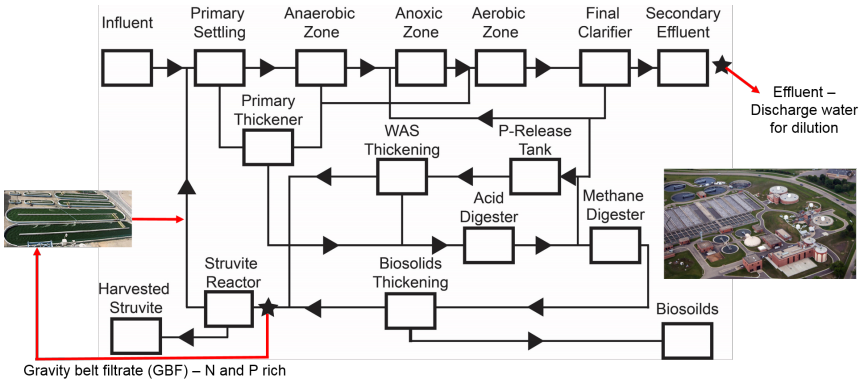

Figure 40: An overview of the process for treating municipal waste at the nine springs wastewater treatment plant. A series of digestors under different conditions is used to eliminate excess nutrients. The effluent from those processes is clarified and sterilized for discharge into fresh water sources. The remaining streams are concentrated and processed to biosolids or the rich gravity belt filtrate, which can be used for cyanobacterial growth or processed to produce struvite. Figure adapted from Travis Korosh.[36]

This would mean that the resulting effluent after cyanobacterial growth would need some further processing before discharge. This would likely be in the form of a struvite reactor. On the other hand, pretreatment with a struvite reactor to remove the majority of the phosphate may present an opportunity for a low phosphorus GBF that still contains high nitrogen content. This would allow for cyanobacterial growth to remove all remaining nutrients from the wastewater. When selecting the wastewater stream to use for growth, we focused primarily on the nitrogen requirement.

This work expands upon previous findings about the toxicity of GBF to *S.* PCC 7002.[37] GBF was shown to have a variety of toxic compounds, including humic material, biological aromatics, and fulvic acids. These compounds, which are included in dissolved organic compounds, have been shown to disrupt membrane integrity and inhibit the electron transport chain.[54] GBF media was found to be toxic to *S.* PCC 7002 under standard growth conditions. When the temperature for growth was decreased from 37°C to 27°C, *S.* PCC 7002 was able to recover growth on short time scales.[37] This work aims to produce glycogen at appreciable levels from a wastewater derived media. We technoeconomic analysis to determine the value of this work in reducing the cost of cyanobacterial biomass production.

Methods

Wastewater collection and processing

Wastewater samples were collected from the Nine Springs Wastewater Treatment Plant in Madison, WI. Effluent samples were taken before UV sterilization and GBF was collected directly from the gravity belt runoff. Raw GBF samples were brought to the lab and used immediately for experiments or frozen. Filtered GBF samples were filtered using vacuum filtration and coffee filters, which removes large solids. Autoclaved GBF was first filtered and then placed in an autoclave on a liquids cycle at 121°C for 30 minutes. Sterilized GBF samples for the microbiome assessment were made using raw GBF filtered through 0.22um syringe filters in small volumes due to filter blockage from solids.

Analysis of wastewater

Total nitrogen, ammonia, total phosphate, reactive phosphate were measured using color-based assays purchased from Hach Company for water analysis. Nitrate and Nitrite were measured using high performance liquid chromatography (HPLC) with a Ultra AQ C18 column, photodiode array detector, and 50mM potassium phosphate monobasic + 1% acetonitrile running buffer. Samples were measured with a 5 minute sample time. This HPLC method is adapted from [30]. pH was measured using pH strips. Dissolved metals were measured through a nitric acid extraction and measurement through inductively coupled plasma atomic emission spectroscopy (ICP-AES). ICP-AES analysis method is adapted from [48]. Measurements were taken as quickly as possible after sample collection.

Excitation-emission spectral scans were completed using a Tecan M1000 plate reader and a UV transparent 96-well plate. Each sample was scanned in 10nm steps from excitation range of 230-450nm and emission range of 280-510nm. Measurements were taken in QSU, quinine sulfate units. QSUs are measured as the fluorescence of 1ppm of quinine sulfate in 0.1M sulfuric acid at an

excitation wavelength of 350nm and emission wavelength of 450nm.

Cyanobacteria culturing

Cyanobacteria are first struck onto an appropriate antibiotic media A plate and allowed to grow for 3 to 4 days. A streak of cells are added to a 30mL starter culture and grown for 1-2 days and then subcultured into 60mL of media A at an optical density of 0.05. All cultures are grown in 250mL baffled flasks in a light shaking incubator at 27°C. When using wastewater sources as a media, GBF, effluent, and sea water mimic are mixed in specified concentrations to 60mL in a 250mL baffled flask. During growth, sterile water is added to cultures to supplement water lost by evaporation. Water loss is estimated by weight change of each sample. In the case where cultures are grown diurnally, the cultures are grown at 27°C in the shaking incubator with a diurnal cycle programmed into an 8-cycle controller. The controller is programmed by setting the length of time and light intensity for each of the 8 segments of the controller scheme. Light is measured as a percentage of maximum intensity.

Biomass titer measurements

Biomass titers were estimated in one of two ways. First, we use optical density measurements with light at a wavelength of 730nm. This required sample dilution to within the linear range of the spectrophotometer used. Optical density (OD) measurements will detect both cell biomass and other components that absorb light. This becomes relevant when producing glycogen because OD730 measurements will detect glycogen as well as total cell biomass. Second, Biomass titers were also directly measured through dry cell weight measurements. A pre-weighed conical tube is filled with a recorded volume of cell culture. The conical tube is centrifuged at 5000xg for 20 minutes. The supernatant is vacuum aspirated and the pellet is resuspended in 1 volume of water. Next, the suspension is centrifuged at 5,000xg for 20 minutes and the supernatant is vacuum aspirated. The samples are then flash frozen in liquid nitrogen or frozen overnight in a -80C freezer. Once frozen,

the samples are lyopholized and final weights are measured.

Glycogen content and glycogen titer measurements

Glycogen content is measured by extracting glycogen as glucose from lyopholized biomass samples through hydrolysis. A direct biomass titer is calculated using the dry cell weight method described above. Next, 5-20mg of dessicated biomass is added to a 5mL glass reactor. To this, 1mL of 4% sulfuric acid is added. The reactor is sealed with a cap containing a second septa to prevent vapor loss during hydrolysis. The reactors are placed in a silicon oil bath at 121°C for 1 hour and then cooled in an ice water bath for 20 minutes. Samples are transferred into 1.7mL microfuge tubes, centrifuged for 10 minutes at 20,000xg, filtered through a 0.22um filter, and stored at -20C until analysis. This is based on the biomass hydrolysis process used by NREL.[69]

Glucose concentration of the hydrolyzed sample is measured using HPLC. A 5mM sulfuric acid mobile phase is used with a Rezek ROA-Organic Acid column. Samples are measured for 25 minutes using a refractive index detector detector and compared to a prepared standard curve.

Wastewater sample analysis

In order to conduct growth experiments in municipal wastewater, we must fully understand the general qualities of the feedstock and what might cause the toxicity effects we have seen previously. Previous work in the Pfleger Lab has identified that *S.* PCC 7002 cultures grown in wastewater media experience loss of membrane integrity.[37] To attempt and recover robust cyanobacterial growth in wastewater, we will need to understand the potential pitfalls to growth in wastewater. We decided to evaluate the nutrient composition and potential toxins through a variety of analyses. We performed direct chemical measurements of nitrogen content, phosphorus content, and heavy metals. Further, we applied a multi-dimensional excitation-emission spectral scan to check for the presence of certain categories of toxins expected in wastewater (Figure 41).

To determine the nutrient availability and form, we analyzed the nitrogen and phosphorus content

using colorimetric kits purchased from Hach Company as well as HPLC. Nitrogen content was measured as total nitrogen, ammonia, nitrate, and nitrite. The nitrogen detected in the total analysis that is not accounted for by ammonia, nitrate, and nitrite is likely in more complex biomolecules that have not been fully broken down in municipal wastewater processing. This could include amino acids, proteins, or biological products. In comparison to media A, the GBF has primarily ammonia, not nitrate, as its nitrogen source. This is advantageous for cyanobacteria because nitrate must be reduced to ammonia for biological assimilation, so *S.* PCC 7002 prefers growth on ammonia to nitrate.[70] This means there is an energetic savings in using ammonia as a nitrogen source and that wastewater media has low energy cost nitrogen available for cyanobacteria.

Analysis	GBF	Effluent
Total Nitrogen (mg/L)	1510.5	44.05
Ammonia (mg/L)	1301.2	NM
Nitrate (mg/L)	12.8	OVER
Nitrite (mg/L)	<1mg/L	<1mg/L
Total Phosphate (mg/L)	220.9	ND
Reactive Phosphate (mg/L)	253.6	NM
pH	8-8.5	6.5-7

Figure 41: Summary of the chemical analysis of collected samples of gravity belt filtrate (GBF) and effluent from the Nine Springs Wastewater Treatment Plant.

Phosphate analysis reveals that all phosphate appears to be free reactive phosphate that is bioavailable. The ratio of phosphate to nitrogen in GBF is much higher that the nutrient requirement for cyanobacteria or the ratio in media A. This excess phosphorus will not be removed during cyanobacterial growth in the wastewater media and acts as one of the major limiting factors in wastewater detoxification by cyanobacteria. Finally, the pH of the GBF matches media A closely and the effluent is slightly more acidic than media A. These raw measurements are not as meaningful

because the media acidifies when exposed to higher CO_2 concentrations. This means buffering capacity is likely the more important measure for comparison.

Next, we tested for presence of toxic levels of heavy metals as well as what metals are available within the GBF media (Figure 42). Appreciable levels of calcium, iron, potassium, magnesium, and sodium are present and beneficial for cyanobacterial growth. The boron and chromium levels are also appreciable, but neither should have a strong effect on growth. Lead is detectable below our lowest standard and is unlikely to be a concern for growth. Overall, there are no heavy metals present that are predicted to inhibit cyanobacterial growth.

Analysis	Average (mg/L)	STD Dev	Detected?	In range?
Al 396.152	0.23	0.025	Yes	No
B 249.678	1.63	0.81	Yes	Yes
Ba 233.527	0.21	0.038	Yes	No
Ca 422.673	36.6	0.32	Yes	Yes
Co 238.892	-0.13	0.022	No	No
Cr 267.716	0.26	0.025	Yes	No
Cu 327.395	-0.014	0.024	No	No
Fe 238.204	4.34	0.050	Yes	Yes
K 766.491	133	0.83	Yes	Yes
Li 670.783	0.095	0.030	No	No
Mg 280.270	16.2	0.20	Yes	Yes
Mn 257.610	0.25	0.025	Yes	No
Na 589.592	154	0.70	Yes	Yes
Ni 231.604	-0.27	0.023	No	No
Pb 220.353	0.19	0.064	Yes	No
Zn 213.857	0.13	0.027	Yes	No

Figure 42: Summary of the ICP-AES analysis of the metals present in the GBF samples.

To test the GBF and effluent for toxic compounds, we completed an excitation-emission scan. This scans for fluorescence over a range of excitation and emission wavelengths and can be used to identify general classes of toxic compounds. Specifically, humic compounds, aromatic compounds, and fulvic acids can be identified using this method. Humic compounds have been shown to intercalate the cell membrane and cause membrane instability.[58] ”Soluble microbial products”, most likely aromatic compounds, have been shown to disrupt the electron transport chain and, when combined with membrane damage, can cause significant energetic losses for the cell.[4] The heat

maps in Figures 43 and 44 show the presence of all three compounds within GBF and, to a lesser extent, the effluent. This implies that GBF could have toxic compounds that have induced the membrane damage and cell death seen in previous work.[37] This toxicity was overcome to some extent by a decrease in temperature, meaning that methods that stabilize the *S.* PCC 7002 membrane are more likely to provide resistance to the toxicity of GBF.

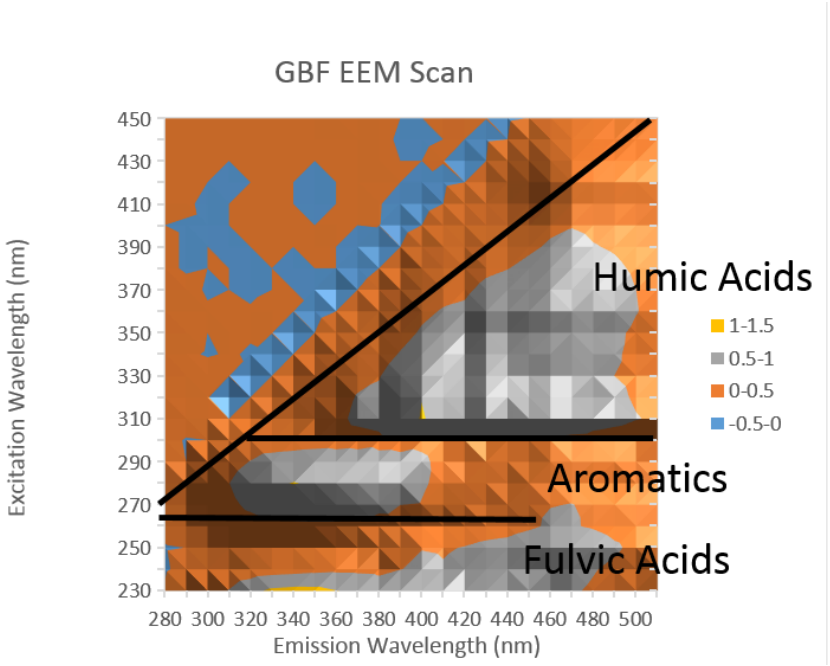

Figure 43: An excitation-emission scan of the GBF sample which covers the regions representing humic compounds, aromatics, and fulvic acids.

Overall, our analysis of wastewater streams used for the growth of cyanobacteria reveals the potential for toxicity from organic compounds. Our analysis of phosphate and nitrogen show that GBF is nitrogen limited and after cyanobacterial growth will contain leftover phosphate. Further, nitrogen is in the form of ammonia, which is energetically advantageous for growth. Our analysis of dissolved metals through ICP-AES shows that there are no heavy metals present that are likely to inhibit cyanobacterial growth. Finally, an excitation-emission scan shows the presence of multiple classes of toxic compounds that can disrupt the cell membrane and electron transport chain. We predict that overcoming the toxicity of GBF based on its composition will require improving

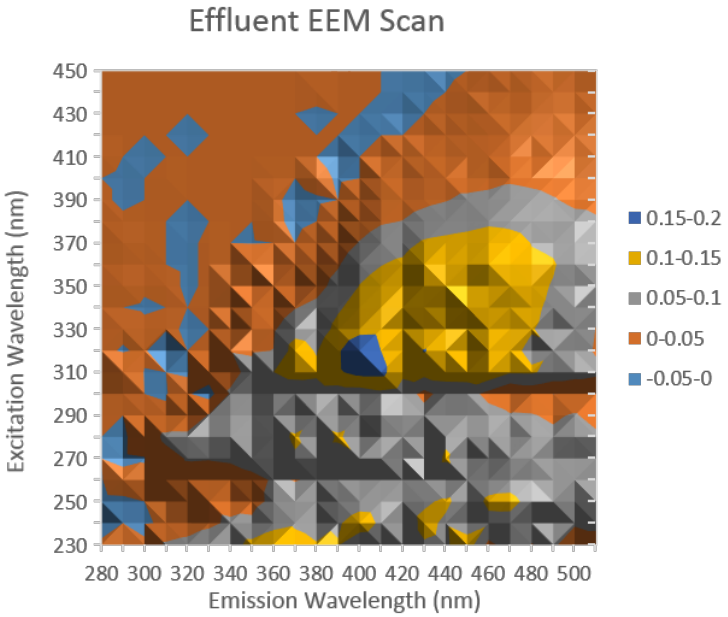

Figure 44: An excitation-emission scan of the effluent sample which covers the regions representing humic compounds, aromatics, and fulvic acids.

cyanobacterial membrane stability.

Refactoring individual components of wastewater media

In order to capture the advantages of using wastewater media, we used a range of environmental and media changes to reduce GBF toxicity. Previous work showed that cells grown in GBF have lower membrane fidelity and high rates of cell death. Further, we showed that reducing culturing temperature from 37°C to 27°C reduced the short-term effects and allowed for better growth of *S.* PCC 7002.[37] These conditions are most industrially relevant, as evaporative cooling keeps ORPs at lower temperature. However, this change will need to improve growth until stationary phase in order to take advantage of high glycogen and biomass titers. Upon repeating the reduced temperature condition in a 12.5% GBF media for long-term glycogen production, we found the cultures would still fail to grow under continuous light conditions (Figure 45). We decided to try and refactor the GBF media in order to fully recover growth to match production levels in media A.

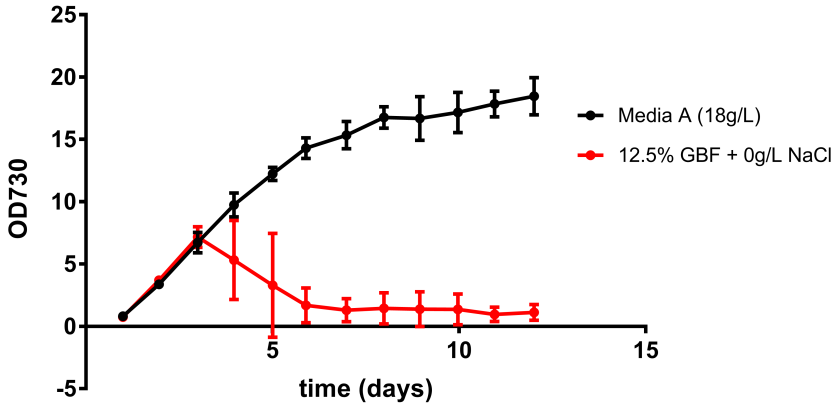

Figure 45: Measured biomass production as optical density at a wavelength of 730nm for samples grown in 12.5% GBF diluted in effluent and grown in media A. The growth recovery observed previously at 27°C is not maintained after early growth.

Given that *S.* PCC 7002 prefers brackish water conditions, we predicted that altering the salinity or ionic state of wastewater media could improve membrane stability. Although studies have shown that *S.* PCC 7002 has a high range of salt tolerance, the best production for glycogen occurs under brackish water mimic conditions (media A).[1] In addition to improving cyanobacterial growth, the

addition of salt to an ORP may reduce the range of contaminating organisms that can survive in the media. We decided to use a similar approach and tested fresh water, brackish water (18g/L NaCl), and salt water (36g/L NaCl) conditions using GBF as the nutrient source compared to growth in Media A (Figure 46).

The brackish water condition is the closest mimic to media A and showed the best growth compared to both salt and fresh water. *S.* PCC 7002 has been shown to support growth in both salt water and fresh water, but production of both biomass and glycogen is reduced. These results imply that the toxicity of the GBF may exacerbate that effect given the very low growth of *S.* PCC 7002 in salt water media with GBF. Further, after 10 days of growth, the brackish water GBF culture matches biomass production and has similar glycogen production as the media A grown culture. This is a substantial improvement over the original GBF media formulation.

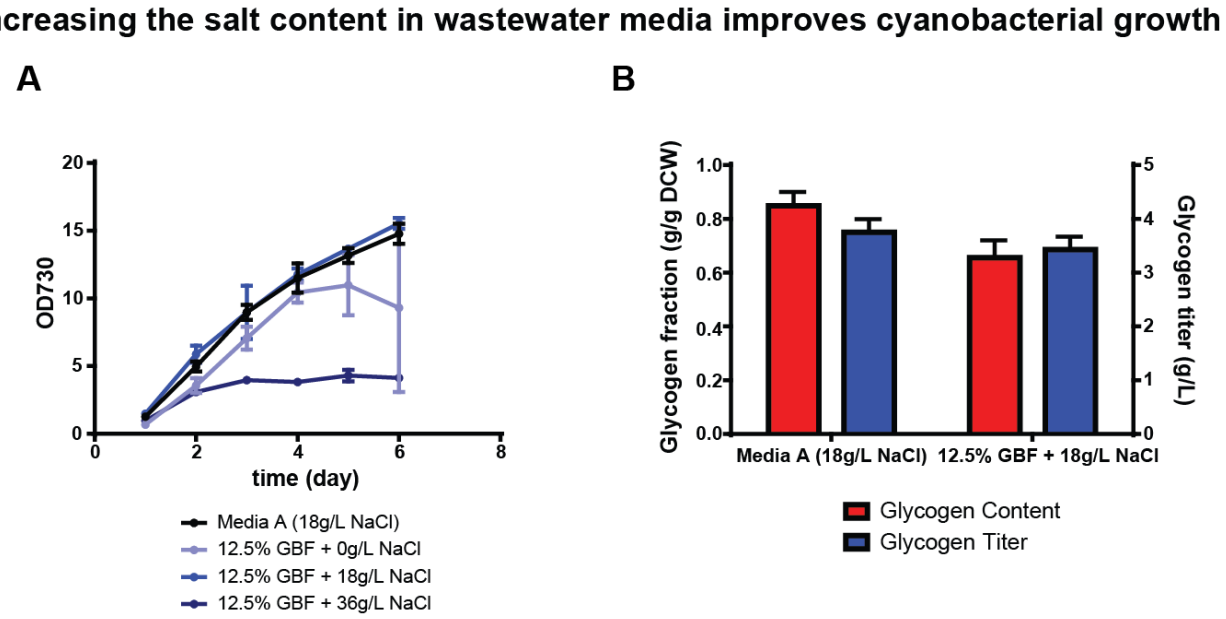

Figure 46: Summary data from a comparison of growth and glycogen production in GBF medias supplemented with different levels of salt. Panel A describes the biomass production as measured by optical density at 730nm. Panel B describes final glycogen content and glycogen titer as measured through acid hydrolysis and HPLC.

In order to understand the full effect of working with GBF, we decided we should confirm that our processing of raw GBF was not altering the chemical signature significantly. There are three

processing states we have considered for our experiments: unprocessed GBF, filtered GBF, and autoclaved GBF. By removing solids through filtration or sterilizing through autoclaving, we were altering the chemical composition of GBF, possibly removing or breaking down both toxins and other microorganisms. Given that both filtration and autoclave-based sterilization are economically inviable for a cyanobacterial biomass production process, we wanted to confirm we were not biasing our results. In addition, previous experiments in our lab used exclusively autoclaved GBF, so comparing our current results with past results had a confounding factor. Further, the inconsistency of GBF could also be problematic because the variable composition of GBF could lead to variable experimental results over time. We decided to test the effect of processing in a single collected sample of GBF to account for sample variance over time. We hypothesized that both filtration and autoclaving were reducing the toxicity of GBF.

Our comparison of raw, filtered, and autoclaved GBF as the nutrient source for wastewater growth medium shows that filtration has only a small effect on growth and autoclaving has a substantial negative growth effect (Figure 47). Cultures were grown for 10 days, with additional GBF added after 6 days and growth was tracked using optical density. The raw and filtered GBF samples show similar propensity for cyanobacterial growth. However, the autoclaved sample showed a strong growth defect. We hypothesize that this could be due to chemical breakdown of different products in the GBF or destruction of the microbiome. This experiment disproves out hypothesis that GBF processing could decrease toxicity and bias our results.

To fully probe the changes in GBF due to processing, we used the previously discussed excitation-emission scan to analyze gross changes in GBF media caused by processing (Figure 48). The filtration process could remove certain compounds in the GBF and the autoclaving process could cause chemical breakdown of the toxic components. The results of excitation-emission scan show that filtration has little effect on GBF content, but autoclaving appears to decrease the concentration of aromatics and fulvic acids marginally, and substantially increases the humic compounds in the GBF. This alteration in the distribution of potentially toxic compounds could account for the growth

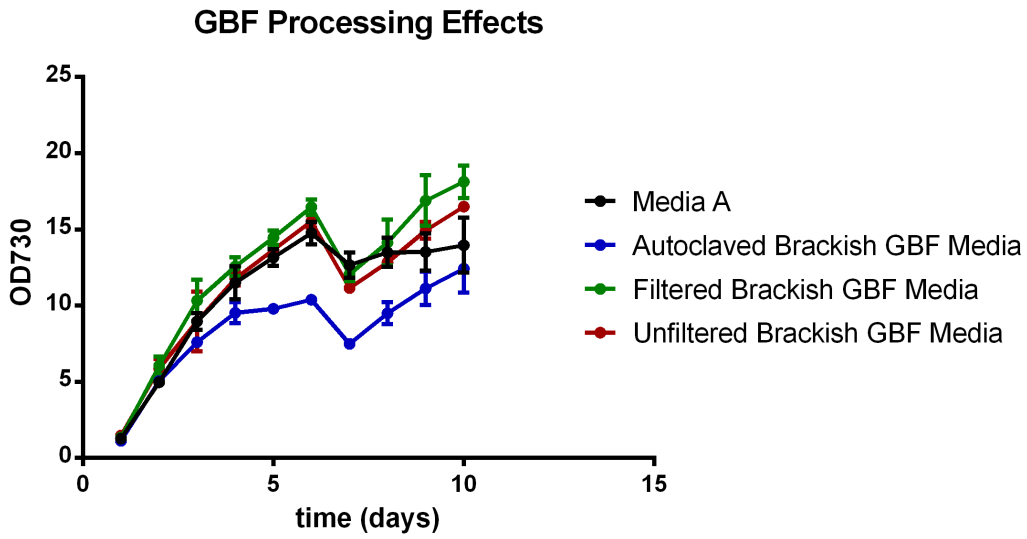

Figure 47: The effect of processing GBF is teased out through comparison between growth in media A and salt-supplemented GBF media that has been either unaltered, filtered, or autoclaved and filtered. Biomass production was measured as optical density at 730nm.

changes caused by processing GBF.

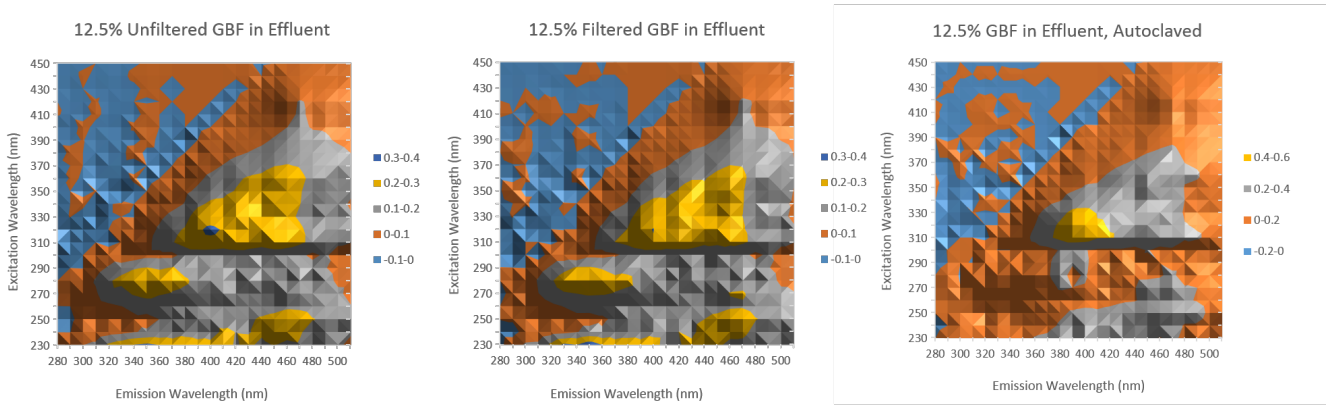

Figure 48: Excitation-emission spectra of the different GBF medias used in Figure 47. The effect of processing can be seen in variations in peak height.

After determining that altering the salt content of the GBF media greatly improves growth of cyanobacteria, we decided to probe the changes in cyanobacterial tolerance to GBF at higher concentrations in this media. Previously, 12.5% GBF media was toxic to cyanobacteria beyond short growth periods. By increasing the salt content, we have altered the ionic environment to more

closely mirror that natural environment of *S.* PCC 7002. This environmental shift may improve membrane stability. We tested the increased tolerance by growing cyanobacteria in increasingly concentrated starting medias of GBF diluted with effluent and supplemented with salt (Figure 49).

With the salt concentration adjustment, we observe growth in 25% GBF with a nearly imperceptible growth defect. At higher concentrations of 50-100%, GBF is still highly toxic to cyanobacterial growth. This shows that the salt concentration adjustment has greatly improved growth in GBF media. This adjustment would make the GBF much more similar to the natural environment that *S.* PCC 7002 resides in and thus is most likely to have optimized membrane conditions for survival. Membrane stability is crucial for microbial defense against toxic compounds. This experiment supports our hypothesis that adjusting the ionic state of wastewater media has improved GBF tolerance.

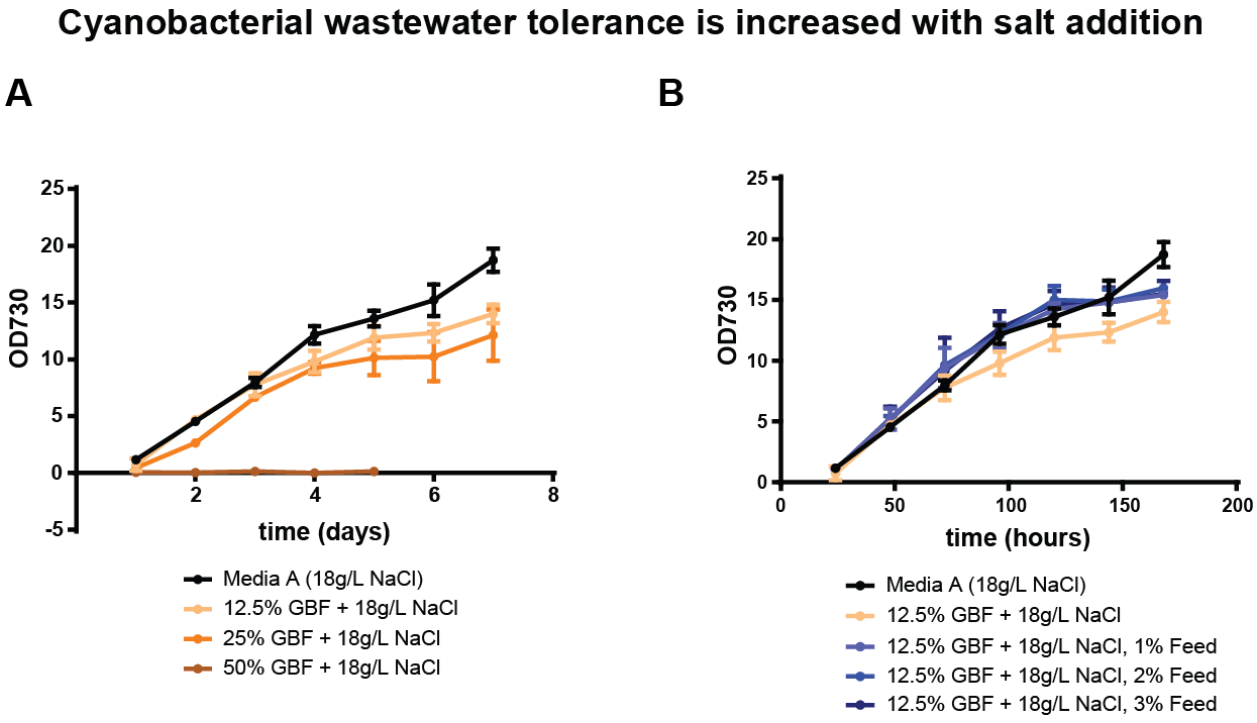

Figure 49: Tolerance to GBF media under salt-supplementation is higher than media without salt supplemented. Panel A describes the growth as measured by optical density at 730nm among cultures with different starting concentrations of GBF. Panel B describes the growth as measured by optical density of cyanobacterial cultures grown with different daily feed rates measured as percent of original volume.

To determine if a continuous feed of nutrients could further improve growth in wastewater media, we tested continuously feeding wastewater to cultures. We considered feed rates of 1%, 2%, and 3% of initial volume per day in GBF. This would supplement consumed nitrogen and mimic the high and low nitrogen conditions tested in Chapter 4. We were able to show a very modest increase in growth rate, but not final titers, with a GBF feed of 1%. There was no further improvement with higher feed rates. The fed cultures also did not reach significantly higher final optical densities, implying that a feed may help to produce cells more quickly, but they are still limited by light delivery. This increased feed rate will also result in excess nitrogen in the cyanobacterial culture, which will result in less glycogen production and enhanced biomass production. While using a feed of GBF appears to improve growth rate, it might have a negative effect on high carbon partitioning to glycogen in the final culture.

To probe whether any key growth enhancers are missing from lab media, we considered the addition of different supplements from media A. This could provide a limiting nutrient to the culture or further balance the environment with critical conditions found in brackish water. The two nutrients we focused on most were iron limitation in the form of iron(II) chloride and sulfur limitation in the form of magnesium sulfate. Media A is theoretically quite close to being iron limited, and the large dose of magnesium sulfate provides critical metal in the form of magnesium as well as sulfur for growth. In addition, we considered increasing the dose of trace metals provided in the GBF media to double or triple the standard dose in media A.

The results for supplementing wastewater media show only a growth benefit with magnesiuim sulfate addition (Figure 50). We show that increasing iron(II) chloride or trace metals provids no benefit to growth. However, magnesium sulfate provided a minimal improvement in growth. Overall, the additives seem to be of relatively low importance compared to the effect of salt concentration. We decided to include magnesium sulfate in an improved formulation of GBF media because it did show improvement over the salt adjusted GBF media alone. Interestingly, high doses of additional trace metals caused growth defects or a no growth phenotype.

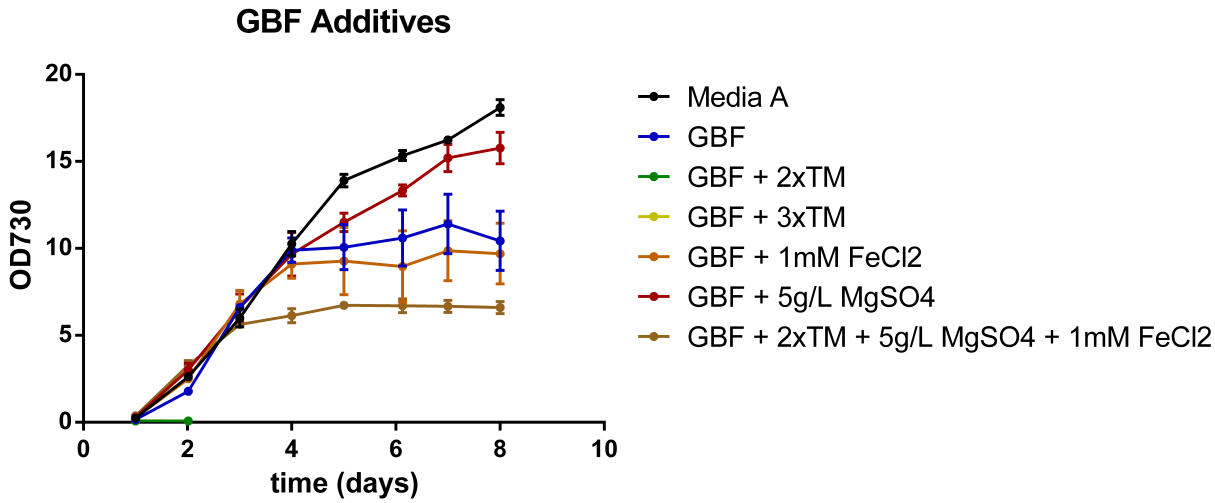

Figure 50: Measured cyanobacterial growth as optical density at 730nm of cultures grown in different GBF medias or media A. The base GBF media is 18g/L NaCl and 1x trace metals (TM). Noted additives are in addition to the base formulation of GBF media.

Overall, we have been able to show the effects of refactoring GBF media and how GBF processing may affect growth. Adjusting the concentration of salt in wastewater media improved growth drastically. Beyond this, we found small growth improvements from magnesium sulfate addition, avoiding highly processed GBF, and continuously feeding nutrients to cultures. We will need further experimentation to determine if the benefits of a continuous GBF feed on biomass growth rate are of value for glycogen production. We decided to rigorously test the refactored GBF media for glycogen production.

Testing refactored wastewater media

To provide a true test of our improvements to the GBF media, we decided to do comparative growth studies for glycogen production under continuous and diurnal conditions. We tested the improved GBF media with the following formulation: 12.5% GBF, 18g/L sodium chloride, 5g/L magnesium sulfate, and trace metals. We considered the addition of a 1% by volume daily GBF feed to probe its benefits under production conditions. Improving growth in a wastewater media can significantly decrease costs.

We tracked dry cell weight, glycogen content, and glucose titer over time for each set of cultures (Figure 51). Under continuous light conditions, we show that growth in media A is robust and produces high levels of glycogen after 12 days of growth. On the other hand, the GBF media shows poor growth with all cultures dying off after 4 days of growth. Finally, the GBF improved media with and without a feed both show robust growth similar to media A. We show that the improved GBF media produces a higher biomass titer with a lower glycogen content compared to media A, which results in the same glycogen titer after 12 days of growth.

This implies that our refactored wastewater media can successfully support cyanobacterial growth and product formation. Additionally, the refactoring has produced a robust resistance to the toxicity effects of the GBF. This media could still cause toxicity effects if the product of interest has a negative effect on membrane stability. This shows that we are able to match control media growth of *S.* PCC 7002 using our refactored GBF media under continuous light conditions. One major factor in this improved growth could be synergy with organisms found in the GBF used for the growth medium. It has been shown that cyanobacteria can form synergistic relationships where a heterotrophic organism can consume a byproduct of cyanobacterial growth. This will produce locally increased concentrations of CO_2, which improve cyanobacterial carbon uptake and growth rate.[3] This synergy boosts growth of both organisms and can even consume organic acids that are normally excreted in the media and could be inhibitory to repeated use of the spent media as a diluent in future growth runs.

To probe the effect of wastewater in industrially relevant conditions, we compared the same set of media conditions under diurnal light conditions. We decided to use the same refactored media formulation, but programmed an 8 period diurnal cycle designed to imitate sunlight exposure over a day under outdoor conditions. We hypothesize that diurnal cycling has a variety of effects on cyanobacterial growth. We predict that the cyanobacteria should reach a lower biomass titer, lower maximum productivity, and not grow during night cycles.[14, 19] These conditions allow for other organisms in the wastewater to grow at night given the stagnation of the cyanobacteria and may reveal that the microbiome has a greater effect on the culture than in continuous light conditions. Further, we predict that less glycogen would be accumulated because glycogen is consumed during the dark cycle to keep the cell alive.[19] This would result in less glycogen being stored because the cell will need to accumulate glycogen during the day to make up for consumed glycogen at night.

In considering the results of this experiment in Figure 52, the effect of diurnal cycling on cyanobacterial growth can be seen in the ”saw-tooth” pattern in the optical density measurements. The final biomass titers of the refactored wastewater media and media A are similar and both lower than under continuous light conditions. The unaltered wastewater media shows the same rapid death phenotype from continuous light conditions, but appears to partially recover late in the experiment. The glycogen content for the media A condition is higher than either refactored wastewater media condition, although only marginally. All of the glycogen contents are lower than in continuous light, reaching only 60% of biomass titer. The decrease in both glycogen content and biomass titer reduces glycogen titer by 25-30%.

As in the continuous light experiment, *S.* PCC 7002 grown in media A and grown in refactored GBF media has similar biomass titers. Further, the original GBF media still shows poor growth and complete culture death early in the growth cycle. Interestingly, the cultures seem to recover after a very long stagnation. This recovery could be due to detoxicification from light exposure or other organisms in the GBF. The most interesting variation between the diurnal and continuous light conditions is that the improved GBF media appears to grow more quickly at early time points

in comparison to media A. This faster growth rate represents a higher potential production in a continuous process where separation costs are minimal. Further, in batch processes, it appears that the GBF cultures could be grown almost 2 days faster than in media A, although this would not be at a maximum glycogen content. This could represent a fairly significant cost savings in capital expenses, especially when this effect is emphasized by the slower growth rates offered by the geometry of open raceway ponds.

The glycogen production from wastewater media is similar to that from media A. This means we can match production targets for media A growth conditions using wastewater media. Utilizing wastewater for biomass production will decrease the cost of the final product. This cost could become important as further technical improvements make algal production economically viable. The addition of a daily wastewater feed to the wastewater media increases the biomass titer and decreases the glycogen content. This difference results in identical titers that are marginally lower than *S.* PCC 7002 grown in media A and aligns closely with expectations given the increased dose of nitrogen associated with the nutrient feed. It is also interesting that the growth under diurnal conditions is much more variable than under continuous light conditions for GBF media. This could be for a variety of reasons including increased effect of the wastewater microbiome due to periods of non-growth for the cyanobacteria in the culture.

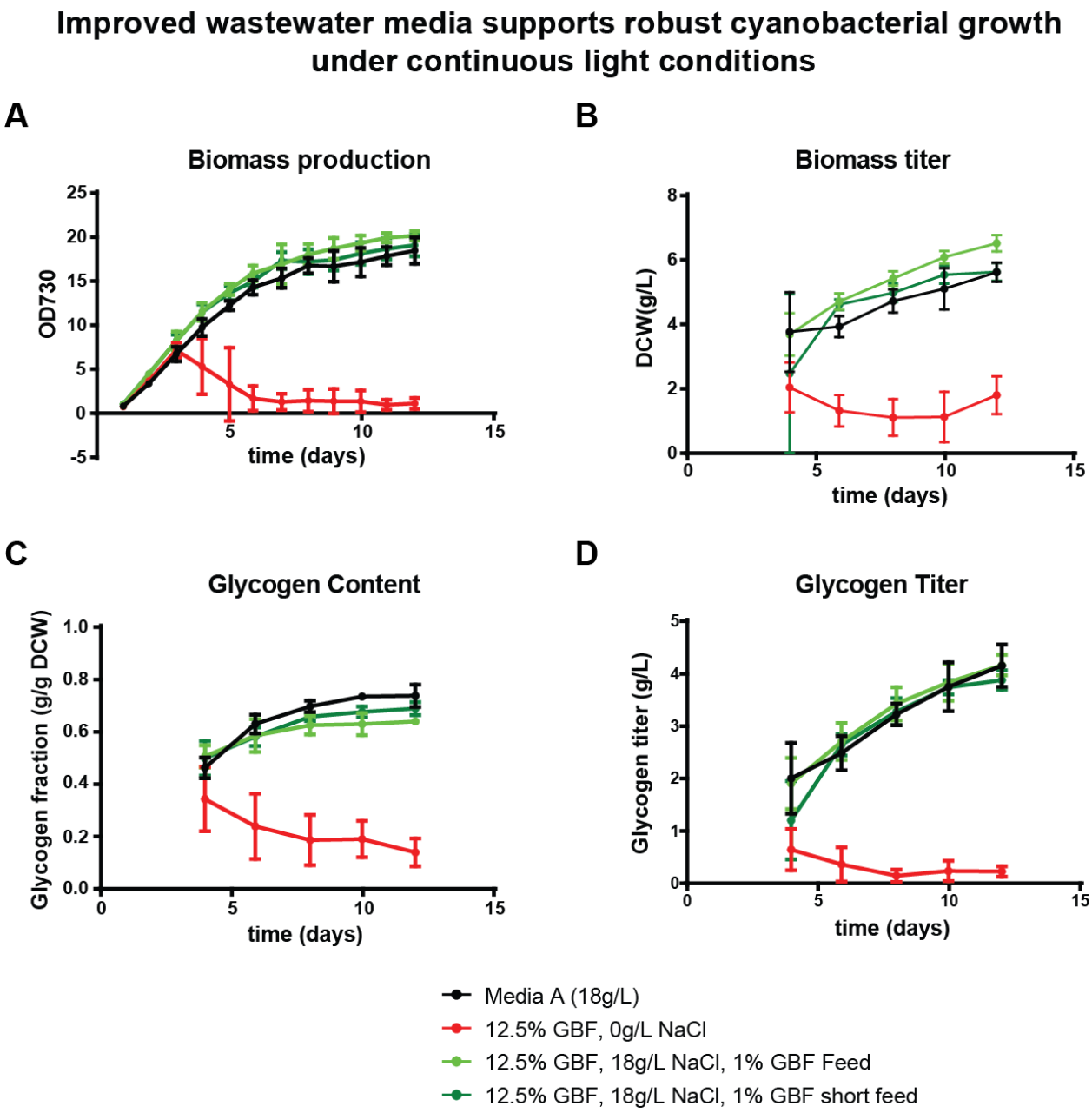

Figure 51: We tested the effectiveness of the refactored GBF media in comparison to media A and the original GBF media formulation under continuous light conditions. All tested GBF media are 12.5% GBF diluted in effluent and salt water mixtures with 1x trace metals and 5g/L magnesium sulfate. The GBF media without salt also has no magnesium chloride and represents the original GBF formulation. A 1% vol/vol feed of GBF was completed for 4 or 12 days for the short feed and feed samples, respectively. Panel A describes the biomass production as optical density measured at 730nm. Panel B describes the biomass titer measured as dry cell weight (DCW). Panel C describes the glycogen content as a fraction of total biomass titer. Panel D describes the measured glycogen titer.

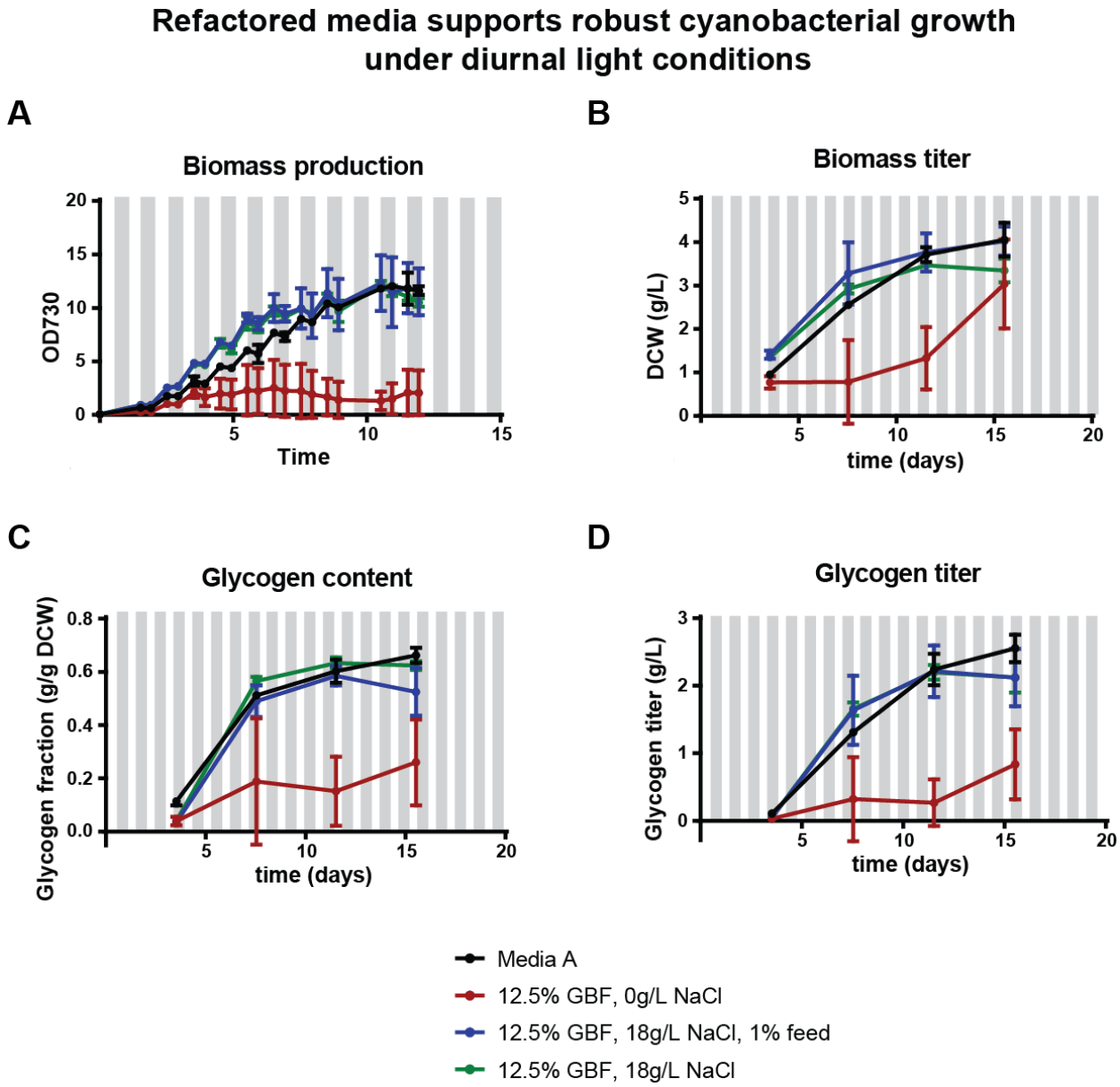

Figure 52: We tested the effectiveness of the refactored GBF media in comparison to media A and the original GBF media formulation under diurnal light conditions. All tested GBF media are 12.5% GBF diluted in effluent and salt water mixtures with 1x trace metals and 5g/L magnesium sulfate. The GBF media without salt also has no magnesium chloride and represents the original GBF formulation. A 1% vol/vol feed of GBF was completed for 0 or 4 days for the no feed and feed samples, respectively. Panel A describes the biomass production as optical density measured at 730nm. Panel B describes the biomass titer measured as dry cell weight (DCW). Panel C describes the glycogen content as a fraction of total biomass titer. Panel D describes the measured glycogen titer.

Testing mixed culture and microbiome effects indirectly

The increased instability in cultures grown in GBF media under diurnal light conditions led us to investigate potential effects of the microbiome and controlled co-culturing on cyanobacterial growth. We first considered analyzing the effect of the microbiome on the growth potential of *S.* PCC 7002 apart from the effect that it may have on the media itself. We tested this by inoculating new cultures from the grown cultures at the end of the diurnal light experiment testing the improved GBF media. We subcultured into both media A and into sterilized GBF media. We sterilized GBF through microfilitration to remove contaminating organisms and allow the cyanobacteria to grow with only the influence of the final microbiome present in the cultures of the diurnal light condition experiment. This should help to determine if the microbiome has increased the survivability in the media or has otherwise impacted the growth of the cyanobacteria.

This experiment provided a variety of interesting results (Figure 53). First, the cultures grown in GBF grew worse when subcultured into sterile GBF than the media A culture that was subcultured into media A. This could imply that the microbiome is critical to effective growth in GBF, that not enough non-cyanobacterial microbiome was transferred to the new culture, or that the microfiltration has removed some of the critical nutrients for growth. If the microbiome of GBF is critical to growth in GBF, this may give us more tools to improve cyanobacterial growth in wastewater. Second, the GBF grown cyanobacteria that are subcultured into media A do not grow at all. These cultures completely photo-bleached and did not recover over the measured growth period. I hypothesize that this is caused by an adaptation to growth in GBF that results in death when transferred immediately into media A. It might be possible to transition these cultures back to growth in media A by first transferring into a mixed media.

In addition, we decided to do controlled tests to show that co-culturing cyanobacteria with another organism could have an effect on the growth and biomass titer potential of the cyanobacteria. Theoretically, cyanobacterial co-culturing with heterotrophic organisms could increase overall culture growth. This occurs by the heterotroph consuming an excreted by-product of cyanobacterial

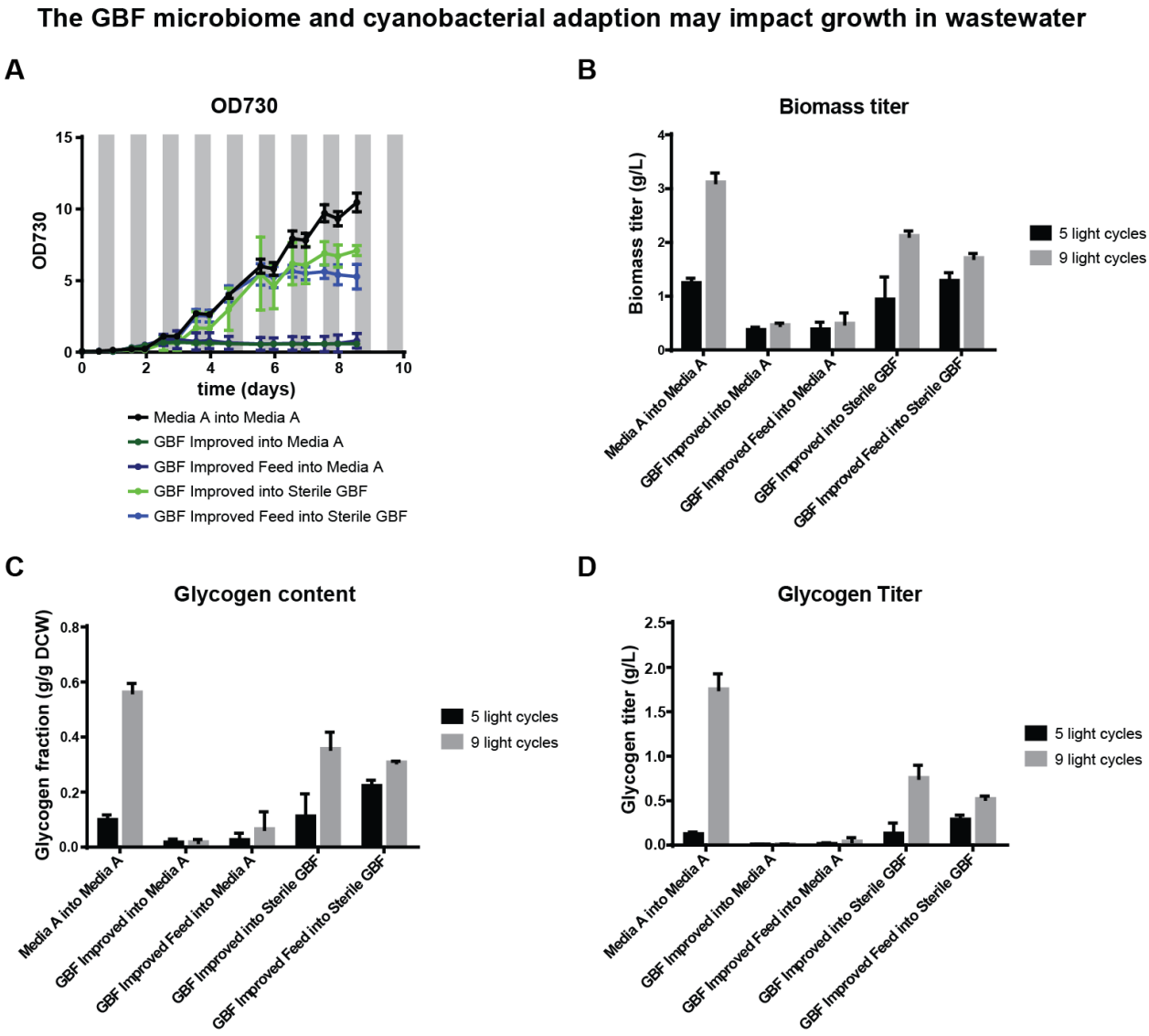

Figure 53: Estimated effect of the microbiome by sub-culturing from the cultures at the end of the diurnal GBF media experiment into either media A or sterilized GBF media. Panel A describes the biomass production as optical density measured at 730nm. Panel B describes the biomass titer measured as dry cell weight (DCW). Panel C describes the glycogen content as a fraction of total biomass titer. Panel D describes the measured glycogen titer.

growth and producing increased local concentrations of carbon dioxide in the media. The increased concentrations of carbon dioxide, in turn, allow for more efficient and faster uptake of carbon for the cyanobacteria.[3] This relationship can be symbiotic under the previously described conditions, but co-culturing has additional effects. If the cyanobacteria can utilize the excreted carbon source,

than the relationship may be less advantageous. In addition, the heterotrophic organism will absorb incoming light that could be used for photosynthesis by the cyanobacteria. This may mean that a low concentration of the heterotroph in the culture provides the greatest benefit to phototrophic growth. We co-cultured *S.* PCC 7002 with both *E. coli* and *P. putida* to see if growth benefits or penalties occur for the total culture. We decided to grow cultures with a 90% inoculum of cyanoabcteria and 10% inoculum of the heterotroph by optical density measurements in media A. This media lacks any carbon source for heterotrophic growth besides carbon captured and excreted by the cyanobacteria. These cultures were then grown under diurnal conditions for 10 days with biomass and glycogen production tracked.

Under diurnal growth conditions, the co-culturing with *E. coli* and *P. putida* have opposite impact on growing cyanobacteria (Figure 54). *P. putida* seems to provide a slight benefit when co-cultured with *S.* PCC 7002, while *E. coli* tends to reduce overall growth when co-cultured with *S.* PCC 7002. These effects are minor in comparison to the overall growth rate. In addition, the *E. coli* co-culture has a lower final glycogen content than the *P. putida* culture. This could be caused by more nitrogen remaining in the final media, which allowed for less time for glycogen production, or it could be that the ratio of *E. coli* in this culture is very high. This could result in lower relative glycogen levels because less of the total biomass accumulates glycogen.

Overall, we have identified a method to refactor wastewater media to support robust growth of *Synechococcus sp strain* PCC 7002. This approach adjust the salt water content and includes minor additives to make growth more robust. The refactored media supports robust growth instead of providing a toxic environment. Further, we show that this robust growth may be impacted by the microbiome present in wastewater media and that co-culturing cyanobacteria with individual heterotrophs can impact total biomass titer of the mixed culture. Overall, the use of wastewater can save money in an industrial setting and this data can support a technoeconomic analysis completed in Chapter 6 to evaluate the value of the refactored media.

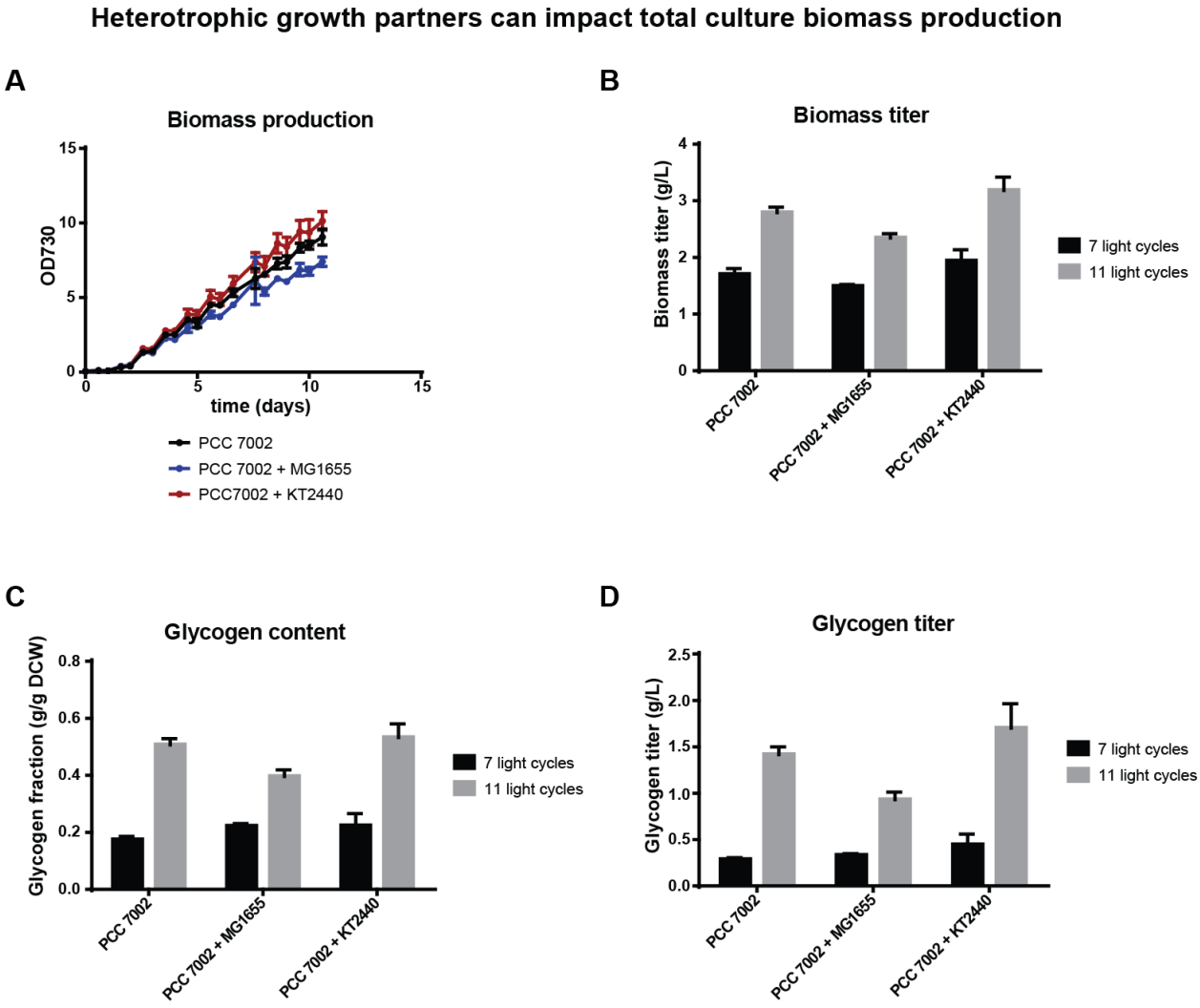

Figure 54: Proof of concent that mixed phototrophic/heterotrophic cultures can have variable overall growth rates. Cultures were mixed with either *E. coli* or *P. putida*. Panel A describes the biomass production as optical density measured at 730nm. Panel B describes the biomass titer measured as dry cell weight (DCW). Panel C describes the glycogen content as a fraction of total biomass titer. Panel D describes the measured glycogen titer.

Chapter 6: Construction and testing of an open raceway pond system for cyanobacterial growth

Introduction

In order to produce data that correctly mimics the growth rates and yields we expect when growing cyanobacteria at industrially relevant levels, we have constructed a small open raceway pond (ORP) system that imitates ORPs used for industrial algae growth.[4] These systems have more accurate geometry and growth conditions to mimic the scaled-up ORPs used in industrial algae growth. We can use the data from our system along with detailed measurements of system parameters to more closely estimate the titers and productivities we can achieve in an industrial setting. We have decided to construct and test a two 50-100L pond ORP system with tight control schemes and use these to probe cyanobacterial growth potential under industrial conditions. We follow a detailed description of the construction and modification of such a system with a short series of tests aimed at determining sacle-up growth factors for a technoeconomic analysis. Finally, we present a technoeconomic analysis of an industrial scale process for the production of cyanobacterial biomass, which incorporates data collected from Chapters 4, 5, and 6.

Design, construction, and modification of an open raceway pond growth system

The ORP system was originally purchased from MicroBio Engineering and contained the following parts: culture growth containers (the physical ORPs), supporting table, internal dividers for circular flow, impellers, probe holders, pH probes, temperature probes, diffuser stones, Apex controller and supporting units, CO2 manifold with attached solenoid valves, waterproof controller

[4]This work was done in collaboration with Hugh Purdy and Wenzhao "Tony" Wu. Hugh helped with ORP operation as well as sample collection and analysis, and Tony completed the technoeconomic analysis and associated figures.

housing, and controller support struts. In order to begin construction of the ORP system, we first had to meet safety requirements set forth by EH&S. We built a retaining wall to hold the maximum volume of liquid in the tub in case of a leak or critical tub failure. This wall and the floor were lined with a thick, double-layered waterproof tarp. This acts as secondary containment for any spills that may occur.

Figure 55: **Left:** The early ORP constructed within a retaining wall. The retaining wall acts as secondary containment in case there is a spill. **Right:** The plumbing system beneath the ORP is shown. This drainage allows for easy draining of the ORP after use or during cleaning.

Next, we needed to include tertiary containment in order to protect against secondary containment failure. This included protecting the entrances and exits to the laboratory as well as any drains in the floor from receiving any live cyanobacterial cells. We accomplished this by using automatically inflating sandbags that would stop fluid flow on contact with water. Within this containment setup, we assembled one table with two ORPs on top. We connected a set of temperature and pH probes to their appropriate controller components and secured them into each ORP using the magnetic probe holders. Finally, we placed the impellers into the ORPs aligned to induce circular flow around the internal barriers. This constituted the basic setup of the ORPs using the majority of the supplies that came with the system. In order to remove media or culture from the ORPs, we had to plumb the bottom of each ORP. This required assistance from Steven Shumacher in the machine shop, who bore holes into the bottom of the plugs for each ORP that were compatible with PVC fittings. We then used PVC connections to connect to a ball valve, a right angle turn, and

then a fitting for a hose. This allows for controlled removal of spent media and cells into separate containers to be bleached.

Figure 56: **Left:** The pH and temperature probes placed inside their magnetic probe holders. **Center:** Diffuser stone set on the bottom of the ORP. **Right:** Impeller fixed in place using magnets.

We decided to supplement this system by constructing a gas delivery system and adding a set of actuators for more effective control of ORP conditions. The gas delivery system was designed to deliver a stream of carbon dioxide that is diluted with air to a certain concentration. We connected a carbon dioxide tank and regulator to a mass flow controller (MFC) to allow for precise control of CO_2 delivery and maximum downstream pressure. Next, we connected the in-house air available within out lab to a pressure regulator and a second MFC. This allows for the same precision control of downstream pressure and mass flow of air. The only potential weakness in this system is the need to carefully balance the pressure upstream of each MFC. An imbalance in the deliverable pressure downstream under increased pressure drop requirements from the diffuser stones or other downstream elements could cause one MFC to be unable to control mass flow because the upstream pressure cannot overcome the pressure downstream from the MFC. This presents problems when a carbon dioxide tanks gets below the regulator pressure as it empties. After the pair of MFCs, we combine the gas flows and pump them to the two ORPs, splitting flow evenly between the two ponds and delivering the carbon dioxide through diffuser stones. The gas flow to the ORPs can be controlled through a manifold built into the controller box. This manifold is made up of a series of solenoid valves that can be opened or closed by the controller based on preset commands. We can use this system to create pH control against excessive carbon dioxide delivery by allowing carbon dioxide to vent to the room through an alternate solenoid valve instead of being delivered to the

ORPs. By setting the MFC flow rates, we can deliver 5% CO_2 continuously to the ORPs. This matches a low concentration from an industrial source. We are delivering carbon dioxide at a rate much higher than what should be required for effective carbon delivery to the culture for growth.

Figure 57: The gas delivery system where carbon dioxide from the compressed tank on the right and air delivered from the house air line from the left are mixed using a pair of mass flow controllers and a pressure regulator mounted to a wooden baseboard. Carbon dioxide concentration is controlled by the delivery rate of the two mass flow controllers and pressure is controlled by the lower pressure setting between the two pressure regulators.

Next, we considered approaches for controlling temperature of the entire system. There are a number of hurdles to temperature control in the lab setting for these ORPs. First, the systems are large and impacted by a number of variables, so the controller is likely to overshoot the temperature set points and the system will require large amounts of energy to change the temperature. Second, the room the ORPs are housed in has poor temperature control, meaning the system will need both reliable heating and cooling elements. Third, the lighting system we are planning to build out is likely to produce a large amount of heat. Finally, the controller cannot carry the high electrical load of some of the actuators we will need to use for temperature control.

Given that the amount of heat we will need to provide to the ORP system at any given time is relatively low, we decided to try using heaters designed for use in fish tanks. These heaters have a maximum temperature of around 84°F and have internal controllers. This allows them to be used through the controller or separately. These heaters are rated for large-sized fish tanks, so they have the ability to heat the ORPs. Our first two tests have shown consistent ability for the heaters to hold the ORPs at temperature with the lights on and most of the time with the lights off.

Figure 58: A 150W fishtank heater purchased to maintain temperature within the ORP.

Next, we designed a system for cooling the ORPs. First, we decided to use chilled water supplied to the laboratory as a simple cooling source. We wrapped tubing around the pair of ORPs and hooked one end to the water supply and the other to a drain. This would introduce continuous cold water to the tubing while the water was running. This system presented two difficulties. First, the continuous use of water is very wasteful. Second, the temperature of the water was cold enough to reduce the temperature of the ORPs, but the difference in temperature was low enough that changes were slow or the ORPs could not hold temperature. We then decided to make two separate upgrades to the chilling system. First, we were able to acquire a chiller to chill and recirculate cold water (4C). Next, we upgraded the tubing we used to wrap the tub to improve contact and heat transfer. Unfortunately, the power demands of the chiller were too great to consider using the controller as the power source. Instead, we needed to use a relay to allow the low-powered controller to control whether the high-power chiller had electricity. This relay required a power converter in order to run a direct current from the controller. Eric Codner helped us to design and implement the electrical changes required to make such a system work and provided us with the chiller.

Finally, we set up a lighting system to attempt to deliver high levels of light to the ORP system. We initially considered the purchase of either high lux fluorescent lights or very high lux LED strips. The LED strips were unfortunately cost prohibitive for this project and we decided to use fluorescent lighting. We purchased two 40,000 lumen grow lights to cover the area of the two ORPs. This should result in a lux of somewhere between 40,000 and 80,000 depending on the efficiency of light delivery, bulb brightness decay, and how the actual brightness compares to advertised brightness. We found after considering these factors, the ORPs receive an average lux of approximately 20,000. This represents a photon delivery of 15-20% the maximum brightness of the sun. We also wanted to have timing control over this system to be able to more closely mimic diurnal cycling. Unfortunately we lack automated methods for light dimming, but we could install timers for ON/OFF cycling. This mimics diurnal cycling, but is not as accurately as the programmable shaker that was used in GBF and glycogen production experiments.

Figure 59: A large recirculating chiller that uses a tubing wrap to maintain the temperature of the ORPs. The chiller is set to a constant 4°C and recirculates constantly when powered by the controller and relay.

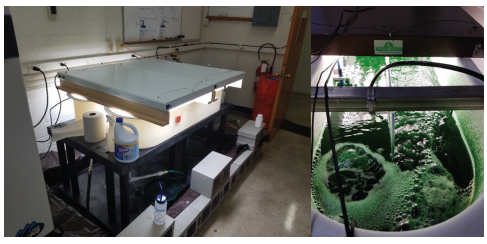

Figure 60: An image of the fully upgraded ORP system. This includes the upgraded brighter lighting that delivers light at volumetric delivery rates similar to the sun in an industrial system.

Methods

Cyanobacterial culturing

Cultures were grown in 50L of media A in the ORP system. The media A was prepared as salts added to deionized water without any form of sterilization beyond using deionized water. Water was first measured to the correct volume and then media A salts were added with the impellers running at 50% of maximum or 2,833RPM. The ORPs were then allowed to heat to 27C before being inoculated to a starting optical density 0.05 with cyanobacterial starter culture. Once inoculated, optical density measurements were taken 2 to 4 times daily, and biomass samples were taken twice a day. The biomass samples were used to determine biomass titer, glycogen content, and glycogen titer. Lights were set to be on continuously or for 12hr on/off cycles.

ORP turnover

The ORPs were shut down by draining the culture into 5 gallon plastic carboys to be sterilized with bleach. Sterilized cultures can be disposed of safely and the ORPs can undergo sterilization. The ORPs are surface sterilized with disinfecting wipes and ethanol. The plumbing is cleaned using bleach. Impellers, probes, probe holders, and heaters are cleaned using disinfecting wipes and soaking in an ethanol bath. Finally, any buildup of salts on the lighting is cleaned off with disinfecting wipes.

Biomass titer measurements

Biomass titers were estimated in one of two ways. First, we use optical density measurements with light at a wavelength of 730nm. This required sample dilution to within the linear range of the spectrophotometer used. Optical density (OD) measurements will detect both cell biomass and other components that absorb light. This becomes relevant when producing glycogen because OD730 measurements will detect glycogen as well as total cell biomass. Second, Biomass titers were also

directly measured through dry cell weight measurements. A pre-weighed conical tube is filled with a recorded volume of cell culture. The conical tube is centrifuged at 5000xg for 20 minutes. The supernatant is vacuum aspirated and the pellet is resuspended in 1 volume of water. Next, the suspension is centrifuged at 5,000xg for 20 minutes and the supernatant is vacuum aspirated. The samples are then flash frozen in liquid nitrogen or frozen overnight in a -80C freezer. Once frozen, the samples are lyopholized and final weights are measured.

Glycogen content and glycogen titer measurements

Glycogen content is measured by extracting glycogen as glucose from lyopholized biomass samples through hydrolysis. A direct biomass titer is calculated using the dry cell weight method described above. Next, 5-20mg of dessicated biomass is added to a 5mL glass reactor. To this, 1mL of 4% sulfuric acid is added. The reactor is sealed with a cap containing a second septa to prevent vapor loss during hydrolysis. The reactors are placed in a silicon oil bath at 121°C for 1 hour and then cooled in an ice water bath for 20 minutes. Samples are transferred into 1.7mL microfuge tubes, centrifuged for 10 minutes at 20,000xg, filtered through a 0.22um filter, and stored at -20C until analysis. This is based on the biomass hydrolysis process used by NREL.[69]

Glucose concentration of the hydrolyzed sample is measured using HPLC. A 5mM sulfuric acid mobile phase is used with a Rezek ROA-Organic Acid column. Samples are measured for 25 minutes using a refractive index detector detector and compared to a prepared standard curve.

Testing cyanobacterial growth in an open raceway pond

In order to test the ORP system and calculate scale-up parameters for technoeconomic analysis, we must grow a cyanobacterial culture under carefully defined conditions. The ORP system has the capability to run with continuous or diurnal light conditions, both of which provide interesting challenges to temperature control. The continuous light test will inform maximum growth rates and allow us to compare our growth system to smaller growth methods. The diurnal light condition gives an accurate estimate of growth expectations in an industrial environment.

We tested this system using wild-type *S.* PCC 7002 under continuous light at 27°C for one month. The cultures reach an average biomass titer of approximately 2g/L with a glycogen content of approximately 20%. This gives a total glycogen titer of only 0.4g/L, which is less than we had hoped for. There is a distinctly visible exponential phase in the optical density measurements. Once the exponential phase ends there is a very rapid transition to the linear growth phase and an extended growth retardation phase.

The geometry of an ORP in combination with our limited ability to supply light results in a slower cellular growth rate and lower cellular yields. The lower biomass titer also reduces the potential for starvation in media A because there is not enough cell mass produced to reduce the nitrogen below critical levels. This results in lower cellular glycogen content compared to growth conditions that allow for high cell density cultures. This could potentially be altered with brighter lighting conditions or lower nitrogen. On the other hand, out ability to measure light delivery per volume and growth under the geometry of an ORP allows for more accurate scale-up parameters for technoeconomic analysis.[14]

Large-scale growth being slightly slower does allow for a more detailed resolution of the growth cycle of cyanobacteria. Interestingly, we can resolve both the short exponential phase and the transition to linear phase growth more clearly than in faster, smaller growth conditions. Exponential phase seems to occur until an optical density of approximately 1.5. In that time, the cyanobacteria reach a much faster growth rate than seen at any other time during growth. There is a very rapid

switch into linear phase where the growth rate drops drastically. Theoretically, the very fast rate of growth at the end of the exponential phase could be used in a turbidostat-style photobioreactor to increase biomass productivity.

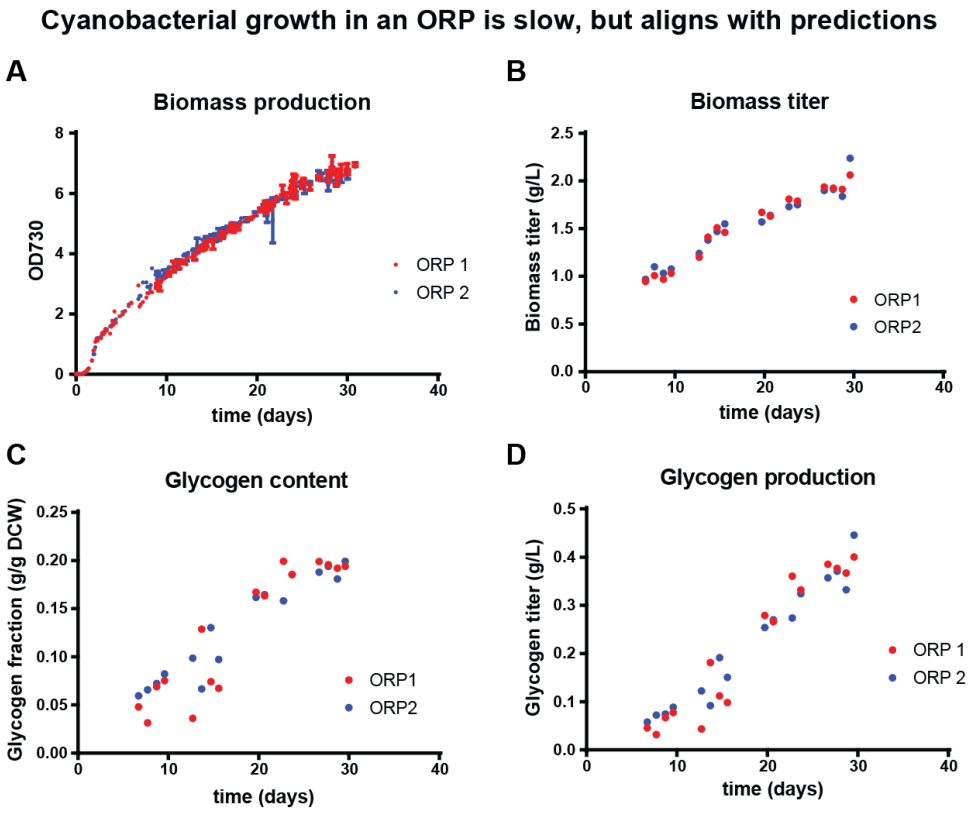

Figure 61: Results of cyanoabcterial growth int he open raceway ponds for 30 days under continuous light conditions. Panel A shows the biomass production as optical density measured at 730nm. Panel B shows the biomass production measured directly as dry cell weight (DCW). Panel C shows fractional glycogen content measured through biomass hydrolysis. Panel D shows glycogen titer measured as glucose.

The glycogen content of the ORP system under continuous light growth, 20%, in much lower than growth in shake flasks, glycogen contents closer to 70-80%. This difference in primarily due to lower light levels leading to less nitrogen consumption and less opportunity for nitrogen starvation. This difference, combined with lower biomass yields result in a much lower glycogen titer compared to improved growth conditions. One major consideration is that this system has a much lower light delivery than the same geometry in an outdoor system. The maximum delivery of sunlight in 5X to

6X stronger than this indoor ORP system, which offers a significant opportunity for higher density cultures. On the other hand, most outdoor ORP systems use an even poorer geometry.[57]

To test the productive potential of cyanobacteria in an industrial system, we grew a test culture under diurnal conditions. We used the 12 hour on/off light cycles, which will more closely represent an outdoor ORP system and make for more accurate predictions than a continuous light system. We predict a longer growth period, lower biomass titer, and lower glycogen titer. These effects will reduce economic viability of an industrial ORP system in our predictions, but will make for far more accurate estimates. We can see from optical density measurements that growth occurs in a similar fashion as with continuous light, but at a slower rate. There seems to be a lag after exponential phase. This could be caused by a night cycle during the transition to linear phase or possibly by growth of another organism. Given the consistency of the rest of the growth curve to phototrophic growth, contamination seems unlikely.

Biomass titers appear to be slightly more than half of the titer under continuous light. Further, the lack of biomass production did not result in enough nitrogen depletion to trigger a nitrogen starvation effect and induce buildup of glycogen within the cell. This can be seen by flat glycogen fractions within the culture and low total glycogen titers. These titers could be boosted by further nitrogen depletion of the media or increased light delivery. Natural sunlight would provide the boost in light necessary to achieve higher total biomass production and higher glycogen titers.

Overall, we have demonstrated the construction and successful testing of an open raceway pond system for cyanobacterial growth. We can now use the data from this section along with the expected improvements in biomass titer and glycogen fraction achieved from our metabolic engineering and media engineering efforts to create a technoeconomic analysis of this process. The use of an ORP system can provide higher accuracy data as well as the ability to test this geometry in an outdoor setting.

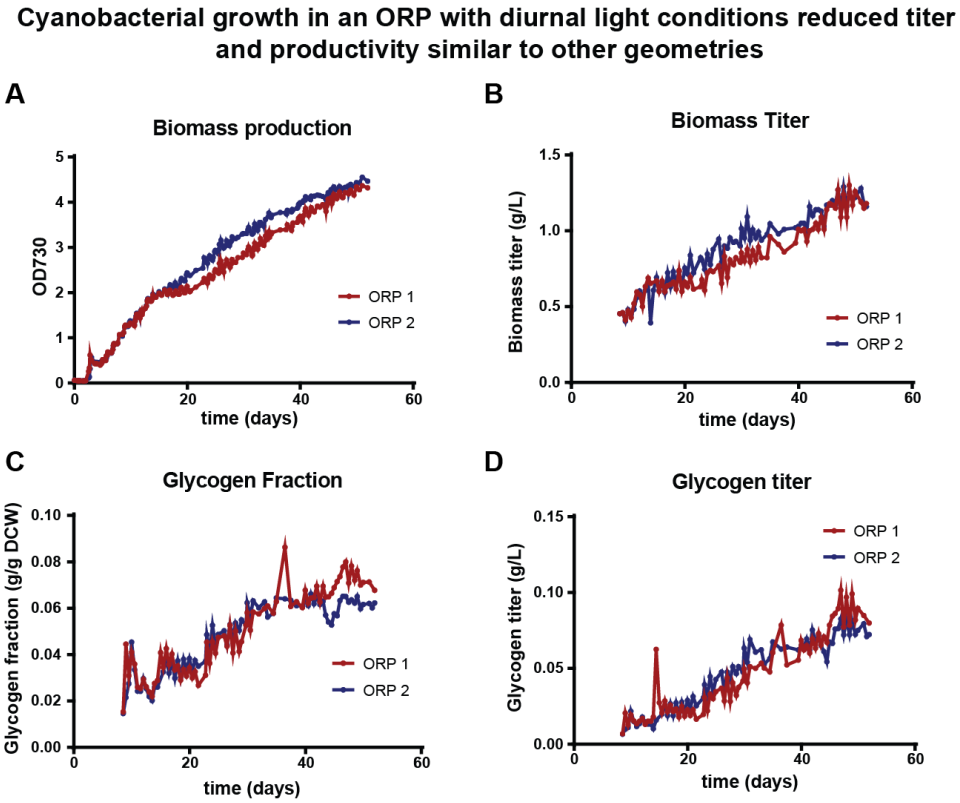

Figure 62: Results of cyanoabcterial growth int he open raceway ponds for 60 days under diurnal light conditions. Panel A shows the biomass production as optical density measured at 730nm. Panel B shows the biomass production measured directly as dry cell weight (DCW). Panel C shows fractional glycogen content measured through biomass hydrolysis. Panel D shows glycogen titer measured as glucose.

Technoeconomic analysis and scale-up factors

Using the data collected from the test runs in the ORP system, we can create a more informed and accurate estimate of the cost of producing glucose from cyanobacteria. In order to run a complete technoeconomic analysis of cyanobacterial growth and biomass collection, we need a range a parameters measured and compared to industrial conditions to adjust our predicted growth rates. The major factors we need to consider are the productivity and yield we were able to achieve under diurnal light conditions, the volumetric light intensity compared to outdoor sunlight, scalable flocculation parameters, and estimates of production targets to compare to another process. The first set of requirements can be found by taking the results from the ORP test runs and adjusting using the remaining parameters.

Previous Pfleger Lab work has elucidated a relationship between light intensity and maximum linear growth rate during the extended growth retardation phase.[14] This relationship is dependent on measuring the term $\frac{IS}{V}$, which is the measured light flux multiplied by the surface area and divided by the culture volume. This measurement is a volumetric measurement of light intensity and more accurately correlates with the amount of light reaching each cell. For the ORP system, light is delivered to 100L of media in a $1m^2$ area across both ORPs, which makes this calculation simple. With a light intensity averaging about 25,000 lux, this translates to approximately 12,000 umol/L/hr compared to approximately 18,000 umol/L/hr for sunlight in the geometry of an industrial scale ORP. This means that our estimates are within 2 fold of the light intensity delivered to an industrial ORP. This calculation does not consider light distribution and which photons are actually usable by a cyanobacteria, which may mean that outdoor growth is more efficient than our calculations. We can safely assume a 50% improvement in titer that will occur over a shorter time period. We measure a maximum linear growth rate of 4mg/L/day, which allows us to test the previous analysis in a scaled-up system. The two squares on Figure 63, adapted from previous work in the Pfleger Lab, represent the locations where the continuous light (upper) and diurnal light (lower) growth of the ORP system lies. The continuous light system is almost exactly in alignment with the

prediction. This validates Ryan Clark's approach to estimating phototrophic scale-up parameters as we maintained the expected relationship when moving to a much larger system.[14]

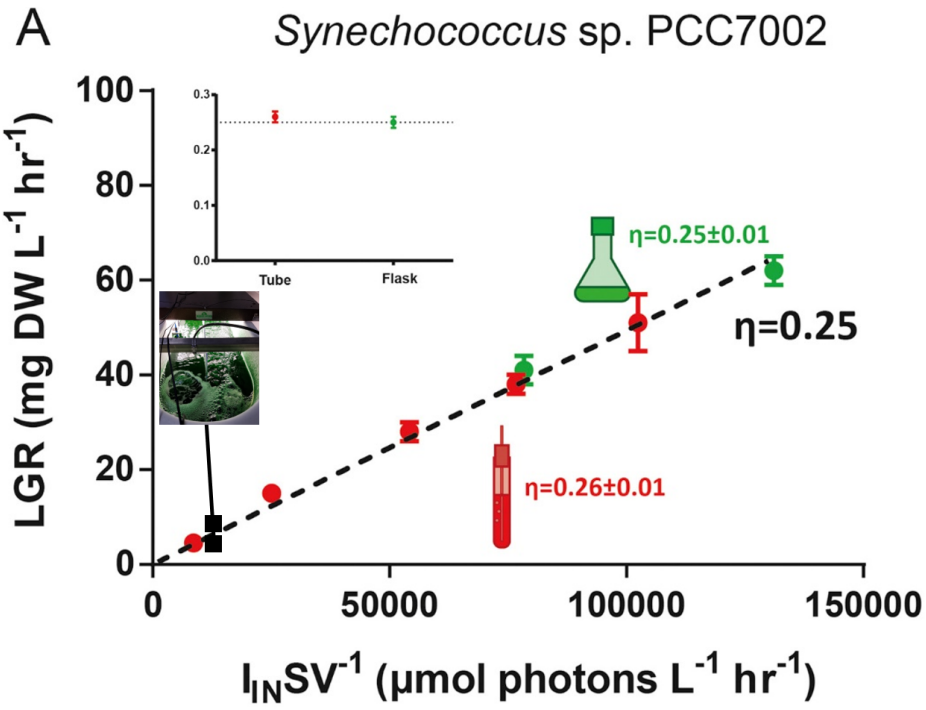

Figure 63: A figure showing how ORP volumetric light deliver compares to other growth systems used in our lab. Figure adapted from [14]

Next, we can calculate flocculation parameters based on the measured sedimentation rates in Chapter 4. These measurements, using stokes law, can allow for an estimate of floc size. Floc size can then be used as a variable to estimate separation costs. We will also use information about flocculant required to estimate the material costs associated with this process as well as information about optimal nitrogen levels to produce high glycogen biomass. This relationship allows for estimation of the nutrients that must be purchased for cyanobacterial growth. This also provides a point of reference to compare the use of wastewater. Growth in wastewater gives a mild benefit to growth, but should also reduce nutrient costs through the use of a waste stream from a wastewater treatment plant. We can represent this by simply decreasing the cost of the supplied nutrients. Finally, we used a series of studies on corn ethanol production and required carbon output

for such a system to use as a basis for the size of the production facility.

Based on this set of information, we constructed a technoeconomic model to represent this process shown in Figure 64. This structure uses nutrients and fresh water as well as recycled spent media to provide the growth medium. After growth for 30 days, we expect titers of approximately 1.8g/L. The culture is then mixed with calcium hydroxide, flocs are allowed to form for 30 minutes, sedimented, and then neutralized with sulfuric acid. This process matches the density of rehydrated corn starch at 300g/L.

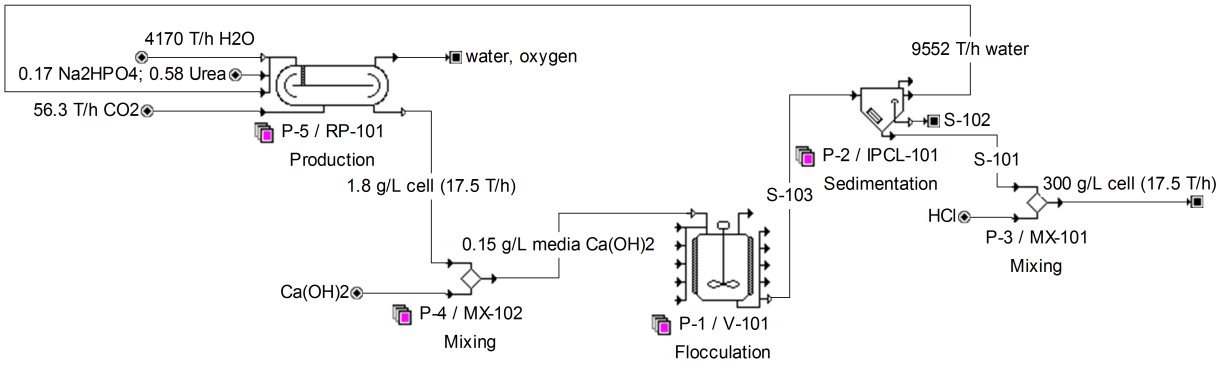

Figure 64: The design of the process for the production and concentration of cyanobacterial biomass to be hydrolyzed downstream.

This structure was used to evaluate 2 additional scenarios beyond the one described here in order to estimate the value of the improvements this work has achieved. The second scenario considers the use of wastewater as a nutrient source as well as using a $\Delta glgP$ strain. These alterations increase glycogen production and total biomass in the same growth time frame. The final scenario we directly evaluated is a system in which we grow cyanobacteria in very low nitrogen media with a short time to harvesting to achieve a very high productivity. This scenario will likely suffer from high separation costs while decreasing capital costs. These scenarios are summarized in Figure 65. Finally, we use case 1 as a reference point for a sensitivity analysis.

Case 1 is the base reference case and represent a standard growth process using purchased fertilizer for growth. This should represent the production potential of cyanobacteria currently

Entries	Units	Case 1	Case 2	Case 3
Cell titer out of pond	g/L	1.8	2.28	0.5
Product content in cells	wt%	70%	75%	75%
Residence time	days	30	30	3
Flocculated cells diameter (est.)	um	51	92	51
Nutrient cost	% of pure	100	50	100

Figure 65: Table describing the differences between the 3 case studies performed in this technoeconomic analysis. These cases vary in multiple areas making it difficult to compare to the original case using sensitivity analysis.

without any improvements suggested in this thesis. The cost breakdown of case 1 is shown in Figure 66. The overall cost for producing a concentrated biomass stream that could be hydrolyzed at low cost is $2.76/kg. This is substantially higher than the $0.60/kg cost of pure glucose or the $0.2/kg cost of preprocessed corn starch based on our calculations. The primary cost driver under our current parameter estimates is the capital expense of ponds, which is explained by the low productivity we estimate. Pond capital expenses are determined by the cost of constructing an ORP and the number of ORPs required to meet a constant production rate of biomass. These will be affected by any parameters that improve growth. Both water and sedimentation costs scale with higher volume to process, so decreasing the number of ponds needed for biomass production also decreases these other costs.

Case 2 is the case that combines the improvements we can make in growth and glycogen accumulation using growth on wastewater and the Δ*glgP* strain. These alterations help bring down capital costs by improving both glycogen accumulation and biomass titer. Further, flocculation occurs much more quickly in wastewater media. This scenario can represent the monetary improvement in glycogen production achieved by the work in this thesis. Figure 67 shows the cost breakdown for case 2. Case two shows significant cost savings over case 1. At a cost of $1.95/kg of biomass, this scenario cuts costs by nearly 30%. This improvement is primarily in two places. First, flocculation costs decrease significantly due to the use of a wastewater media. Second, biomass titer is higher in the same production window, meaning that average productivity is higher and the capital expense of pond construction is lower. This case still has enormous room for improvement in the productivity

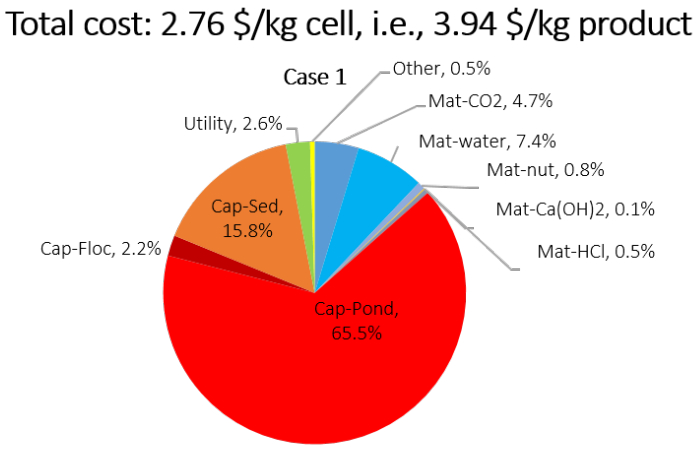

Figure 66: The total cost and cost breakdown for the production of cyanobacterial biomass using case 1 described in Figure 65.

to further improve capital expenses.

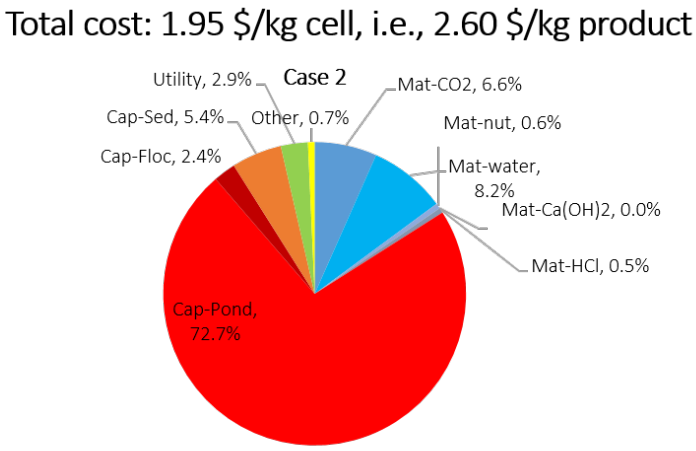

Figure 67: The total cost and cost breakdown for the production of cyanobacterial biomass using case 2 described in Figure 65.

Case 3 probes the scenario where cultures are harvested after a short growth phase with low biomass titer and high glycogen content. This offers increased average productivities aimed at decreasing capital costs. The results of this case study are shown in Figure 68. This case has the highest resulting cost of the three cases. The primary culprit for this case is a very large increase in

sedimentation cost. This increase is due to the high volume of low biomass titer culture that must be sedimented. This analysis assumes that decreased titers will have lower flocculation rates, which we have shown to be experimentally invalid. This scenario does have much lower capital expenses for pond construction than either of the other scenarios. If the low titer culture could be efficiently flocculated with a newer flocculation technology, then these costs could be much lower and offer a price near or even below case 2. Water costs are also significant in the scenario and would be possible to reduce with water conservation methods. This case could see further improvement if we added the advancements from case 2, which would improve sedimentation substantially.

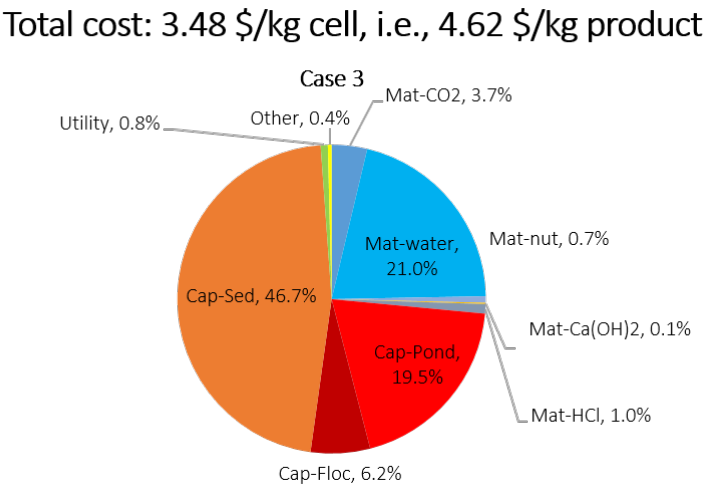

Figure 68: The total cost and cost breakdown for the production of cyanobacterial biomass using case 3 described in Figure 65.

Finally, we completed a sensitivity analysis of case 1 to investigate the economic benefit of different improvements. It is interesting to first note that most costs are not significant compared to out current challenges of separation and productivity. Nutrient and material costs all have a minimal impact on price even if available for free (Figure 69). Glycogen content does improve cost on a glucose basis, but not a total biomass basis.

Alternatively, flocculation and productivity are significant cost drivers (Figure 70). Even small improvements in these areas are worth significant cost savings. The strongest cost factor is total

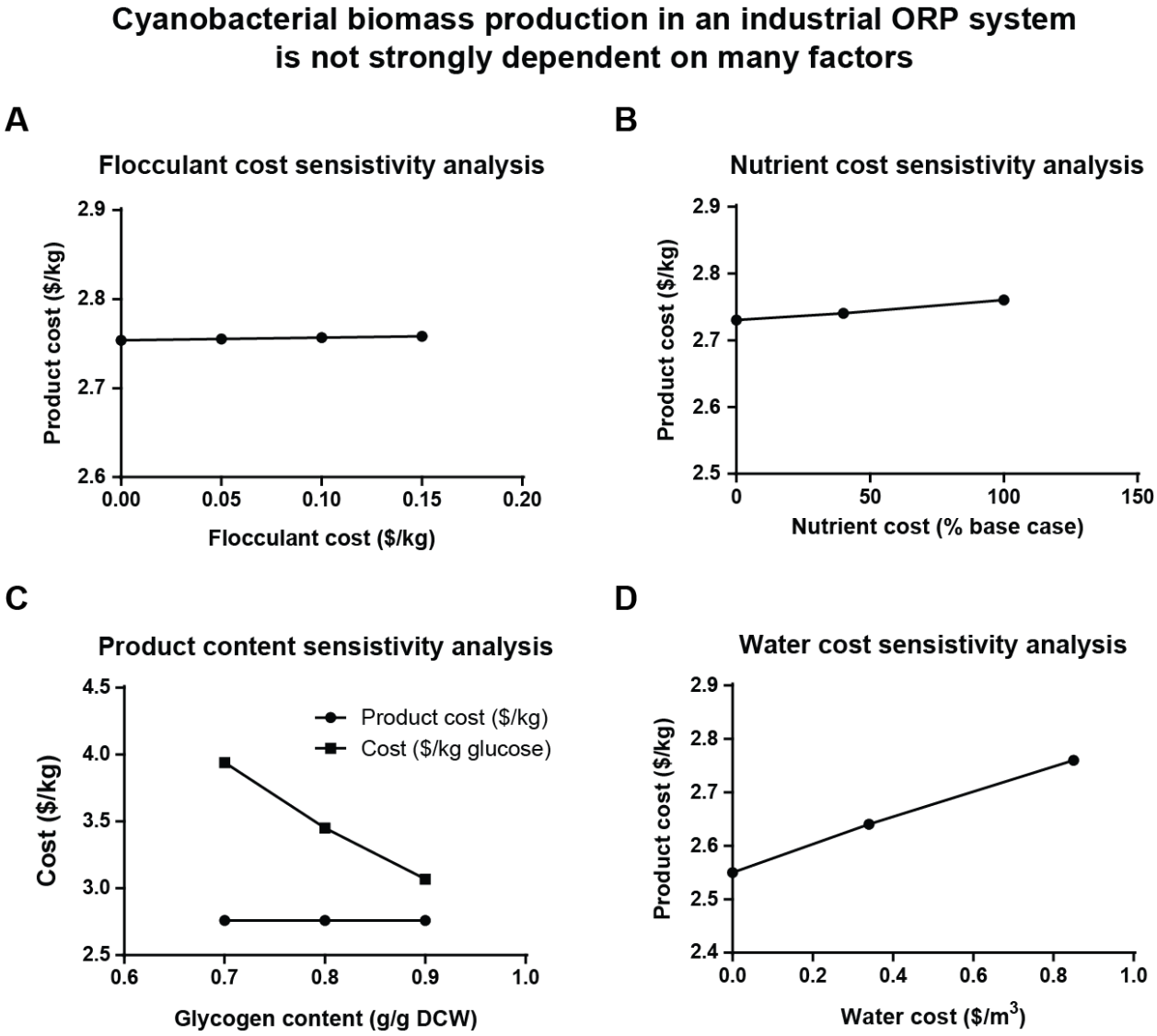

Figure 69: The sensitivity analysis of case 1 reveals that under our current production capabilities, product cost is not particularly responsive to many variables.

titer. This impacts the cost of flocculation and ORP capital expense, which are the main cost drivers. The second strongest factor is retention time. This only affects ORP capital expense by maintaining final titer and increasing productivity. Finally, flocculation improvements can drive costs down. In cases 1 and 2, this is a smaller factor, but in case 3 this is strongest cost driver.

Our system is currently limited by final titer, productivity, and flocculation costs

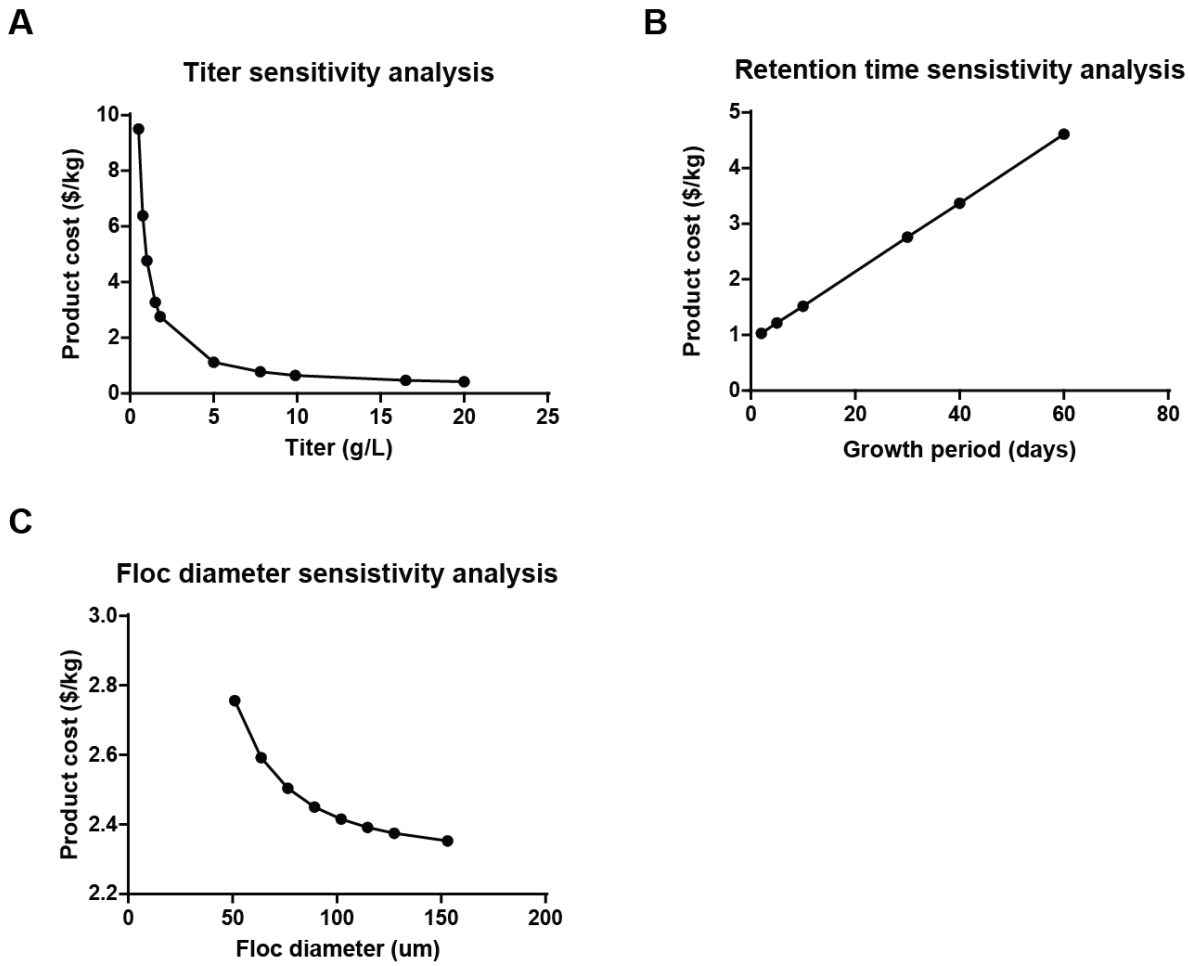

Figure 70: The sensitivity analysis of case 1 reveals that under our current production capabilities, product cost is responsive to some variables.

We can probe the individual effects of changing different production variables using the sensitivity analysis of the base case. For example, inclusion of baffling inside an ORP has been shown to increase biomass titer by up to 40%. We can estimate cost savings of $0.6-0.8/kg with this

variation alone if the capital cost is minimal. Further, alternate flocculation techniques can reduce sedimentation costs by up to $0.4/kg. Finally, choosing conditions or reactor geometries that reduce residence time has a linear effect on cost. Halving residence time without any increase in final biomass titer can decrease cost by $0.8-1.0/kg.

There are two potential products to compare our production cost to in this analysis. First, the direct product of interest is glycogen, which is converted to glucose when hydrolyzed, which has a price point of approximately $0.6/kg, based on bulk purchase prices. The other target of interest is simply cell biomass. This makes up the non-glycogen part of biomass and can be used as a replacement for yeast extract. We can use the $\Delta glgC$ to achieve a strain of cyanobacteria that accumulates no biomass. Yeast extract has a wider range of prices that average about $0.6/kg, based on current bulk purchase prices. These price points are both well below what we can currently achieve with this production system. The most significant barrier to production is the technical hurdles around $\frac{IS}{V}$ level. Building low cost growth systems with higher volumetric light delivery will increase productivity and titer.

This technoeconomic analysis lays a clear foundation to guide cyanobacterial growth improvements for industrial applications. Although the lowest cost for the production of cyanobacterial biomass that we can calculate, $1.95, is much higher than current glucose or yeast extract prices, we now understand what areas pose the largest technical challenges and best opportunities. This analysis points us to increasing biomass titer, biomass productivity, and sedimentation rates as the areas ripe for improvement. Further, we can estimate the value of this body of work at a 30% reduction in cost for production of algal biomass, which is a substantial improvement over the calculated base case before this work.

Chapter 7: Conclusions and future research directions

Conclusions

This body of work has made progress in understanding and improving feedstocks used in industrial bioprocesses. In Chapter 3, we analyzed potential replacements for glucose as a carbon source for biocatalytic processes. We identified methane and acetate as low cost alternatives to glucose. Under current market prices, we can eliminate methanol as a relevant feedstock to replace glucose. Following this analysis, we explored a range of engineering approaches to improve the intracellular production of glycogen in the cyanobacteria *Synechococcus sp. strain* PCC 7002 in Chapter 4. We showed a 20% increase in glycogen content under diurnal light conditions and eliminated a number of alternate methods for glycogen accumulation. We also showed the nitrogen dose within a cyanobacterial culture can control glycogen production and biomass yield, providing a better understanding of nitrogen starvation as a tool for industrial-scale glycogen production. Further, we show that cyanobacteria can be flocculated, sedimented, and hydrolyzed under industrially relevant conditions as well as support growth of heterotrophic bacteria. Next, we refactored wastewater media to support robust cyanobacterial growth under both continuous and diurnal light conditions in Chapter 5. This advancement allows for low cost biomass production due to decreased nutrient costs, faster flocculation, and increased biomass production. Finally, in Chapter 6, we demonstrate a scaled-up open raceway pond system that can provide accurate data for a complete technoeconomic analysis of cyanobacterial biomass production. The technoeconomic analysis shows that the improvements in glycogen production made in this work decrease production costs of cyanoabacteria at industrial scales by 30%.

Future directions for this work

This thesis has laid the foundation for future work to elucidate more information about the selection, analysis, and engineering of feedstocks for industrial bioprocesses. While I can say I wish I had more time to learn all of the details that there are to learn about my research and about the effect it could have on the world at large, I recognize that research is an institutional art. My work is based of the work of those that came before me, and I can only hope my work will provide some basis of knowledge for another researcher to expand upon. Here I will describe some of the directions I believe are promising and could yield more valuable information about industrial bioprocess feedstocks.

My work in metabolic modeling and its associated economic analysis is not inherently groundbreaking. It is just a thorough analysis that allows for quick comparisons between feedstocks. This framework would allow for quick comparisons between feedstocks, ignoring downstream costs, for rapid decisions about feedstock choices. This could be expanded to new feedstocks and new organisms without any alterations. The deeper expansion on this work would be to complete the technoeconomic analysis of the downstream effect of changing feedstocks. If it was possible to predict downstream costs for a range of products under each feedstock, then a full effect of feedstock selection on cost could be achieved. It might be possible that within certain categories of products, the same consistent ratio of cost from one feedstock to another holds, independent of specific product within the class. This would require that the set of products within a class hold to a consistent set of unit operations for purification.

The other major expansion on this work that could be valuable is evaluating substrate mixtures to divide energy production and carbon conversion to products. This would open the door to using low cost substrates, such as methane, for their energy and reducing power alone. This could act as the powerhouse for carbon efficient conversion of another more complex carbon substrate into a value-added chemical. An approach like this could help to fix energetic and reductive imbalances within biosynthetic pathways and possible improve yields. Understanding if this type of system

could work well and if there would be a need for metabolic isolation of the energy providing substrate could prove to be a valuable undertaking.

Our work in metabolic engineering of *Synechococcus* PCC 7002 has multiple potential expansions upon the work I have completed. The overexpression of the complete glycogen synthesis pathway in tandem with the *glgP* knockout could drastically increase glycogen accumulation under diurnal conditions. This enhanced accumulation could result in higher titers of glycogen, higher intracellular glycogen content, or possibly much higher productivity. All of these improvements would decrease costs further for cyanobacterial glycogen production.

This could be taken one step further by engineering the master nitrogen regulator for continuous signaling for glycogen production. We would likely have to complete this as an inverse to the project where the master nitrogen regulator was engineered to bind to only a single signaling partner and avoid signaling towards glycogen production. To complete such a task, the engineered regulator would have to be inducibly expressed, while the natural regulator would need to be rapidly degraded. This creates the need for development of both rapid protein degradation and improved induction tools for the cyanobacterial toolbox. Successful implementation could allow for a culture to have a faster growth phase followed by an efficient glycogen conversion phase. Its possible that this would improve yield and overall productivity. Unfortunately, the very low biomass titers derived from cyanobacterial growth in an open raceway pond would limit the applicability of this approach. This work would create a better strain, but it would still require that an improved industrial growth system be used to harness that production potential.

One of the advancements that personally excited me the most is improvements in flocculation and sedimentation. While this analysis shows separation is not the largest cost driver in our case study, it quickly becomes limiting as growth limitations are overcome. I believe investigating self-flocculation techniques, specifically the use of a covalent bond forming protein pair called SpyTag/SpyCatcher.[89] This protein pair creates a covalent bond that would link bacterial cells together. This technology could work by surface displaying each protein on a different cyanobacterial

strain constitutively. These strains would be grown in separate ORP or PBR systems, mixed en route to a sedimentation tank, and then undergo rapid sedimentation. There is one major challenge to this effort: effective surface display of the SpyTag and SpyCatcher proteins. This could be attempted by integrating each protein into proteins already displayed on the cyanobacterial membrane surface using long flexible linkers. These could even be separately expressed copies of native genes to avoid disrupting native gene activity. Based on unpublished work I have encountered at a conference, the flocculation rate of mixed cells surface displaying these proteins is much faster than any system shown here, which could drop flocculation costs both through lower material costs and much higher sedimentation rates. This could possibly make case study 3 more economically viable or allow for alternate continuous separation technologies to be used.

The efforts discussed in the growth of cyanobacteria in municipal wastewater derived media sets the groundwork for better understanding of how this nutrient source affects growth. Deeper studies of the live microbiome within the gravity belt filtrate (GBF) stream as well as how this microbiome changes upon interaction with cyanobacteria can help us to understand the strengths and weaknesses of this low-cost feedstock. It could be possible to clearly identify the organisms that benefit cyanobacteria growth and those that are detrimental. Further, overall analysis of the outputs within a wastewater treatment plant may be able to identify additional or alternate feedstock streams that are more nitrate and phosphate balanced for nutrient removal by cyanobacteria. Alternatively, maybe effective phosphate removal from spent GBF media can be removed more efficiently than recycling through the wastewater treatment plant. Although technoeconomic analysis has been completed to study integrated algal growth and wastewater treatment facilities, these studies do not often consider the details of algal growth potential outdoors.

Finally, our work in establishing and testing a lab-scale open raceway pond system has laid the groundwork for collecting accurate and detailed data about cyanobacterial growth under industrial conditions. As this thesis has shown, cyanobacterial growth varies greatly with the geometry of the growth system and the intensity of the light provided for growth. Most cyanobacterial research is

performed used extremely optimized conditions that are clearly not present in industrial settings. The ORP system allows for more accurate studies on growth potential under industrial growth conditions. With this basis, our work could be expanded in many ways. First, the ORP system could be moved outdoors to get a more accurate understanding of the effect of sunlight on the growth system. An intermediate step that reduces contamination risk would also be growth within a closed greenhouse. These experiments could validate our expectations for cyanobacterial growth in sunlight. In addition, detailed studies about the effect of nitrogen starvation on productivity under this alternate geometry could help establish a better model of glycogen production in relation to nitrogen starvation. Further, testing cyanobacterial growth in an ORP with wastewater media could show the scalable benefits of growth within wastewater. This experiment has a number of safety concerns that would need to be addressed for implementation. Finally, I think there is great value in testing different cyanobacterial strains under growth conditions in an ORP. This could help us to understand what the production potential between cyanobacterial strains is under industrial conditions. I would suggest comparing a number of model and fast-growing cyanobacteria and algae.

Appendices

Fast-folding, fast-degrading fluorescent protein design

At the start of my graduate career, I joined the Pfleger Lab and joined a project focused on better understanding how we can use transcription activator-like effectors (TALEs) as gene expression tools in *E. coli*. I was given a small role on this project to make a highly responsive reporter protein.[5] We needed a tool to rapidly identify changes in gene expression for both expression increases and decreases. This meant the protein needed to be expressed quickly and needed to stop providing a signal if expression stops.

I decided to find a fast expressing fluorescent protein variant, which would express quickly after induction. I decided to acquire a green fluorescent protein (GFP) variant called superfolder GFP (sfGFP). This reporter was designed to fold quickly and thus give a very rapid signal. Next, I needed to find a way to either induce rapid degradation of the reporter, or naturally have a high basal degradation rate of the reporter. I achieved this by adding a C-terminal ssrA tag for the native *E. coli clpXP* protein degradation system. This system can identify proteins with the ssrA tag and rapidly deliver the proteins to proteasomes for degradation. This system would result in continuous degradation of the reporter protein, such that any decrease in expression should result in an analogous decrease protein level and, thus, fluorescence.

To test this system, we grew samples in a 96-well plate comparing the tagged and untagged versions of sfGFP under a trc IPTG-inducible promoter. The samples were grown with IPTG for 6 hours before one set of samples were washed twice with fresh media containing no IPTG and the other was washed with IPTG containing media. Then growth and fluorescence were measured for an additional 18 hours. Under the conditions in which the culture was washed with IPTG (the control) both the ssrA tagged and untagged strains show fluorescence. The fluorescence of the untagged strain is much higher than that of the tagged strain. This is presumably because active degradation

[5]This work was done in collaboration with Dr. Matthew Copeland.

results in a lower steady state concentration of the sfGFP with the ssrA tag. Next, we can compare this result to when we wash the cultures with fresh media containing no IPTG. Under this condition, the untagged sfGFP strain has slowly increasing and then very steady fluorescence, while the ssrA tagged sfGFP strain has decreasing fluorescence to a very low steady state. This system would be best compared to an uninduced culture for a baseline fluorescence of the lac system, but it appears that most of the protein was degraded in a short time frame. Although this could happen more quickly, this does show the successful construction of a fast-folding, fast-degrading reporter protein that can be used to evaluate the effectiveness of different gene expression tools.

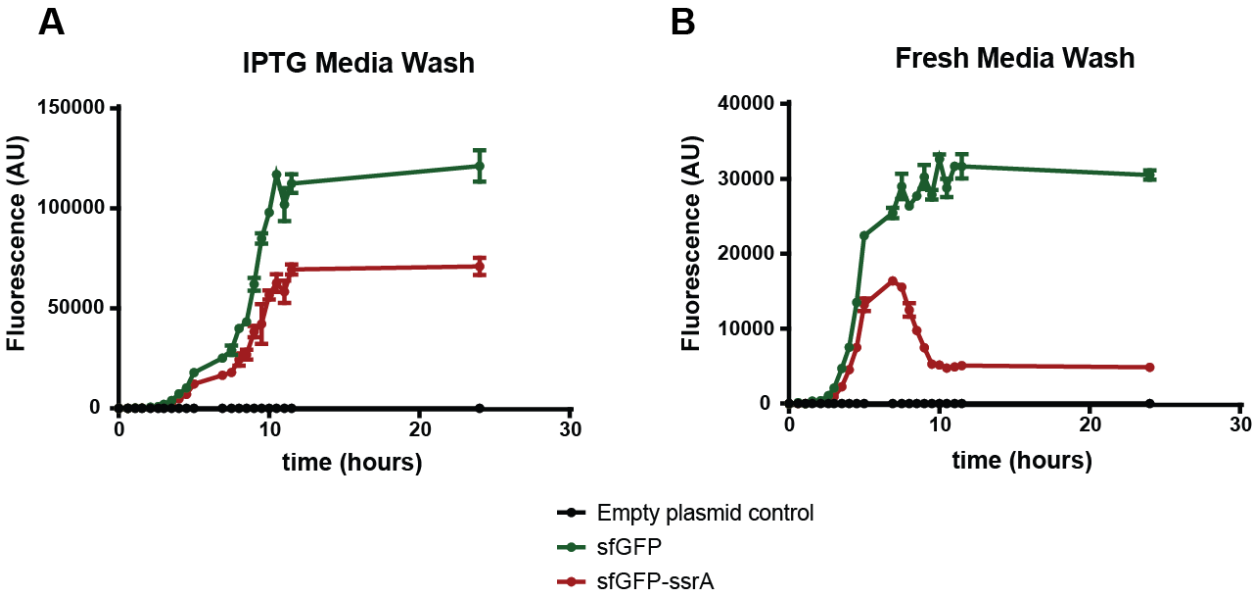

Figure 71: The fluorescence of ssrA tagged reporter proteins over a growth phase with inducer maintained (left) or removed (right)

Design and initial implementation of a terminator library in *Synechococcus sp. strain* PCC 7002

A previous Pfleger lab member made an observation that *Synechococcus* PCC 7002 expression of the reporter protein yellow fluorescent protein (YFP) was consistent between different integration

sites when using an inducible promoter, but inconsistent when using a constitutive promoter.[6] This was an interesting observation given that the difference between the two promoters was only the presence of the lac operator sites. These sites appeared to act as insulators to avoid read-through from upstream transcriptional activity. This insulation effect can be vital for effective gene expression when consider multiple integrations into the same genome. This motivated our interest in discovering effective insulation elements for *S.* PCC 7002.

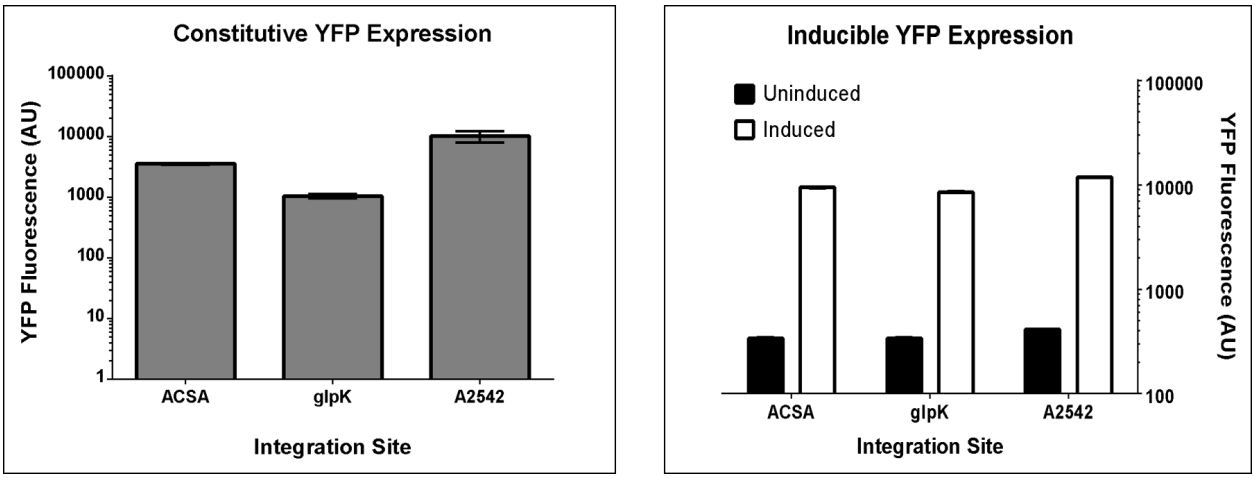

Figure 72: This compares data collected by Dr. Christopher Jones (left) and Andrew Markley (right) showing that expression from uninsulated sites (left) is variable, while expression from insulated sites (right) is not.

The most common insulating element is the use of a terminator. Often genomic insertions will include flanking terminators to reduce read-through into the integrated cassette. This protects against expression of repressed elements, production of non-sense proteins, or disruption of carefully balanced systems. Given that *S.* PCC 7002 is a prokaryote, it makes sense that we can use commonalities to *E. coli* to probe for insulators. We decided to take advantage of the work from the Voigt Lab at MIT to make and test a large library of terminators in *E. coli*.[10] This was a large library covering many natural *E. coli* terminators as well as a variety of synthetic terminators. The data was used to create a computational model of termination in bacteria.

[6]This work was motivated by observations by Dr. Chistopher Jones using data collected by both Dr. Jones and Dr. Andrew Markley (Figure 72). The initial progress on this project was made as a collaborative effort with Alexander Steiner.

We decided to run a comparison of a small set of the terminators from the Voigt Lab analysis in *S.* PCC 7002 in order to compare termination efficiency and rank order of terminator strength. There were 9 terminators and the spacer control stored in the online plasmid repository, Addgene. We ordered this set of plasmids and adjusted the system for *S.* PCC 7002. In the original screen, terminator strength was determined by placing a terminator to be tested between two fluorescent proteins.[10] The difference in the fluorescence ratio of these reporters between the strain with a terminator and a control strain containing a spacer gave a measurement of terminator efficiency. The original screen used GFP and red fluorescent protein (RFP). We have been unsuccessful in integrating any RFPs into *S.* PCC 7002. Instead, we switched the downstream RFP to YFP. Although YFP is more likely to have some leakage with the GFP detection and visa versa, both reporters can be expressed in our cyanobacteria.

After adjusting the original set of plasmids, we then moved each expression cassette onto a cyanobacterial integration plasmid for the *glpK* locus. We used natural transformation ability of *S.* PCC 7002 and gentamycin selection to integrate each cassette into the *glpK* locus. Integrations were confirmed by colony PCR to by homogeneous. We then measured the fluorescence of each reporter after 24 hours of growth under continuous light conditions for both the integrated cyanobacterial system and the same system on a plasmid in *E. coli*. This was completed in 96 well plates using a Tecan M1000 plate reader with GFP and YFP excitation/emission wavelengths of 485/510nm and 510/530nm, respectively. This differs significantly from the use of flow cytometry for more detailed analysis, but should work effectively for an initial estimate. Termination strength is measured in AU and is calculated using the following formula.

$$T_s = Averageof\frac{GFP_{term} - Avg(GFP_0)}{YFP_{term} - Avg(YFP_0)} \tag{7}$$

Below are a set of measurements taken by Alex Steiner to determine terminator strength (Figure 73). The most obvious result of this data is that our measurements are much less sensitive to

variations in termination strength than those taken using flow cytometry (small variations instead of orders of magnitude). This could be due to the measurement method or it could be due to the chosen reporters. The control measurements are very low for both measurement in *E. coli* and *S.* PCC 7002. The highest termination strength from the Voigt Lab measurements is one of the highest strength terminators in our measurements. The easiest way to compare this bulk data is the use of a Spearman rank correlation. This compares the rank order of the terminators by strength as opposed to using the raw values. The correlation between the Voigt Lab analysis in *E. coli* and ours was 0.82. This means our method is capturing terminator strength variation, despite being less sensitive. Further, the correlation between the Voigt Lab *E. coli* data and our *S.* PCC 7002 analysis shows a correlation of 0.75. This is a reasonable correlation given the difference in measurement technique and species. This may imply that termination systems between the two bacteria are very similar and the Voigt Lab terminator analysis may be directly applied in *S.* PCC 7002.

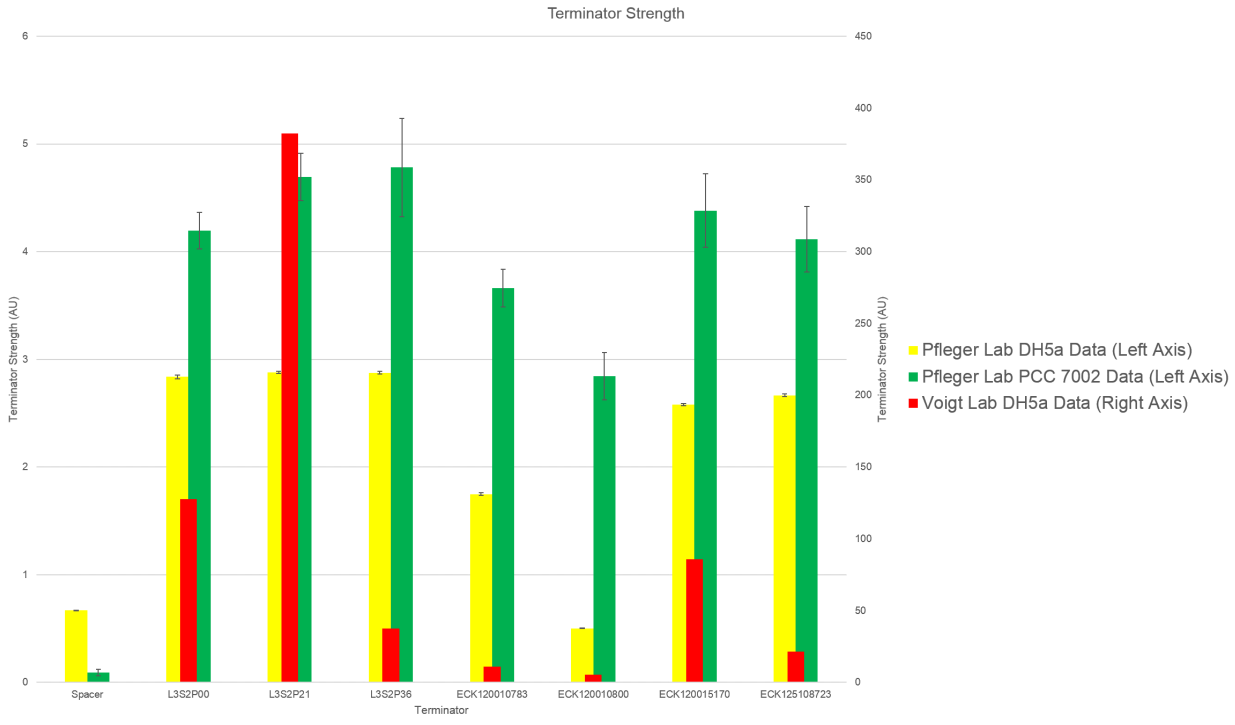

Figure 73: Analysis by Alex Steiner showing the measured variation in termination strength from a set of *E. coli* and synthetic terminators.

After completing this analysis, Alex realized that the strains he constructed for this experiment had mutations in some key areas for a subset of the constructs. This means this promising data would need to be re-analyzed once the mutations were repaired. We decided to pass this project onto two people in the Pfleger Lab that would be here long-term to see the project through testing terminators using flow cytometry and testing a wider range of terminators.[7] This would give us a better comparison to the results obtained by the Voigt Lab and open the door to a better understanding of termination in cyanobacteria. We have laid out a plan to test for termination strength for a number of constructs that probe different aspects of bacterial termination. We have seen in transcriptome-wide RNAseq analysis that termination efficiency seems to be generally low in cyanobacteria, which may imply that analogous terminators will have different strengths between *E. coli* and cyanobacteria, but may still maintain a relative strength. This would be the value of using Spearman rank correlation on a larger set of more carefully measured integrands.

Supplemental data and figures

[7] Dr. Michael Engstron and Francesca Gambacorta will be taking over this project to see it through to completion

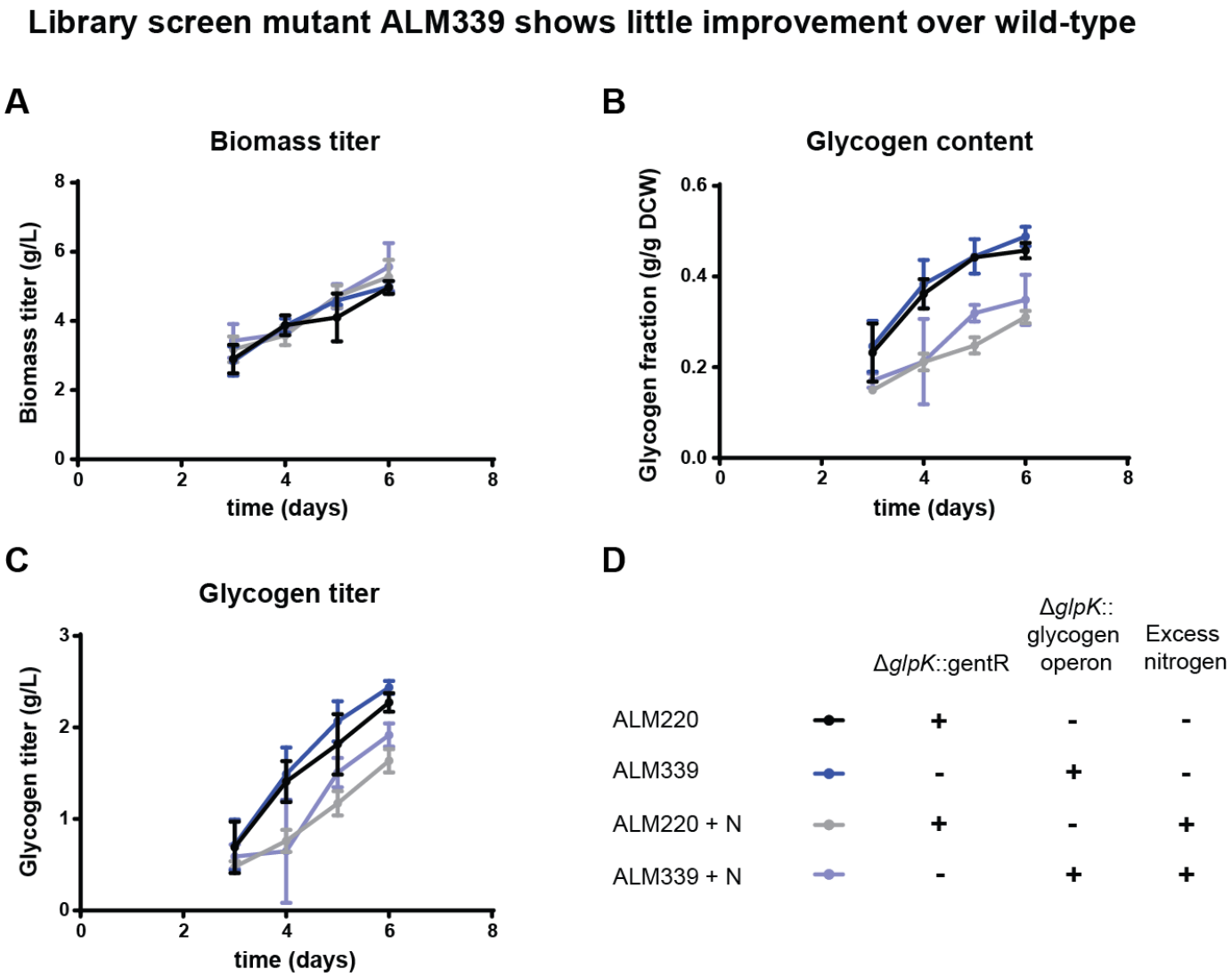

Figure 74: Biomass and glycogen production by *S.* PCC 7002 strains under continuous light conditions in media A. This experiment investigates the effects of the random mutant from the glycogen screen library on glycogen production. Panel A shows the biomass production measured directly as dry cell weight (DCW). Panel B shows fractional glycogen content measured through biomass hydrolysis. Panel C shows glycogen titer measured as glucose. Panel D describes the genotypes and media conditions of the strains measured in Panels A-C.

Maximum ATP Hydrolysis in mmol/gDW/hr per mmol/gDW/hr Substrate							
	C1 Pathways	Glucose	Methane	Methanol	Acetate	Glycerol	Xylose
E. coli	None	19.75	0	0	5.125	11.25	16.208
	RuMP	19.75	3.292	4.667	5.125	11.25	16.208
	DHA	19.75	3.292	4.667	5.125	11.25	16.208
	Serine	19.75	3.25	4.625	5.125	11.25	16.208
	All	19.75	3.292	4.667	5.125	11.25	16.208
S. cerevisiae	None	17	0	0	4		
	RuMP	17	2.833	3.958	4		
	DHA	17	2.25	3.375	4		
	Serine	17	2.25	3.375	4		
	All	17	2.833	3.958	4		
S. PCC 7002	None	30	0	0	8	15.25	
	RuMP	30	5.5	8	8	15.25	
	DHA	30	5.5	8	8	15.25	
	Serine	30	5.5	8	8	15.25	
	All	30	5.5	8	8	15.25	

Figure 75: ATP hydrolysis rates under different conditions for the FBA scenarios used in Chapter 3.

Name	Reaction	Pathway
aox1	methanol + oxygen --> formaldehyde + hydrogen peroxide	All C1 assimilation pathways
aox2	methanol + NAD+ --> formaldehyde + NADH + proton	All C1 assimilation pathways
aox3	methanol + NA(P)D+ --> formaldehyde + NAD(P)H + proton	All C1 assimilation pathways
mmo1	methane + oxygen + NAD(P)H + proton --> methanol + water + NAD(P)+	All C1 assimilation pathways
mmo2	methane + oxygen + NADH + proton --> methanol + water + NAD+	All C1 assimilation pathways
dha1	xyulose 5-phosphate + formaldehyde --> dihydroxyacetone + glyceraldehyde 3-phosphate	DHA
rmp1	ribulose 5-phosphate + formaldehyde --> hexulose 6-phosphate	RuMP
rmp2	hexulose 6-phosphate --> fructose 6-phosphate	RuMP
ser1	formaldehyde + tetrahydrofolate --> water + 5,10-methylene-tetrahydrofolate	Serine
ser2	5,10-methylene-tetrahydrofolate + water + glycine --> serine + tetrahydrofolate	Serine
ser3	serine + glyoxylate --> glycine + hydroxypyruvate	Serine
ser4	hydroxypyruvate + proton + NAD(P)H --> glycerate + NAD(P)+	Serine
ser4b	hydroxypyruvate + proton + NADH --> glycerate + NAD+	Serine
ser5	glycerate + ATP --> 2-phosphoglycerate + ADP + proton	Serine
ser6	malate + ATP + Coenzyme A --> malyl-CoA + ADP + Inorganic Phosphate	Serine
ser7	malyl-CoA --> glyoxylate + acetyl-CoA	Serine
ser8	glyoxylate + 2 water + 2NAD(P)H --> acetyl-CoA + proton + Coenzyme A + 2 NAD(P)+	Serine, represents a set of poorly understood pathway steps
ser8b	glyoxylate + 2 water + 2NADH --> acetyl-CoA + proton + Coenzyme A + 2 NAD+	Serine, represents a set of poorly understood pathway steps
cof1	formaldehyde + water + 2 NAD(P)+ --> carbon dioxide + 2 NAD(P)H	Formaldehyde detoxification
cof2	formaldehyde + water + 2 NAD+ --> carbon dioxide + 2 NADH	Formaldehyde detoxification

Figure 76: The formaldehyde assimilation and detoxification pathways added to each genome-scale metabolic model used in Chapter 3.

Name	Reaction	Pathway
but1	2 acetyl-CoA --> acetoacetyl-CoA + coenzyme A	butanol from acetyl-CoA
but2	acetoacetyl-CoA + NADH + proton --> (S)-3-hydroxybutanoyl-CoA + NAD+	butanol from acetyl-CoA
but2b	acetoacetyl-CoA + NAD(P)H + proton --> (S)-3-hydroxybutanoyl-CoA + NAD(P)+	butanol from acetyl-CoA
but3	(S)-3-hydroxybutanoyl-CoA --> crotonyl-CoA + water	butanol from acetyl-CoA
but4	crotonyl-CoA + NADH + proton --> butanoyl-CoA + NAD+	butanol from acetyl-CoA
but4b	crotonyl-CoA + NAD(P)H + proton --> butanoyl-CoA + NAD(P)+	butanol from acetyl-CoA
but5	butanoyl-CoA + NAD(P)H + proton --> butanal + coenzyme A + NAD(P)+	butanol from acetyl-CoA
but5b	butanoyl-CoA + NADH + proton --> butanal + coenzyme A + NAD+	butanol from acetyl-CoA
but6	butanal + NADH + proton --> butanol + NAD+	butanol from acetyl-CoA
but6b	butanal + NAD(P)H + proton --> butanol + NAD(P)+	butanol from acetyl-CoA
isobut1	2 pyruvate + proton --> 2-acetolactate + carbon dioxide	isobutanol from pyruvate
isobut2	2-acetolactate + NAD(P)H + proton --> 2,3-dihydroxy-3-methylbutanoate + NAD(P)+	isobutanol from pyruvate
isobut2b	2-acetolactate + NADH + proton --> 2,3-dihydroxy-3-methylbutanoate + NAD+	isobutanol from pyruvate
isobut3	2,3-dihydroxy-3-methylbutanoate --> water + 3-methyl-2-oxobutanoate	isobutanol from pyruvate
isobut4	3-methyl-2-oxobutanoate + proton --> isobutanal + carbon dioxide	isobutanol from pyruvate
isobut5	isobutanal + NADH + proton --> isobutanol + NAD+	isobutanol from pyruvate
isobut5b	isobutanal + NAD(P)H + proton --> isobutanol + NAD(P)+	isobutanol from pyruvate
kivD	4-methyl-2-oxopentanoate + proton --> 3-methylbutanal + carbon dioxide	3-methylbutanol production
ADH2	3-methylbutanal + NADH + proton --> 3-methylbutanol + NAD+	3-methylbutanol production
ADH2b	3-methylbutanal + NAD(P)H + proton --> 3-methylbutanol + NAD(P)+	3-methylbutanol production

Figure 77: The heterologous production pathways added to each genome-scale metabolic model used in Chapter 3.

Name	Reaction	Pathway
fxp	fructose 6-phosphate + inorganic phosphate --> acetyl-phosphate + erythrose 4-phosphate + water	NOG
xkp	xyulose 5-phosphate --> glyceraldehyde 3-phosphate + acetyl-phosphate	NOG
wljp1	carbon dioxide + NAD(P)H + proton--> formate + NAD(P)+	WLJ
wljp1b	carbon dioxide + NADH + proton --> formate + NAD+	WLJ
wljp2	formate + ATP + tetrahydrofolate --> N10-formyl-tetrahydrofolate + ADP + inorganic phosphate	WLJ
wljp3	N10-formyl-tetrahydrofolate + proton --> 5,10-methenyltetrahydrofolate + water	WLJ
wljp4	5,10-methenyltetrahydrofolate + NAD(P)H + proton --> 5,10-methylene-tetrahydrofolate + NAD(P)+	WLJ
wljp4b	5,10-methenyltetrahydrofolate + NADH + proton --> 5,10-methylene-tetrahydrofolate + NAD+	WLJ
wljp5	5,10-methylene-tetrahydrofolate + NADH + proton --> N5-methyltetrahydrofolate + NAD+	WLJ
wljp5b	5,10-methylene-tetrahydrofolate + NAD(P)H + proton --> N5-methyltetrahydrofolate + NAD(P)+	WLJ
wljp6	carbon dioxide + proton + NADH --> carbon monoxide + water + NAD+	WLJ
wljp6b	carbon dioxide + proton + NAD(P)H --> carbon monoxide + water + NAD(P)+	WLJ
wljp7	N5-methyltetrahydrofolate + carbon monoxide + coenzyme A --> tetrahydrofolate + acetyl-CoA	WLJ
hphb1	acetyl-CoA + bicarbonate + ATP --> malonyl-CoA + ADP + inorganic phosphate	3H4H
hphb2	malonyl-CoA + NADH + proton --> malonate semialdehyde + coenzyme A + NAD+	3H4H
hphb2b	malonyl-CoA + NAD(P)H + proton --> malonate semialdehyde + coenzyme A + NAD(P)+	3H4H
hphb3	malonate semialdehyde + NADH + proton --> 3-hydroxypropanoate + NAD+	3H4H
hphb3b	malonate semialdehyde + NAD(P)H + proton --> 3-hydroxypropanoate + NAD(P)+	3H4H
hphb4	3-hydroxypropanoate + ATP + coenzyme A --> 3-hydroxypropanoyl-CoA + AMP + pyrophosphate	3H4H
hphb5	3-hydroxypropanoyl-CoA --> acryloyl-CoA + water	3H4H
hphb6	acryloyl-CoA + NADH + proton --> propanoyl-CoA + NAD+	3H4H
hphb6b	acryloyl-CoA + NAD(P)H + proton --> propanoyl-CoA + NAD(P)+	3H4H
hphb7	propanoyl-CoA + ATP + bicarbonate --> (S)-methylmalonyl-CoA ADP + inorganic phosphate + proton	3H4H
hphb8	(S)-methylmalonyl-CoA --> (R)-methylmalonyl-CoA	3H4H
hphb9	(R)-methylmalonyl-CoA --> succinyl-CoA	3H4H
hphb10	succinyl-CoA + NADH + proton --> succinate semialdehyde + coenzyme A + NAD+	3H4H
hphb10b	succinyl-CoA + NAD(P)H + proton --> succinate semialdehyde + coenzyme A + NAD(P)+	3H4H
hphb11	succinate semialdehyde + NADH + proton --> 4-hydroxybutanoate + NAD+	3H4H
hphb11b	succinate semialdehyde + NAD(P)H + proton --> 4-hydroxybutanoate + NAD(P)+	3H4H
hphb12	4-hydroxybutanoate + ATP + coenzyme A --> 4-hydroxybutanoyl-CoA + AMP + pyrophosphate	3H4H
hphb13	4-hydroxybutanoyl-CoA --> crotonyl-CoA + water	3H4H
hphb14	crotonyl-CoA + water --> 3-hydroxybutanoyl-CoA	3H4H
hphb15	3-hydroxybutanoyl-CoA + NAD+ --> acetoacetyl-CoA + NADH + proton	3H4H
hphb15b	3-hydroxybutanoyl-CoA + NAD(P)+ --> acetoacetyl-CoA + NAD(P)H + proton	3H4H
hphb16	acetoacetyl-CoA + coenzyme A --> 2 acetyl-CoA	3H4H

Figure 78: The carbon efficient assimilation pathways added to each genome-scale metabolic model used in Chapter 3.

Exchange Reaction	Reaction Name	Lower Limit
Maintenance ATP	ATPM	3.15
Calcium	EX_ca2_e	-1000
Cob(I)alamin	EX_cbl1_e	-0.01
Chloride	EX_cl_e	-1000
Carbon Dioxide	EX_co2_e	0
Cobalt	EX_cobalt2_e	-1000
Copper	EX_cu2_e	-1000
Iron (II)	EX_fe2_e	-1000
Iron (III)	EX_fe3_e	-1000
Proton	EX_h_e	-1000
Water	EX_h2o_e	-1000
Potassium	EX_k_e	-1000
Magnesium	EX_mg2_e	-1000
Manganese	EX_mn2_e	-1000
Molybdate	EX_mobd_e	-1000
Sodium	EX_na1_e	-1000
Ammonium	EX_nh4_e	-1000
Nickle	EX_ni2_e	-1000
Phosphate	EX_pi_e	-1000
Selenate	EX_sel_e	-1000
Selenite	EX_slnt_e	-1000
Sulfate	EX_so4_e	-1000
Tungstate	EX_tungs_e	-1000
Zinc	EX_zn2_e	-1000
Oxygen	EX_o2_e	-1000

Figure 79: The exchange reactions used in the *E. coli* genome scale metabolic model.

Exchange Reaction	Reaction Name	Lower Limit
Ammonium	EX_nh4_e	-1000
Sulfate	EX_so4_e	-1000
Iron	EX_fe2_e	-1000
Sodium	EX_na1_e	-1000
Potassium	EX_k_e	-1000
Oxygen	EX_o2_e	-1000
Carbon Dioxide	EX_co2_e	0
Water	EX_h2o_e	-1000
Proton	EX_h_e	-1000
Phosphate	EX_pi_e	-1000

Figure 80: The exchange reactions used in the *S. cerevisiae* genome scale metabolic model.

Exchange Reaction	Reaction Name	Lower Limit
Nitrate	r_EX_no3_e	-1000
Photosystem 1	r_EX_photonPSI_e	0
Photosystem 2	r_EX_photonPSII_e	0
Water	r_EX_h2o_e	-1000
Proton	r_EX_h_e	-1000
Oxygen	r_EX_o2_e	-1000
Phosphate	r_EX_pi_e	-1000
Sulfate	r_EX_so4_e	-1000
Magnesium	r_EX_mg2_e	-1000

Figure 81: The exchange reactions used in the *S.* PCC 7002 genome scale metabolic model.

Bibliography

[1] S. Aikawa et al. Glycogen production for biofuels by the euryhaline cyanobacteria Synechococcus sp. strain PCC 7002 from an oceanic environment. *Biotechnology for biofuels* 7 (2014), 88.

[2] I. Andersson and A. Backlund. Structure and function of Rubisco. *Plant Physiology and Biochemistry* 46 (2008), 275–291.

[3] S. d. Angelis et al. Co-culture of microalgae, cyanobacteria, and macromycetes for exopolysaccharides production: process preliminary optimization and partial characterization. *Applied biochemistry and biotechnology* 167 (2012), 1092–1106.

[4] H. Bährs et al. Does quinone or phenol enrichment of humic substances alter the primary compound from a non-algicidal to an algicidal preparation? *Chemosphere* 87 (2012), 1193–1200.

[5] C. M. Beal et al. Energy return on investment for algal biofuel production coupled with wastewater treatment. *Water environment research : a research publication of the Water Environment Federation* 84 (2012), 692–710.

[6] M. B. Begemann et al. An organic acid based counter selection system for cyanobacteria. *PloS one* 8 (2013), e76594.

[7] B. M. Berla et al. Synthetic biology of cyanobacteria: unique challenges and opportunities. *Frontiers in microbiology* 4 (2013), 246.

[8] I. W. Bogorad, T.-S. Lin, and J. C. Liao. Synthetic non-oxidative glycolysis enables complete carbon conservation. *Nature* 502 (2013), 693–7.

[9] R. J. Bothast and M. A. Schlicher. Biotechnological processes for conversion of corn into ethanol. *Applied Microbiology and Biotechnology* 67 (2005), 19–25.

[10] Y.-J. Chen et al. Characterization of 582 natural and synthetic terminators and quantification of their design constraints. *Nature methods* 10 (2013), 659.

[11] J. Cheng et al. Alternatively permutated conic baffles generate vortex flow field to improve microalgal productivity in a raceway pond. *Bioresource Technology* 249 (2018), 212–218.

[12] K. Chojnacka and A. Noworyta. Evaluation of Spirulina sp. growth in photoautotrophic, heterotrophic and mixotrophic cultures. *Enzyme and Microbial Technology* 34 (2004), 461–465.

[13] A. F. Clarens et al. Environmental life cycle comparison of algae to other bioenergy feedstocks. *Environmental Science and Technology* 44 (2010), 1813–1819.

[14] R. L. Clark et al. Light-Optimized Growth of Cyanobacterial Cultures: Growth Phases and Productivity of Biomass and Secreted Molecules in Light-Limited Batch Growth. *Metabolic Engineering* (2018).

[15] R. L. Clark et al. Construction and Operation of an Affordable Laboratory Photobioreactor System for Simultaneous Cultivation of up to 12 Independent 1 L Cyanobacterial Cultures. *bioRxiv* 1 (2017).

[16] A. D. Comer et al. Flux balance analysis indicates that methane is the lowest cost feedstock for microbial cell factories. *Metabolic Engineering Communications* 5 (2017), 26–33.

[17] R. J. Conrado and R. Gonzalez. Envisioning the bioconversion of methane to liquid fuels. *Science (New York, N.Y.)* 343 (2014), 621–3.

[18] O. Darwazah, J. Floren, and M. Laughlin. Demand surge buoys methanol above crude declines, producers say ().

[19] S. Diamond et al. The circadian oscillator in Synechococcus elongatus controls metabolite partitioning during diurnal growth. *Proceedings of the National Academy of Sciences* (2015), 201504576.

[20] R. A. Dixon. Natural products and plant disease resistance. *Nature* 411 (2001), 843.

[21] P. M. Doran. *Bioprocess Engineering Principles (2nd Edition)*. Vol. 9. 2012, pp. 1–928.

[22] D. C. Ducat et al. Rerouting carbon flux to enhance photosynthetic productivity. *Applied and Environmental Microbiology* 78 (2012), 2660–2668.

[23] E. Essich, E. Stevens, and R. D. Porter. Chromosomal transformation in the cyanobacterium Agmenellum quadruplicatum. *Journal of Bacteriology* 172 (1990), 1916–1922.

[24] G. C. Gordon et al. CRISPR interference as a titratable, trans-acting regulatory tool for metabolic engineering in the cyanobacterium Synnechococcus sp. strain PCC 7002. *Metabolic Engineering* 38 (2016), 170–189.

[25] S. Grierson and V. Strezov. Life cycle assessment of the microalgae biofuel value chain: A critical review of existing studies. *The Third International Conference on Bioenvironment, Biodiversity and Renewable Energies* (2012), 1–6.

[26] M. J. Grisewood et al. Computational redesign of acyl-ACP thioesterase with improved selectivity toward medium-chain-length fatty acids. *ACS catalysis* 7 (2017), 3837–3849.

[27] L. T. Guerra et al. Natural osmolytes are much less effective substrates than glycogen for catabolic energy production in the marine cyanobacterium Synechococcus sp. strain PCC 7002. *J Biotechnol* 166 (2013), 65–75.

[28] T. Hasunuma et al. Dynamic metabolic profiling of cyanobacterial glycogen biosynthesis under conditions of nitrate depletion. *Journal of experimental botany* 64 (2013), 2943–2954.

[29] C. a. Haynes and R. Gonzalez. Rethinking biological activation of methane and conversion to liquid fuels. *Nature chemical biology* 10 (2014), 331–9.

[30] S. He and K. D. McMahon. 'Candidatus Accumulibacter'gene expression in response to dynamic EBPR conditions. *The ISME journal* 5 (2011), 329.

[31] R. W. Howarth, A. Ingraffea, and T. Engelder. Natural gas: Should fracking stop? *Nature* 477 (2011), 271–275.

[32] P. Hu et al. Integrated Bioprocess for Conversion of Gaseous Substrates to Liquids. *Proceedings of the National Academy of Sciences* 113 (2016), 14–19.

[33] P. Hu et al. Integrated bioprocess for conversion of gaseous substrates to liquids. *Proceedings of the National Academy of Sciences* 113 (2016), 3773–3778.

[34] I. Y. Hwang et al. Biocatalytic Conversion of Methane to Methanol as a Key Step for Development of Methane-Based Biorefineries. 24 (2014), 1597–1605.

[35] D. Klein-Marcuschamer, B. A. Simmons, and H. W. Blanch. Techno-economic analysis of a lignocellulosic ethanol biorefinery with ionic liquid pre-treatment. *Biofuels, Bioproducts and Biorefining* 5 (2011), 562–569.

[36] T. C. Korosh. "Advancement Towards a Biorefinery Platform Using the Cyanobacterium Synechococcus Sp. Strain PCC 7002". PhD thesis. University of Wisconsin–Madison, 2018.

[37] T. C. Korosh et al. Inhibition of Cyanobacterial Growth on a Municipal Wastewater Sidestream Is Impacted by Temperature. *mSphere* 3 (2018), e00538–17.

[38] S. H. Kung et al. Approaches and Recent Developments for the Commercial Production of Semi-synthetic Artemisinin. *Frontiers in plant science* 9 (2018), 87.

[39] T. Kusakabe et al. Engineering a synthetic pathway in cyanobacteria for isopropanol production directly from carbon dioxide and light. *Metabolic engineering* 20 (2013), 101–108.

[40] E. I. Lan and J. C. Liao. Metabolic engineering of cyanobacteria for 1-butanol production from carbon dioxide. *Metabolic engineering* 13 (2011), 353–363.

[41] N. S. Lau, M. Matsui, and A. A. A. Abdullah. Cyanobacteria: Photoautotrophic Microbial Factories for the Sustainable Synthesis of Industrial Products. *BioMed Research International* 2015 (2015).

[42] K. S. Le Corre et al. Phosphorus recovery from wastewater by struvite crystallization: A review. *Critical Reviews in Environmental Science and Technology* 39 (2009), 433–477.

[43] Y. Liang, N. Sarkany, and Y. Cui. Biomass and lipid productivities of Chlorella vulgaris under autotrophic, heterotrophic and mixotrophic growth conditions. *Biotechnology letters* 31 (2009), 1043–1049.

[44] P. C. Lin et al. Metabolic engineering of the pentose phosphate pathway for enhanced limonene production in the cyanobacterium Synechocysti s sp. PCC. *Scientific Reports* 7 (2017), 1–10.

[45] M. S. G. Lopes. Engineering biological systems toward a sustainable bioeconomy. *Journal of Industrial Microbiology and Biotechnology* 42 (2015), 813–838.

[46] S. R. Mackey, S. S. Golden, and J. L. Ditty. *The itty-bitty time machine. Genetics of the cyanobacterial circadian clock.* 1st ed. Vol. 74. Elsevier Inc., 2011, pp. 13–53.

[47] A. L. Markley et al. Synthetic Biology Toolbox for Controlling Gene Expression in the Cyanobacterium Synechococcus sp. strain PCC 7002. 7942 (2014).

[48] T. D. Martin et al. Determination of metals and trace elements in water and wastes by inductively coupled plasma-atomic emission spectrometry. *Methods for determination of metals in environmental samples. CRC Press Inc., Boca Raton* (1992), 33–91.

[49] A. Mcaloon, F. Taylor, and W. Yee. Determining the Cost of Producing Ethanol from Corn Starch and Lignocellulosic Feedstocks Determining the Cost of Producing Ethanol from Corn Starch and Lignocellulosic. *National Renewable Energy Laboratory-NREL* 2008 (2000), 44.

[50] J. T. McEwen et al. Engineering Synechococcus elongatus PCC 7942 for continuous growth under diurnal conditions. *Applied and Environmental Microbiology* 79 (2013), 1668–1675.

[51] C. R. Mehrer et al. Anaerobic Production of Medium-Chain Fatty Alcohols via a β-Reduction Pathway. *Metabolic engineering* (2018).

[52] R. Mo et al. Acetylome analysis reveals the involvement of lysine acetylation in photosynthesis and carbon metabolism in the model cyanobacterium synechocystis sp. PCC 6803. *Journal of Proteome Research* 14 (2015), 1275–1286.

[53] J. E. Muller et al. Engineering Escherichia coli for methanol conversion. *Metabolic Engineering* ().

[54] A. D. Neilen et al. Phytotoxic effects of terrestrial dissolved organic matter on a freshwater cyanobacteria and green algae species is affected by plant source and DOM chemical composition. *Chemosphere* 184 (2017), 969–980.

[55] D. J. Newman and G. M. Cragg. Natural products as sources of new drugs over the 30 years from 1981 to 2010. *Journal of natural products* 75 (2012), 311–335.

[56] N. E. Nozzi, J. W. K. Oliver, and S. Atsumi. Cyanobacteria as a Platform for Biofuel Production. *Frontiers in bioengineering and biotechnology* 1 (2013), 7.

[57] Nrel. A look back at the U. S. Department of Energy's aquatic species program: biodiesel from algae. *Report* 328 (1998), 291 p.

[58] L. M. Ojwang' and R. L. Cook. Environmental conditions that influence the ability of humic acids to induce permeability in model biomembranes. *Environmental science & technology* 47 (2013), 8280–8287.

[59] J. D. Orth, I. Thiele, and B. O. Palsson. What is flux balance analysis? *Nature Biotechnology* 28 (2010), 245–248.

[60] J. D. Orth et al. A comprehensive genome-scale reconstruction of Escherichia coli metabolism—2011. *Molecular systems biology* 7 (2011), 535.

[61] O. Osundeko et al. Acclimation of microalgae to wastewater environments involves increased oxidative stress tolerance activity. *Plant and Cell Physiology* 55 (2014), 1848–1857.

[62] E. T. Papoutsakis. Equations and calculations for fermentations of butyric acid bacteria. *Biotechnology and bioengineering* 67 (2000), 813–826.

[63] G. K. Pattanayak, C. Phong, and M. J. Rust. Rhythms in energy storage control the ability of the cyanobacterial circadian clock to reset. *Current Biology* 24 (2014), 1934–1938.

[64] P. P. Peralta-Yahya and J. D. Keasling. Advanced biofuel production in microbes. *Biotechnology journal* 5 (2010), 147–162.

[65] B. F. Pfleger. Microbes paired for biological gas-to-liquids (Bio-GTL) process. *Proceedings of the National Academy of Sciences* 113 (2016), 3717–3719.

[66] Photosynthesis. *Essays In Biochemistry* 60 (2016), 255–273.

[67] S. C. Reddington and M. Howarth. Secrets of a covalent interaction for biomaterials and biotechnology: SpyTag and SpyCatcher. *Current opinion in chemical biology* 29 (2015), 94–99.

[68] A. M. Ruffing. Engineered cyanobacteria: Teaching an old bug new tricks. *Bioengineered Bugs* 2 (2014), 136–149.

[69] R. Ruiz and T. E. Date. “Determination of carbohydrates in biomass by high performance liquid chromatography”. *Laboratory Analytical Procedure No. 002, National Renewable Research Laboratory*. Citeseer. 1996.

[70] T. Sakamoto, K. Inoue-Sakamoto, and D. A. Bryant. A Novel Nitrate/Nitrite Permease in the Marine CyanobacteriumSynechococcus sp. Strain PCC 7002. *Journal of bacteriology* 181 (1999), 7363–7372.

[71] R. Salmon and A. Logan. Flaring Up: North Dakota Natural Gas Flaring More Than Doubles in Two Years (2013).

[72] A. Schlesinger et al. Inexpensive non-toxic flocculation of microalgae contradicts theories; overcoming a major hurdle to bulk algal production. *Biotechnology Advances* 30 (2012), 1023–1030.

[73] E. Simeonidis and N. D. Price. Genome-scale modeling for metabolic engineering. *Journal of Industrial Microbiology and Biotechnology* 42 (2015), 327–338.

[74] S. E. Stevens and R. D. Porter. Transformation in Agmenellum quadruplicatum. *Proceedings of the National Academy of Sciences of the United States of America* 77 (1980), 6052–6056.

[75] S. Stevens and C. Van Baalen. Characteristics of nitrate reduction in a mutant of the blue-green alga Agmenellum quadruplicatum. *Plant physiology* 51 (1973), 350–356.

[76] Y. Sun et al. Boosting Nannochloropsis oculata growth and lipid accumulation in a lab-scale open raceway pond characterized by improved light distributions employing built-in planar waveguide modules. *Bioresource technology* 249 (2018), 880–889.

[77] E. Suzuki et al. Role of the GlgX protein in glycogen metabolism of the cyanobacterium, Synechococcus elongatus PCC 7942. *Biochimica et Biophysica Acta (BBA)-General Subjects* 1770 (2007), 763–773.

[78] G. R. Timilsina. Biofuels in the long-run global energy supply mix for transportation (2014).

[79] C. Van Baalen. Studies on marine blue-green algae. *Botanica Marina* 4 (1962), 129–139.

[80] A. D. Van der Woude et al. Carbon sink removal: Increased photosynthetic production of lactic acid by Synechocystis sp. PCC6803 in a glycogen storage mutant. *Journal of Biotechnology* 184 (2014), 100–102.

[81] T. T. Vu et al. Computational evaluation of Synechococcus sp. PCC 7002 metabolism for chemical production. *Biotechnology Journal* 8 (2013), 619–630.

[82] B. Wang et al. Application of synthetic biology in cyanobacteria and algae. *Frontiers in microbiology* 3 (2012), 344.

[83] W. B. Whitaker et al. Synthetic methylotrophy: engineering the production of biofuels and chemicals based on the biology of aerobic methanol utilization. *Current Opinion in Biotechnology* 33 (2015), 165–175.

[84] D. A. Wood, C. Nwaoha, and B. F. Towler. Gas-to-liquids (GTL): A review of an industry offering several routes for monetizing natural gas. *Journal of Natural Gas Science and Engineering* 9 (2012), 196–208.

[85] Y. Xu et al. Altered carbohydrate metabolism in glycogen synthase mutants of Synechococcus sp. strain PCC 7002: Cell factories for soluble sugars. *Metab Eng* 16 (2013), 56–67.

[86] J. T. Youngquist, T. C. Korosh, and B. F. Pfleger. Functional genomics analysis of free fatty acid production under continuous phosphate limiting conditions. *Journal of industrial microbiology & biotechnology* 44 (2017), 759–772.

[87] J. H. Yun et al. Hybrid operation of photobioreactor and wastewater-fed open raceway ponds enhances the dominance of target algal species and algal biomass production. *Algal Research* 29 (2018), 319–329.

[88] H. Yurimoto, N. Kato, and Y. Sakai. Assimilation, dissimilation, and detoxification of formaldehyde, a central metabolic intermediate of methylotrophic metabolism. *Chemical record (New York, N.Y.)* 5 (2005), 367–75.

[89] B. Zakeri et al. Peptide tag forming a rapid covalent bond to a protein, through engineering a bacterial adhesin. *Proceedings of the National Academy of Sciences* 109 (2012), E690–E697.

[90] S. Zhang, Y. Liu, and D. A. Bryant. Metabolic engineering of Synechococcus sp. PCC 7002 to produce poly-3-hydroxybutyrate and poly-3-hydroxybutyrate-co-4-hydroxybutyrate. *Metabolic engineering* 32 (2015), 174–183.

[91] Y. Zhang, M. A. White, and L. M. Colosi. Environmental and economic assessment of integrated systems for dairy manure treatment coupled with algae bioenergy production. *Bioresource Technology* 130 (2013), 486–494.

[92] Y. Zilliges. Glycogen, a dynamic cellular sink and reservoir for carbon. *The cell biology of Cyanobacteria* (2014), 189–210.